EVALUATION OF MIXED-MODE CHROMATOGRAPHY RESINS FOR ISOLATION OF RECOMBINANT THERAPEUTIC PROTEINS

A Dissertation

by

AYSWARYA RAVI

Submitted to the Office of Graduate and Professional Studies of
Texas A&M University
in partial fulfillment of the requirements for the degree of

DOCTOR OF PHILOSOPHY

Chair of Committee,	Zivko Nikolov
Committee Members,	Carmen Gomes
	Sandun Fernando
	Arul Jayaraman
Head of Department,	Stephen Searcy

August 2019

Major Subject: Biological and Agricultural Engineering

ABSTRACT

Biotherapeutics are lifesaving drugs, but their cost is prohibitively high for widespread use. Multiple chromatography operations required to meet stringent regulatory standards, contributes up to 70% of manufacturing cost. Mixed-mode resins are emerging chromatographic media having multimodal chemistries promising enhanced process selectivity. Their potential to reduce the number of chromatography operations employed, is key to improving affordability of biotherapeutics. This dissertation assessed the capabilities of mixed-mode resins, using two recombinant therapeutic proteins with challenging purification needs.

Mixed-mode ceramic hydroxyapatite (CHT) resin, was tested on microalgae, *Chlamydomonas reinhardtii* lysate, containing phosphorylated bone regenerative protein, osteopontin, in low purity (0.1-0.2% w/w). Complete binding of osteopontin to CHT through electrostatic interactions and Ca^{2+} coordination required 1500 mM sodium phosphate followed by 100 mM NaOH elution buffers to recover 86% of osteopontin. CHT distinguished between phosphorylated and non-phosphorylated *Escherichia coli* osteopontin, however, also co-purified impurity proteins (Rubisco) with similar properties.

Versatility of mixed-mode resins was tested with osteopontin lacking phosphorylation, expressed intracellularly in *E. coli*. High-throughput screening of mixed-mode resins, established HEA HyperCel as the capture chromatography promising 14-fold increase in purity. Interestingly, ensuing protein elution with NaCl from HEA

HyperCel, the interaction with Capto Q resin was orthogonal resulting in 95% purity and 44% overall recovery.

For the potential treatment of cystic fibrosis, human thioredoxin, was expressed in *E. coli* in high titers. HEA HyperCel resin bound thioredoxin at moderate conductivity of 5 mS and provided highest elution purity. However, unlike osteopontin, elution with NaCl buffer had the caveat of 45% thioredoxin recovery. Molecular modelling revealed existence of electrostatic and van der Waals interactions, supplementing experimental results. Simultaneous targeting of all interactions with 0.1 M arginine in 1 M NaCl buffer resulted in 100% recovery of biologically active, monomeric thioredoxin.

This study established that mixed-mode resins fare well in capturing therapeutic proteins from complex lysates, irrespective of the expression titer. Their flexibility in binding conditions eliminate the processing cost and time associated with conditioning operations. However, the protein-ligand interaction is driven by the properties of the target protein and process development with a thorough understanding of interaction mechanism is essential to realize their maximum potential.

DEDICATION

To my beloved grandparents

ACKNOWLEDGEMENTS

I would like to thank my advisor Dr. Zivko Nikolov, for recognizing my potential and taking me under his tutelage. I am forever grateful for his constant support, encouragement and expert guidance. I want to extend my gratitude to my committee members Dr. Carmen Gomes, Dr. Sandun Fernando and Dr. Arul Jayaraman for their valuable insights and contributions to this work.

I would like to acknowledge the monetary contributions from National Science Foundation (CBET grant #1160117) and OrPro Therapeutics, Inc. that enabled this research. The technical expertise and facility support from the team at National Center for Therapeutics Manufacturing, Lab for Molecular Simulations and Institute for Plant Genomics and Biotechnology is much appreciated.

To the members of the Bioseparation lab and my dear friends, thank you for creating a supportive and positive environment to conduct this research. I also extend my thanks to the Texas A&M community, for assistance with various aspects of this research.

I am fortunate to have an extensive network of friends and family, to rely on for unyielding support. To my significant other, thank you for being a tremendous force of motivation, sharing every day of this journey with me, cheering me on through the highs and getting me through the lows. Finally, I am profoundly thankful to my parents and my brother, for giving me the best opportunities, your unconditional love and patience through all my endeavors.

CONTRIBUTORS AND FUNDING SOURCES

Contributors

This work was performed under the guidance of a dissertation committee, chaired by Dr. Zivko Nikolov, committee members Dr. Carmen Gomes, Dr. Sandun Fernando, Department of Biological and Agricultural Engineering and Dr. Arul Jayaraman, Department of Chemical Engineering.

The cells lines expressing osteopontin, transgenic strain of *Chlamydomonas reinhardtii* and recombinant *Escherichia coli* were provided by Dr. Stephen Mayfield's research group, University of California, San Diego. Recombinant *Escherichia coli* expressing human thioredoxin was provided by Dr. Peter Heifetz, OrPro Therapeutic, Inc. Data described in Chapter III was collected in part by Shengchun Guo, former student of Department of Biological and Agricultural Engineering and his contributions are duly recognized. Portions of this research were conducted with advanced computing resources provided by Texas A&M High Performance Research Computing and the Lab for Molecular Simulations, Texas A&M University with guidance and support from Dr. Lisa Perez. All other parts of this dissertation were performed independently by the student.

Funding Sources

The work detailed in Chapter II and III was funded by the National Science Foundation (Chemical, Bioengineering, Environmental, and Transport Systems Grant #1160117). The research described in Chapter IV was supported by OrPro Therapeutics, Inc.

NOMENCLATURE

aa	Amino acids
AS	Ammonium sulfate
BSA	Bovine serum albumin
BSP	Bone sialoprotein
C. reinhardtii	*Chlamydomonas reinhardtii*
cGMP	Current Good Manufacturing Practice
CHO	Chinese hamster ovary
CHT	Ceramic hydroxyapatite
CV	Column volume
DDT	Dithiothreitol
DNA	Deoxyribonucleic acid
DoE	Design of experiments
E. coli	*Escherichia coli*
EDTA	Ethylenediaminetetraacetic acid
ELISA	Enzyme-linked immunosorbent assay
EU	Enzymatic units
Ga-IMAC	Gallium-immobilized metal affinity chromatography
GST	Glutathione-S-transferase
HCl	Hydrochloric acid
HCP	Host cell protein

HPLC	High performance liquid chromatography
HRP	Horseradish peroxidase enzyme
hTrx	Human thioredoxin
HTS	High-throughput screening
IgG	Immunoglobulin G
kDa	Kilo Dalton
LB	Luria-Bertani
mAb	Monoclonal antibody
MMC	Mixed-modal chromatography
MMP	Metallo-protease
mS	Millisiemens
MW	Molecular weight
MWCO	Molecular weight cut-off
NaCl	Sodium chloride
NaOH	Sodium hydroxide
NaP	Sodium phosphate
OPN	Osteopontin
PBS	Phosphate-buffered saline
pI	Isoelectric point
PMSF	Phenylmethane sulfonyl fluoride
PTM	Post-translational modification
RGD	Arginine-glycine-aspartic acid

Rubisco	Ribulose-1, 5-bisphosphate carboxylase/oxygenase
SDS-PAGE	Sodium dodecyl sulfate polyacrylamide gel electrophoresis
TMB	3,3′,5,5′-Tetramethylbenzidine
TP	Total protein
Tris	Tris (hydroxymethyl) aminomethane
TSP	Total soluble protein

TABLE OF CONTENTS

Page

LIST OF FIGURES

Page

LIST OF TABLES

Page

CHAPTER I

INTRODUCTION AND LITERATURE REVIEW

1.1 Introduction

Biopharmaceuticals are biological materials including proteins, nucleic acids, cells and viral vectors that are of therapeutic value [1]. They can mediate several functions including replacement of deficient proteins, effector functions, receptor blocking, enzyme inhibition, stimulating biological response, etc. [2]. Their wide range of applications have been effective in the treatment and alleviating the symptoms of diabetes, cancer, inflammatory and autoimmune diseases, neurodegenerative diseases, cardiovascular disease, genetic diseases and much more.

Biopharmaceuticals or biotherapeutics are a burgeoning market accounting for $188 billion in sales in 2017 alone and growing rapidly [3]. Currently, there are 316 approved biopharmaceutical products in the United States and European Union [3]. The advent of recombinant DNA technology was the driving force behind the rise of biotherapeutics. It enabled large-scale commercial manufacturing of therapeutics with consistent quality, overcoming the variability and complexity associated with native source material. Additionally, it opened up the possibility of novel modifications that would improve the efficacy and impart additional properties to therapeutics. There are several categories of biopharmaceuticals, shown in Figure 1.1. Monoclonal antibodies (mAb) dominate the current biologics market (37%), followed by vaccines (28%) and recombinant therapeutic proteins (10%).

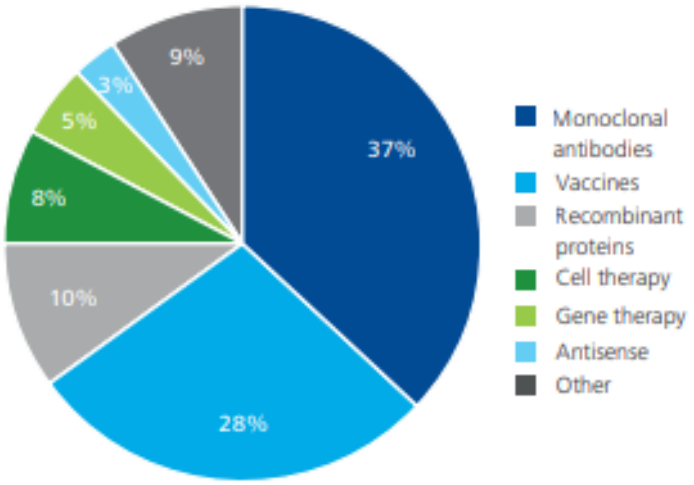

Figure 1.1 Major categories of biopharmaceuticals (Reprinted from Jacoby, R., 2015 [4])

On an average, the cost of a therapeutic ranges from $100-1000/g with a 2-5 g dose required per person per year, compared to $5/g of chemically synthesized drugs [5]. Regulatory authorities Food and Drug Association and European Medicines Agency, have set stringent guidelines for the quality of therapeutic products depending on the route of administration. Typically the final therapeutic should contain ≤ 1 µg concentration per dose of impurity proteins, 10 ng per dose of DNA, 10-100 EU per mg of endotoxins, 0.5% aggregates and 12-20 log reduction in viral loads [6-9]. The regulatory agencies also mandate current good manufacturing practice (cGMP) compliance for biologics manufacturing due to the intended human consumption. Thorough characterization of the product including purity, potency, stability, immunogenicity, pharmacodynamics and pharmacokinetics as well as the contaminant nucleic acids, viruses, pyrogens, residual host cell proteins, etc. need to be analyzed [10]. The manufacturing operation has to be monitored for consistency and extensive quality assurance and quality control is

mandated. Cleaning, sterilization and validation between batches of manufacturing, minimize batch-to-batch variations and contribute to the increased cost of goods. Recent trends of reducing the time for cleaning and validation by switching to disposable single-use components, have also exacerbated the cost of manufacturing. All of these manufacturing requirements and the cost associated with it, reflect in the exorbitant cost of biologics [11].

The process for therapeutic manufacturing can be classified into stages of cell line development, upstream processing, downstream processing and formulation. Because cell line development and product formulation are beyond the scope of this dissertation, only upstream and downstream processing will be further reviewed.

1.1.1 Upstream Processing

Upstream processing entails the propagation and subsequent large-scale fermentation of biological organism to produce biopharmaceutical. A wide-range of organisms ranging from bacteria, fungi, plants, mammalian and human cells have been explored for producing biotherapeutics. The choice of expression system is dependent on the properties of the therapeutic, its proper folding and post-translational modification, immunogenicity, method of delivery, and the contaminants specific to the expression system. The cells are then grown in large-scale to produce the therapeutics during upstream processing. The quantities of therapeutic expressed or "expression titers" dictate the productivity of the expression system. The cost of upstream processing is directly associated with protein expression levels. A tenfold increase in expression titer results in a 25% decrease in upstream costs [5]. Ardent research in the screening of cell lines,

improving cell viability and mode of fermenter operation have successfully enhanced the expression titers [12]. Advancements in chemically defined and serum-free media have reduced batch-to-batch variations of cell culture, simplified media optimization and reduced contamination [13]. Taken together, currently the process scale for mammalian cell stands at 20,000 L bioreactors operated for 2-3 weeks under fed-batch or perfusion conditions to accumulate 10^7/mL cell density [12]. Biomass accumulation and therapeutic protein concentration vary depending on expression system and mode of growth, but high density *E. coli* cultures accumulate biomass of 20-175 g dry weight/L expressing 5 g/L therapeutics while yeast cells report 130 g dry weight/L expressing 4-14 g/L of therapeutic [14]. Plant cell cultures can accumulate 0.02-0.2% w/w of their dry weight in recombinant therapeutic and mammalian cells can now regularly secrete 5 g/L of monoclonal antibodies [15]. As a result of the explosive improvement in expression titers and cell viability, upstream processing costs have been on a steady decline.

1.1.2 Downstream Processing

Downstream processing is defined as a sequence of unit operations employed to isolate the therapeutic product from the impurities. The process begins with large volumes of relatively low product concentration generated from upstream processing with the end goal of increasing product concentration and purity, conforming to the guidelines set by regulatory bodies. First, removal of the cells used for expressing the biotherapeutic (extracellular product), or extraction of the product from the cells and consequent removal of cell debris is entailed in primary recovery. Figure 1.2 shows a typical downstream process applied to achieve the therapeutic compliant with regulatory standards. Packed-

bed chromatography is the workhorse of downstream processing, because of its unparalleled resolution [16]. In order to achieve the desired purity, three chromatography operations are typically employed. The first chromatography is called capture, with the goal to reduce the handling volume and separate major impurities. The second or intermediate chromatography is employed to enhance the purity followed by an optional polishing step to concentrate and obtain the therapeutic in the desired specification. In order to maximize the process selectivity, each chromatography is required to be orthogonal targeting different properties of the protein. Often, a complimentary chromatography is preferred where the end product from the previous operation is compatible for direct loading on the next operation. Contrary to that, an additional conditioning operation, such as buffer exchange, salt addition or removal would be necessary, which increases the number of unit operations in the downstream process. Minimal processing steps would be ideal for the following reasons- 1) each unit operation contributes to product loss 2) reduce the cost associated with each operation 3) keep the processing time to minimal.

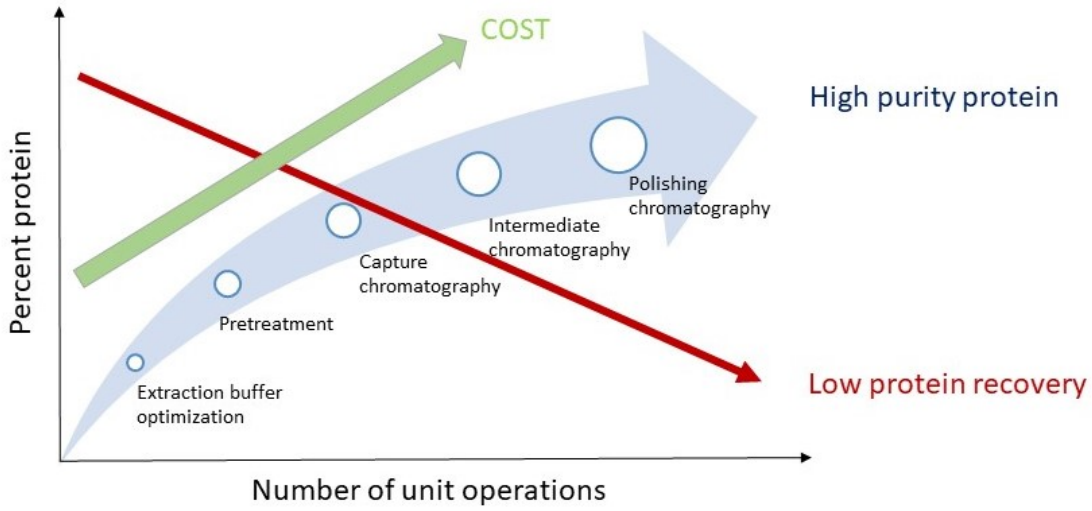

Figure 1.2 Strategy for downstream process development to isolate recombinant biotherapeutics

Upstream productivity (combined cell density and titers) is critical prerequisite for an efficient downstream processing. With the advances in upstream processing, production of therapeutics has become extremely efficient. However, downstream processing is the bottleneck and accounts for 50-80% of the total manufacturing cost [17]. Chromatography is the most expensive part, accounting for up to 70% of the cost of therapeutics manufacturing in some cases [18]. The high cost associated with chromatography mainly arises from the cost of resin, long cycle times, cleaning and validation requirements for reuse [18]. The current processes are often inefficient resulting in 50% waste of product [19]. Comprehensive downstream process development embracing new technologies is key to minimizing the cost of manufacturing which would translate to affordable therapeutics. Currently, the basis for downstream process development is built on "rule-of-thumb" which is followed by a knowledge-based

selection of unit operations for each product and expression system [17]. The resulting process is often suboptimal with inefficient resource utilization and extensive experimental requirements. Significant time and resource is spent on optimizing each unit operation that fails to conform to the scale of operation.

Recent developments in automation and modelling, have allowed for high-throughput experimental screening and algorithm-based methods for process development. Miniaturization, automation and parallelization combined led to the development of robotic liquid-handling instruments capable of processing up to 1536-well plates. Several process parameters such as chromatography conditions, binding isotherm and resin binding capacity can be monitored by high-throughput screening [20]. On the other hand, an algorithmic approach minimizes the number of experiments by mathematic modelling and computer simulations to predict the purification behavior. However, for accurate predictions, extensive database on chromatography resin properties, product and protein impurity information and biological thermodynamics are necessary [17]. Therefore, a hybrid approach combining the advantages of these developments has emerged as a promising candidate [21]. Combination of a hybrid-approach and thorough optimization, improves the process productivity resulting in lower production cost. Using the hybrid approach a platform could be created for downstream process development of therapeutic proteins with similar properties that fall under the same category. An example of such a template is with mAbs that constitutes 37% of all biologic drugs [4]. Since, mAbs have a shared fragment crystallizable (Fc) region, the downstream process often involves Protein A affinity chromatography for capture, followed by ion-exchange chromatography

and additional orthogonal viral clearance steps. Such a cascade template, allows for standardization with reduced time-to-market [17]. However, recombinant therapeutic proteins, the other major class of therapeutics (Figure 1.1), are diverse in properties, application and expression system. They do not have a common motif, therefore a generalized downstream purification platform is not possible for recombinant proteins. Therefore, the downstream process design is strenuous and has to be custom developed without prior knowledge of the compatible chromatography. In the absence of a purification platform, downstream processing cost could be lowered by designing an efficient process based on knowledge of protein chemistry, properties of impurities and novel non-affinity resins, preferably reducing the number of chromatography steps. Process flow diagram in Figure 1.2 suggests that the optimization of capture chromatography would have the maximum impact on process efficiency, improving its selectivity could render multiple chromatography steps redundant. The technological advances in chromatography adsorbents offering enhanced selectivity and their performance as capture chromatography were explored.

1.1.3 The Promise of Mixed-Mode Resins

Mixed-mode resins are an emerging class of chromatography adsorbents. They interact with the solutes through two or more interaction mechanisms that are orthogonal, promising enhanced selectivity [22]. As the capabilities of traditional chromatography methods stagnated, mixed-mode resins have emerged as a potential alternative in downstream processing. They offer higher resolution, high binding capacity, better sample loading properties and flexibility in loading condition. Most importantly, the enhanced

selectivity could replace the need for multiple single-mode chromatography resins, reducing the number of unit operations and consequently the cost of downstream processing [23]. Currently, mixed-mode resins have been applied as the capture and polishing chromatography for mAb to minimize the number of chromatography steps in mAb platform [24, 25]. Mixed-mode resins have not been tested extensively for direct capture of other classes of biotherapeutics expressed in different expression hosts.

There are multiple possible chemistries of mixed-mode ligands, some of which are shown in Figure 1.3, they offer a range of interaction combinations, enabling improved selectivity. However, the multiple interactions make it hard to predict the protein-ligand interaction behavior. Thermodynamic modelling and experimental isotherms have been developed to predict behavior of model protein bovine serum albumin (BSA) with mixed-mode resins [26]. Quantitative structure–property relationship models and molecular simulations have also been explored for other model proteins [27, 28]. These efforts have immensely contributed to understanding the possible interaction chemistries offered, but are not equipped to handle the experimental reality of complex feed material. The performance of mixed-mode resins in situations with complex lysates and unexplored therapeutic proteins is still unclear. The selectivity of these novel adsorbents could be the solution to improving downstream processing efficiency and have to be explored.

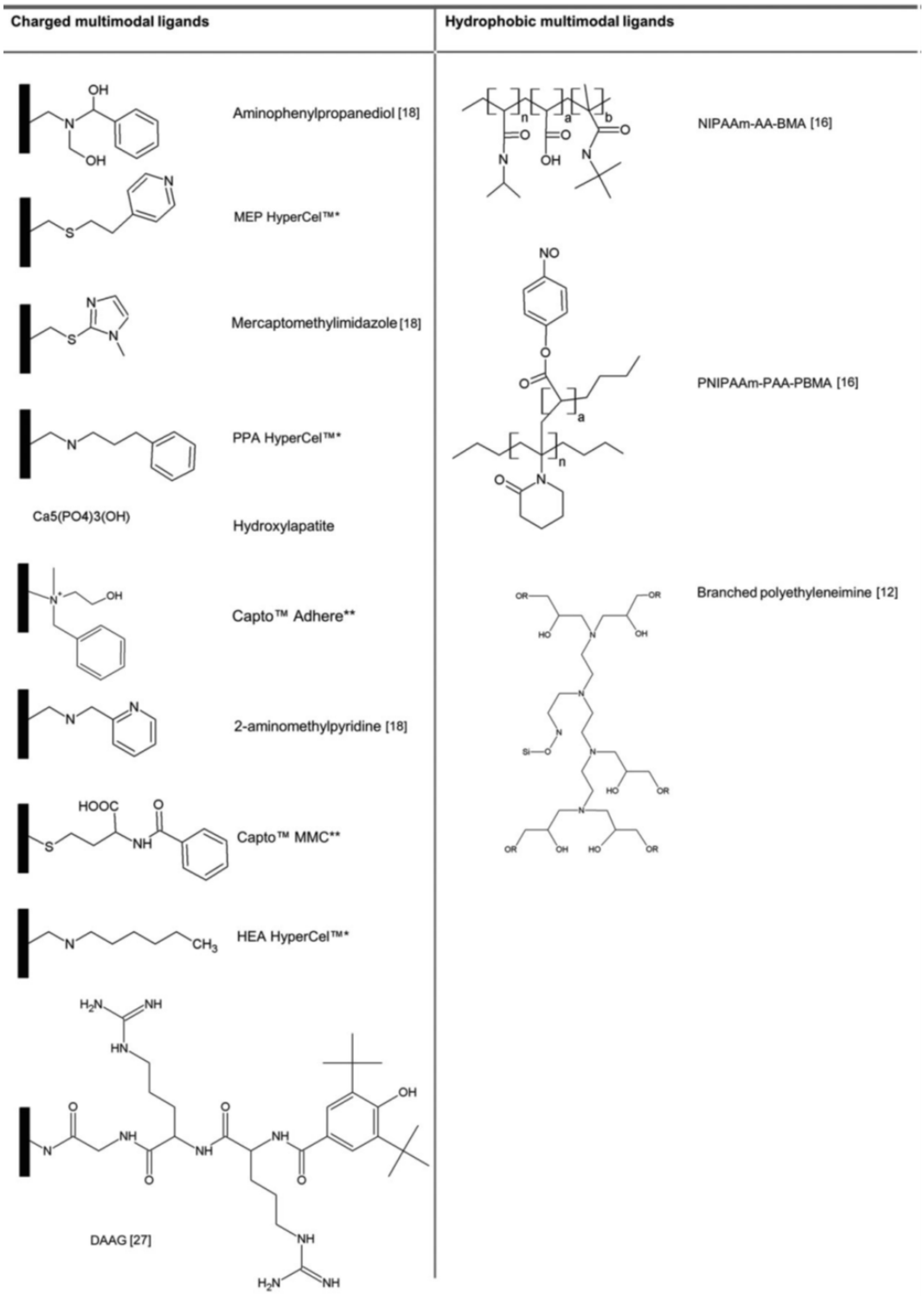

Figure 1.3 Possible chemistries of mixed-mode ligands (Reprinted from Kallberg, K. et al., 2012 [29])

This dissertation aims at addressing some of the following lacking information around the promise and pitfalls of mixed-mode resins-

i. Selectivity of mixed-mode resins as a capture chromatography when applied to different feed streams and challenged with separating isoforms or impurities with similar properties
ii. Impact of starting purity and expression titer on efficiency of the resin
iii. Explore the possible protein-ligand interaction mechanisms and variation depending on the protein properties
iv. Investigate the suitability for direct capture from complex lysates and flexibility of binding conditions
v. Study protein recovery and the mechanism of action of buffer modifiers

These parameters were evaluated by employing mixed-mode resins in the downstream processing of two radically different recombinant therapeutic proteins with challenging purification needs.

1. A low concentration acidic protein (osteopontin) with post-translational modifications, expressed in *Chlamydomonas reinhardtii*, containing plant-like lipids, chloroplast protein impurities.
2. A high concentration acidic protein (thioredoxin) with low ionic and hydrophobic properties, expressed in *E. coli,* containing possible aggregates, endotoxins and numerous host cell protein (HCP) impurities.

1.2 Literature Review

Detailed literature review on the mixed-mode chromatography resins and proteins that are the focus of this dissertation are discussed next.

1.2.1 Mixed-Mode Resins

Yang et al., reviewed the history of mixed-mode resins, the first recognized resin was hydroxyapatite in 1956 by Tiselius et al. [23, 30]. Hydroxyapatite was predominately used in DNA separation till Burton and Harding's work on Hydrophobic Charge Induction Chromatography in 1998 [31]. They discovered that hydrophobic ligands with charge interactions interacted with chymosin in a salt-independent, pH dependent condition and offered enhanced selectivity [32]. This renewed the interest in mixed-mode resins for therapeutic protein application. The technological advancement to manufacture designer ligands and control their uniform distribution on resin beads has fueled their rise [22]. Currently, mixed-mode resins have predominantly been applied as a pseudo-affinity alternative to Protein A chromatography in mAb isolation, both as capture or polishing step [24]. IgG1 isolation incorporating mixed-mode resins MEP and CHT after Protein A chromatography, showed increased reduction in aggregates and improved the protein recovery [33]. Successful isolation of recombinant human vascular endothelial growth factors from *E. coli* inclusion bodies using mixed-mode resin, Capto MMC was accomplished on pilot and manufacturing scales [22]. Other than proteins, peptides and biopolymer separations have also benefited from mixed-mode resins.

The multiple protein-ligand interactions can be simultaneous or separate. When the interactions are separate, or individual retention mode, each mode of interaction can be brought on and controlled by manipulating the process conditions. As a result, a "U-shaped" elution profile ensues, due to the shift between interaction chemistries. For example, BSA interacts electrostatically with benzylamine ligand on Cell-SSP-BA mixed mode resin at pH 4.2. As the NaCl concentration increases, the protein desorbs from the ligand by reversal of electrostatic interaction due to electrostatic shielding. When the NaCl concentration increases beyond 0.5 M, hydrophobic interactions cause BSA to interact with the ligand again [34]. The advantage of individual retention mode is that it can be easily understood and implemented [23]. When the multiple interactions are simultaneous, combined retention mode occurs. With such interactions, it becomes hard to predict the retention and elution behavior of proteins. Predictive approaches with adsorption isotherms, molecular modeling and quantitative structure–property relationship have been applied to forecast the interactions for process development.

The complex nature of these interactions make process development with mixed-mode resins notorious for low protein recovery. Eluents such as NaCl, pH changes or addition of competitor are often insufficient. Extraordinary efforts are necessary to counteract all the interactions and release the bound proteins. Several additives to the elution buffers have been studied for this purpose, called elution buffer modifiers, which include arginine, guanidine, sodium caprylate, various polyols, urea, glycine, ethanol, etc. [35, 36]. The impact of these modifiers on mixed-mode resins have been explored, however not all of the exact mechanism of action are clearly understood. Glycerol can

impact the hydrophobic interaction and promote ionic interactions [37]. Chaotropes such as urea and guanidine affect hydrogen bonds and hydrophobic interactions, exposing the secondary structure, especially with large proteins. Arginine, typically used in protein formulation to maintain structural conformational stability has been extensively used as an elution modifier. Due to the guanidinium group in its structure, it elicits the same properties, combined with aggregate solubilization and possible structural changes [35, 36]. Kalease et al., in the study with recombinant human vascular endothelial growth factors, they employed 0.8-1 M arginine in combination with NaCl to elute the protein from Capto MMC, inconclusively questioning whether arginine acted on the hydrophobic or hydrogen bonding [22]. In another study, the same Capto MMC mixed-mode resin displayed complete desorption of ubiquitin and papain with 0.1 M arginine, while lysozyme and avidin required arginine in combination with high NaCl concentrations for elution [36]. Therefore, the protein interactions with mixed-mode resins are not straightforward and require further studies to be fully understood.

1.2.1.1 Ceramic Hydroxyapatite Resin

Ceramic hydroxyapatite (CHT) was the earliest mixed-mode resins, used for therapeutic protein isolation in 1950s [38]. Hydroxyapatite is a naturally occurring mineral crystal composed of calcium, phosphate and oxygen with a chemical formulae of $Ca_{10}(PO_4)_6(OH)_2$. It is widely present in biological materials as the structural component of teeth enamel and bones. When sintered at high temperatures, porous beads of ceramic hydroxyapatite is formed, entailing high selectivity for biomolecules.

CHT has a uniform composition throughout the matrix, in contrast to typical chromatography resins that have functional ligands immobilized on a bead with the help of a spacer arm. As a result, CHT has high pressure tolerance and better flow properties [39]. The possible interactions with CHT resin is shown in Figure 1.4. Electrostatic interactions with the positively charged calcium sites and negatively charged phosphate sites are possible, enabling separations for both acidic and basic proteins. Additionally, coordinate bonds formed by metal affinity interactions with the calcium sites are also possible. The coordinate bonds at calcium sites are much stronger than electrostatic interactions and NaCl is insufficient to elute them even at concentrations up to 4 M [39, 40]. Although the interaction mechanisms can be broadly classified, the elution of target proteins is more complex and cannot be considered as simple reversal of the binding mechanism. Extensive investigation into the available elution salts and modifiers by extensive experimental testing have been performed [41, 42].

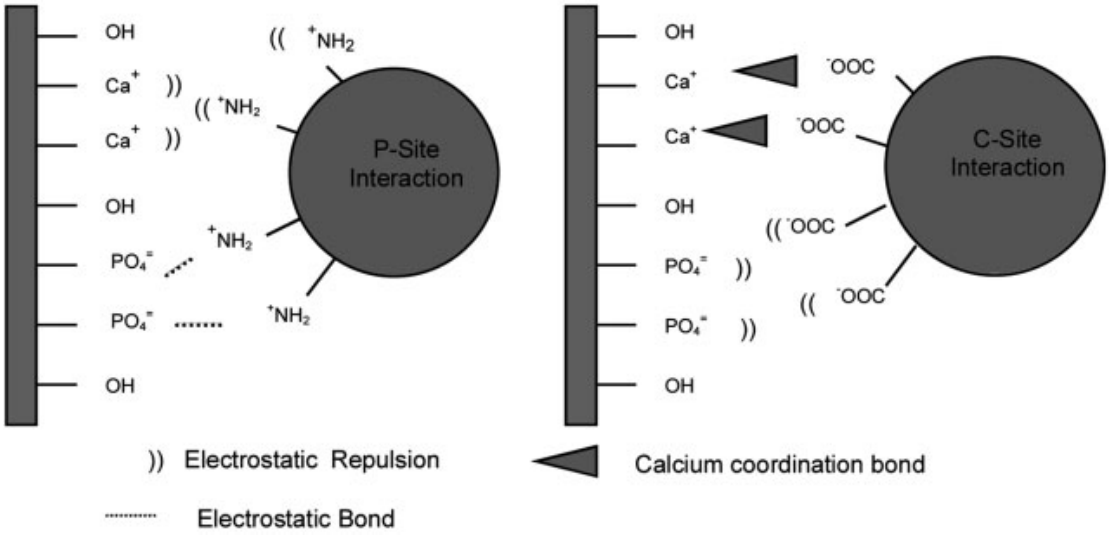

Figure 1.4 Possible interaction mechanisms of CHT resin (Reprinted from Hilbrig, F. et al., 2012 [39])

Monoclonal antibodies, viral vectors, nucleic acids and several proteins have been purified with CHT. Notably, aggregate and fragment separation from mAb is a lucrative property of CHT [43, 44]. The specificity of CHT towards phosphopeptides and phospholipids are of special interest to this study. Fractionation of casein peptides based on the number of phosphorylations has been achieved using a phosphate elution gradient on hydroxyapatite chromatography [45]. The same research group also investigated phospholipids separation from buttermilk and egg yolks. Although the resin successfully separated triacylglycerols from phospholipids, they report that other non-phosphorylated lipids were also bound to the resin by hydrogen bonds. The elution of these phospholipids was also difficult and required extensive testing due to the strong interaction by pseudo-affinity [46]. Finally, phosphoprotein separation using CHT is much less prevalent, due to the complexity of interactions from the distribution of carboxyl groups, and secondary and

tertiary structure [47]. Phosvitin, a phosphorylated egg protein reportedly required exceptionally high concentrations of phosphate in the elution buffers [48]. Therefore, CHT is a powerful and complex chromatography resin, but the success of its application is dependent on the biochemical characteristics of the material to be separated.

1.2.1.2 HyperCel Resins

The family of HyperCel resins are commercial mixed-mode resins by Pall Life sciences. They consist of MEP, HEA and PPA HyperCel resins, with ligands on a cellulose bead. MEP (4-Mercapto-Ethyl-Pyridine) is a hydrophobic charge induction chromatography resin that allows for hydrophobic interactions at low salt and elution is achieved by charge repulsion. MEP is prominently used as an alternative to Protein A chromatography for mAb capture [49]. HEA and PPA HyperCel resin have aliphatic and aromatic hydrocarbons respectively, with a charged ligand. The hydrocarbons promote protein binding in low to moderate conductivity, eliminating the need for conditioning [35]. Human IgG isolation process has incorporated HEA HyperCel as the capture chromatography resin in a 3 step orthogonal purification train [50]. Applying design of experiments (DoE) approach, HEA HyperCel was employed on *E. coli* lysate to obtain 89% recovery of granulocyte colony stimulating factor at 99.16% purity [20]. Other recombinant proteins including zinc metalloenzyme, lactoferrin have also successfully incorporated HyperCel resins in their purification train [51, 52].

HyperCel resins offer multiple-mode of interaction with the proteins such as electrostatic, hydrophobic and hydrogen bonding. The types of interactions were shown to be heavily dependent on the physiological condition of binding using model proteins of

different pI [35]. Acidic proteins such as BSA, ovalbumin and catalase were efficiently adsorbed by HEA and PPA HyperCel resins at pH > pI of proteins at low conductivity, but increasing the conductivity was insufficient for their elution [35]. This is due to multiple interaction mechanisms that act simultaneously and need to be reversed for efficient protein elution. Consequently, extensive screening of binding and elution conditions is a crucial part of process development using mixed-mode resins. High-throughput screening on filter plates is a common approach for selecting the appropriate process conditions [24, 53, 54]. Mathematical-model based predictions and molecular simulations are also gaining prominence to relieve the experimental load [26, 27].

Several elution buffers with modifier salts have been carefully tested for efficient protein recovery and to understand the protein-ligand interaction of HyperCel resins. Most commonly, a variety of salts, urea, arginine, guanidine, glycine and glycerol have been tested. In the study of lysozyme retention on HyperCel resins, the nature of anion and cation of the salt used strongly impacted the retention. While sodium chloride and sulfate promotes retention time by improving hydrophobic interactions, sodium acetate was shown to decrease the lysozyme binding [35]. Organic solvents, ethanol, glycerol and ethylene glycol, have been applied to counteract hydrophobic interactions of bovine gamma-globulin with MEP HyperCel [55]. Ethanol in the presence of 1.5 M NaCl was effective in eluting human growth factor, when ethanol by itself was ineffective, highlighting the necessity to break multiple interactions simultaneously [22]. Depending on the protein, arginine has the ability to break electrostatic, hydrophobic and hydrogen bonding [37]. Bovine γ-globulin absorbed to MEP resin did not elute with NaCl, and

arginine was employed to break hydrophobic interactions efficiently [55]. A 80-90% recovery of human granulocyte colony stimulating factor from HEA HyperCel resin was possible with only NaCl elution [20]. Therefore, there are several possible protein-specific interactions with HyperCel resins that need to be explored during process development.

1.2.2 Therapeutic Proteins Structure and Biological Function

1.2.2.1 Osteopontin

Osteopontin (OPN), also called bone sialoprotein (BSP-1), is mammalian protein expressed by a wide range of cells (bone, smooth muscle cells, vascular tissue, brain cells, epithelial cells of mammary salivary glands, macrophages and lymphocytes, etc.) and secreted in bodily fluids (milk, blood, urine, etc.). Nascent OPN is made up of ~300 amino acids, with acidic amino acids (aspartic acid and glutamic acid) making up 25% and serine contributing to 15% of the primary sequence. The resultant protein is acidic with a theoretical pI of 4.5. The primary amino acid sequence varies between mammals, however functional amino acid sequences are predominantly conserved [56]. The functionality of OPN arises from its distinctive amino acid sequences (Figure 1.5), RGD (arginine-glycine-aspartic acid) sequence, polyaspartate domain, thrombin cleavage site, multiple heparin and calcium binding sites [57].

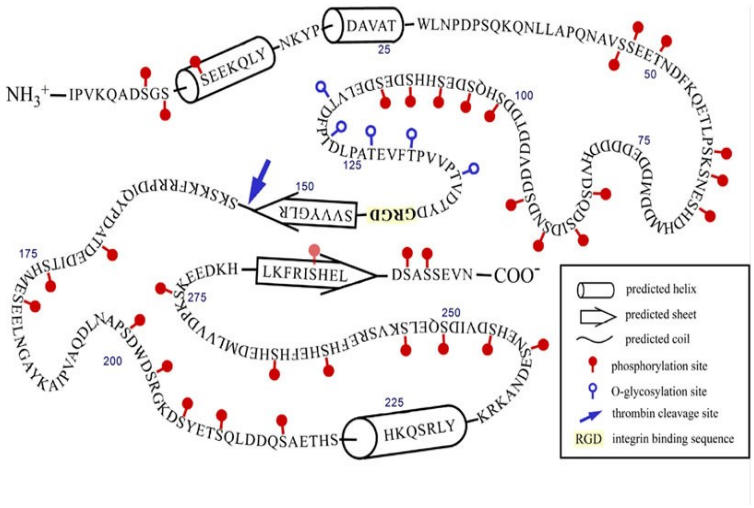

Figure 1.5 Amino acid sequence of OPN showing functional sites (Reprinted from Kazanecki, C.C. et al., 2007 [58])

The primary function of OPN is bone resorption and regeneration during wound healing. The RGD sequence is an integrin binding site that is centrally located (128-130 aa) close to the thrombin cleavage sequence [59, 60]. OPN is secreted by macrophages as a response to injury or inflammation, accumulating at the injury site where it acts as an opsonin. The RGD sequence of OPN attracts the phagocytic osteoclasts to the injury site, promoting debris and bacterial clearance in a process of bone resorption [61]. Osteoclasts in turn secrete OPN, enriching it in the cement layer, the newly exposed surface of the old bone which is primed for regeneration. Here, OPN bridges new osteoblast cells with the hydroxyapatite in the bone matrix through its polyaspartic sequence (70-78 aa), mediating bone regeneration [61]. Calcium binding sites and phosphorylated serines prevent spontaneous precipitation of calcium and impede nucleation of hydroxyapatite or calcium oxalate crystals [56]. The charge distribution in the polyaspartic acid sequence is attributed to the inhibition of calcium oxalate crystals, preventing kidney stones [62]. The heparin

binding regions are involved in immediate response to inflammation and wound healing [63]. OPN is also an immunomodulator of Th1 mediated response to induce antibody production and B-cell proliferation [64].

The secondary structure is predicted based on circular dichroism studies, consists of 8 α-helices in 2 clusters, concentrated towards the C-terminal region [56, 65]. The RGD sequence and thrombin cleavage site are flanked between short β sheets, similar to the structure of fibronectin [65]. The tertiary structure is not defined with reports that characterize OPN with an open, flexible structure by nuclear magnetic resonance and sparse hydrophobic regions [58, 66]. This flexibility in structure allows interaction with multiple proteins such as collagen, fibronectin, osteocalcin, etc. [59].

Several potential post-translational modifications (PTM) sites–28 phosphorylation and 6 glycosylation sites, are present [58, 67] and in some cases sulfation and crosslinking are also possible [68]. Sites for these modifications, vary depending on the source of OPN, bovine milk, human milk and rat bone OPN have 32, 28 and 11 phosphorylations respectively [64]. Glycosylation patterns also vary, bovine and human milk have reported 3 (Thr 115, Thr 124, and Thr 129) and 5 N-linked glycosylations (Thr134, Thr138, Thr143, Thr147 and Thr152) while rat bone OPN has one N-linked and up to six O-linked glycosylated residues [67, 69]. The post-translational modifications in OPN vary with the expressing tissue and as necessitated by its multitude of cellular functionality [69, 70].

Post-translational modifications are key to the immune, mineralization and bone remodeling functionalities of OPN. In wound healing, phosphorylation promotes osteoclast attachment 2-fold [71]. Macrophage synthesis T-cell cytokines for delayed

immunity was dependent on OPN phosphorylation [72]. The ability of OPN to inhibit hydroxyapatite crystal seeding and growth was lost upon dephosphorylation in *de novo* studies [73]. Similarly, preventing calcification of smooth muscle cells was proportional to the dosage and number of phosphorylation in OPN and was lost upon dephosphorylation [74]. Glycosylation affects protein conformation and stability, it reduces phosphorylation and thereby indirectly impacting cell adhesion [75]. N-linked glycosylated rat kidney OPN was not phosphorylated, and retains cell adhesion properties, signifying that cells modify OPN to their intended function [70]. O-glycosylation regulates protein phosphorylation and conformational stability of the protein [75]. Fully glycosylated OPN displayed higher cell adhesion properties [75]. OPN is extensively susceptible to fragmentation and proteolytic degradation by serine proteases, thrombin and multiple metallo-proteases (MMP). The variation in PTMs and fragmentations gives rise to isoforms of OPN with widely different reported molecular weight ranging from 70 to 44 kDa full length OPN and 40 to 20 kDa and smaller peptide fragments, and pI varying from 3 to 4.7 [59, 70, 76]. The fragments of OPN are functionally significant. The amino terminal of thrombin and MMP cleaved OPN contains RGD motif and exhibits integrin binding and cell adhesion properties independent of the full protein [77]. Notably, the fragment displayed 2-fold enhanced cell migration than the full protein [78]. The C-terminal fragment of thrombin and MMP cleavage, suppress the migration of monocyte-derived cells [79]. However, irrespective of the terminal, phosphorylated fragments of OPN retain the functionality to inhibit calcification of smooth muscle cells [74]. The

heterologous isoforms, modifications and fragments of OPN, each with distinct biological and structural properties adds to the complexity of downstream process development.

Therapeutic Properties of Osteopontin

Osteopontin can be administrated as a therapeutic for the following diseases-

Bone health and wound healing- Although OPN is not required for the initial bone development and osteogenesis, it is crucial in maintaining the bone health during remodeling [80]. During wound healing, such as in the case of fractures, osteopontin is responsible for two stages of wound healing. First, it is secreted by macrophages in response to an injury or necrosis site, where it promotes further macrophage secretion. Acting as an opsonin, it is crucial in wound debriment, clearance of bacteria and particulates [61]. Second, OPN is responsible for bone remodeling, a continuous bone regeneration process. It begins with osteoclasts that resorb old bone to expose an interface for new cells to attach. Osteoblasts secrete OPN, to bind to the old bone interface as a "cement line" and promotes adhesion of the new bone cells [61]. Mice with reduced OPN levels developed osteopetrosis, attributed to the inability of osteoclasts to adhere and resorb old bone [81].

Neuroprotection after stroke- Ischemic damage is the loss of blood supply to tissues after a stroke. Due to the reported over expression of OPN in the brain after ischemia, indicative of macrophage mediated cell repair [82], the therapeutic effect was investigated. In *in vivo* mice studies, effects of cerebral focal ischemia was induced surgically for 60 mins with oxygen and glucose starvation of neuron for 120 mins. In a dose responsive to treatments, 0.1 μg/mL OPN dose proved effective in reducing cell

death 2-fold [83]. *In vivo* studies showed 2-fold reduction in the size of infracts with OPN treatment. OPN provided the same neuro protective effect when administered 24-h before or after the ischemia induction. Similarly, OPN has been proved effective in improving cell viability after kidney ischemia. Several studies note the expression of OPN in damaged cells, that affect morphological regeneration [84, 85].

Inflammatory diseases- Osteopontin has been upregulated in several inflammatory diseases, as a result it can be a biomarker in disease prognosis. Multiple sclerosis (MS) affects the brain and nervous system by demyelinating the neurons, primarily attributed to T-cells misregulation. In animal models of MS, autoimmune encephalomyelitis (EAE), expresses increased OPN levels that enable survival of T-cells, that in turn exasperates the disease [86]. In rheumatoid arthritis, a synovial inflammatory disease leading to cartilage and bone destruction, IL-1 and TNF α are the major causative agents. OPN and thrombin cleaved OPN enable the secretion of these pro-inflammatory molecules through T-cell proliferation [87]. A similar role was observed in Crohn's disease and allergic asthma. Therefore OPN is a therapeutic drug target in the treatment of these T-cell mediated inflammatory diseases [87].

In cardiovascular disease, an inflammatory disease of the blood vessels, OPN exhibits dual roles. In the initial stages, OPN induces atherosclerosis lesions by macrophage induced inflammation [88]. As the disease progresses, vascular calcification of the tissue leads to organ failure. In mice studies, OPN deficient mice have accelerated calcification by calcium phosphate deposits. OPN as an injection or adsorption into glutaraldehyde-fixed bovine pericardial implants reduced calcification by 72-91% [89].

Phosphorylation and RGD domain played a key role in inhibition of the calcification [74, 89]. The mechanism of OPN prevention of calcification is three-fold. 1) OPN binds to crystal hydroxyapatite (Ca-Phosphate salt) and consequently prevents further deposition of minerals and avoids crystal growth, 2) Promotes macrophage cytokine secretion to dissolve mineral deposits and 3) opsonin activity with specificity towards mineral and cell adhesion [90]. This similar mechanism is also employed in preventing calcifications of the kidney as well.

Cancer cells also over express OPN, and is often considered a biomarker of tumor metastasis. In a recent review [91], all the applications of OPN as a cancer target to suppress tumors was summarized.

OPN Isolation Processes in the Literature

The various processes reported in the literature for isolation of osteopontin are summarized in Table 1.1.

Table 1.1 Reported downstream processes for isolation of osteopontin

Biological source and reference	**Unit operations in purification method**	**OPN yield**	**OPN recovery**	**Final purity**
Human milk [92]	1) DEAE-trisacryl chromatography 2) Barium citrate absorption 3) RP-HPLC separation	2 mg/300 mL milk	NM	High purity by SDS-PAGE
Bovine milk [93]	1) DEAE-sephacel chromatography 2) Phenyl sepharose chromatography with 4M NaCl 3) Phenyl sepharose chromatography with 5M NaCl	8 mg/L milk	NM	High purity by SDS-PAGE
Human milk [94]	1) DEAE-sephacel chromatography 2) Casein removal by pH and $CaCl_2$ precipitation 3) Hydroxyapatite chromatography 4) Negative affinity chromatography	2 mg/600 mL	NM	NM
Bovine acid milk whey [57]	1) DEAE-sephacel chromatography 2) POROS HQ anion-exchange chromatography	11 mg/L of acidic milk whey	0.14%	~100% by densitometry analysis of SDS-PAGE
Urine [95]	1) DEAE sepharose chromatography 2) RP-HPLC	NM	NM	NM

Table 1.1 continued

Biological source and reference	**Unit operations in purification method**	**OPN yield**	**OPN recovery**	**Final purity**
Recombinant *E. coli* [96]	1) Series of isoelectric precipitations 2) Ammonium sulfate precipitation 3) Q-sepharose anion exchange chromatography 4) S-Sepharose cation exchange chromatography	6 mg from cells grown in 3 L of LB media	12.8%	97% by HPLC-SEC
Recombinant *E. coli* [97]	1) pH 3.0 Isoelectric precipitation 2) DEAE-Sepharose chromatography flow through to remove endotoxins 3) Q-Sepharose chromatography	9.79 ± 1.27 mg	47.46% ± 2.37	100
Recombinant *E. coli* [98]	Glutathione agarose-affinity chromatography	NM	NM	NM
Recombinant *E. coli* [99]	Ni-affinity chromatography	NM	NM	NM
Sweet milk whey concentrate	1) pH 3.6-6.5 4-10mS Isoelectric precipitation 2) Anion exchange chromatography using Q-sepharose	NM	NM	100

(NM- not mentioned)

All the reported processes employ multiple often repetitive chromatography that reduce the process efficiency. The process recoveries are rarely mentioned or are below 50% at best. The new interaction chemistries and selectivity that mixed-mode resins offer could be of immense benefit to isolation of osteopontin.

1.2.2.2 Thioredoxin

Thioredoxin (Trx) is a redox protein, present in all levels of organisms ranging from prokaryotes to higher mammals. The thiol active site (C_{32}-C_{35}) is highly conserved and is responsible for preserving the intra-cellular environment in a reduced state. The mechanism is a reversible redox reaction, Trx is involved in an electron transfer from NADPH in the presence of thioredoxin reductase (TrxR). The active site is then oxidized by donating hydrogens to keep the other proteins reduced. This redox functionality is central for several cellular functions such DNA synthesis, oxidative-stress relief for regulating apoptosis to immunomodulation. Trx is a hydrogen donor to ribonucleotide reductase, facilitating DNA synthesis [100]. It prevents oxidative stress through electron donation to peroxiredoxins, which mediate reduction of H_2O_2. Trx also de-nitrosylates *S*-nitrosoglutathione to release nitric oxide for redox signaling in neutrophils [101]. In mammalian cells, Trx binds to apoptosis signal-regulating kinase 1 and directly inhibits apoptosis to relieve cellular oxidative stress [102]. Trx is an integral structural component of enzymes such as T7 DNA polymerase for phage replication and assembly in *E. coli* [103].

Trx is characterized by a 4 α-helices, 5 β-sheet motif and is found in several forms, differing in amino acid composition. Amongst bacteria such as *E. coli*, *Helicobacter pylori, Rhodobacter capsulatus,* Trx-1 with one active site is more abundant than the second isoform, Trx-2 that has 32 additional N-terminal amino acids and three dithiol active sites [104]. The two forms have identical functionalities, but the expression of Trx-2 is induced by environmental stress [105]. In higher plants and algae, 3 isoforms of Trx: m and f are expressed in the chloroplast and h in the cystol. Each of the isoforms have demonstrated enzyme binding, Trx-f has 550-fold higher affinity to fructose-1,6-bisphosphatase than Trx-m which binds better to malate dehydrogenase [106]. Hence, it can be construed that the evolutionary difference in the amino acid sequence of isoforms is tailored to the target functionality.

Human thioredoxin (hTrx) is found in two forms Trx-1, expressed in the nuclear and cytoplasmic region, and Trx-2 expressed in the mitochondria. The main difference between the two forms is in the structure and function. Trx-1 is a 11.7 kDa protein with 5 cysteines (C_{32}, C_{35}, C_{62}, C_{69} and C_{73}). C_{73} is close to the active site and is prone to oxidation, thereby leading to homodimers and loss of redox activity of proteins. Trx-2 is an 18 kDa protein with a 60 additional amino acids, once cleaved results in 12.2 kDa Trx-2. The main difference is the lack of 3 structural cysteines (C_{62}, C_{69} and C_{73}), leading to higher stability towards some oxidants [107]. Both thioredoxins have displayed redox activities, Trx-2 activity is focused towards mitochondrial reduced state, regulating reactive oxygen species (ROS) and mitochondrial apoptosis signaling pathway [108]. Both Trx are crucial for survival, Trx-1 knockout mice died in early embryonic stage,

immediately following implantation[109]. Trx-2 knockout displayed lethality in mid-embryonic stage, when oxidative phosphorylation (ROS generation) began[110]. hTrx is typically found in concentrations of 28.5 ± 12.6 ng/ml in healthy human plasma [111].

This study focuses on the properties and structure of Trx-1, a short 105 amino acid, acidic protein with a pI of 4.82. The active site C_{32}-C_{35} is present at the end of α_2 helix and protrudes from the structure enhancing accessibility [112]. More than 75% of its amino acids are involved in the 4 α-helices, 5 β-sheet secondary structure, resulting in a highly ordered and stable structure [113]. This contributes to enhanced stability at high temperatures (T_m = 85°C ,pH 7.0) and at pH 2-11.5 [114]. Although, it is not prone to proteolysis due to its conformational rigidity [115], it is cleaved by cyanogen bromide and trypsin at 32 and 73 amino acids, respectively producing fragments with lowered activity [116]. The net charge of the protein is low and the hydrophobic residues are focused towards the C-terminal [113]. hTrx is present in a 90-100% reduced state in the cells with a redox potential of -230 mV [112]. Post-translational modifications are limited to reversible nitrosylation/denitrosylation and glutationylation of C_{73} under oxidative conditions [117, 118].

Therapeutic Potential of Thioredoxin

Diseases attributed to oxidative stress, stand to benefit immensely from the reversible redox functionality of thioredoxin. Numerous *in vivo* and *in vitro* studies in animal models have identified and demonstrated the effectiveness and importance of thioredoxin in cardiovascular, neurodegenerative and inflammatory diseases. Extensive review has been published to summarize these studies on Trx as a therapeutic [119, 120].

Oxidation of proteins has been attributed to aging of tissues, Trx-1 has improved the lifespan in mice by alieving oxidative stress [121]. Cardiovascular diseases (CVD), a leading cause of mortality, are characterized by asymptomatic atherosclerosis, a condition that causes plaques and inflammation of heart tissues. Trx-1 suppresses inflammatory cytokines and down regulates ion channels, combating atherosclerosis [119]. Delivery of Trx-1 through gene therapy using an adeno virus vector has improved myocardial performance in rats by inhibiting proapoptic pathways [122].

Other inflammatory diseases such as rheumatoid arthritis, are also results of oxidative stress. Patients suffer from severe inflammation of synovial fluids due to macrophage and T-cell and cytokine influx. They secrete proteolytic enzymes resulting in cartilage and bone destruction [123]. Trx-1, inhibits protease expression by activation of the Ca^{2+} - Na^{+} ion channels [124]. Additionally, the neutrophils and macrophages release reactive oxygen species (ROS) intensifying the tissue damage through hydrogen peroxide and nitric oxide levels. Trx levels in the plasma of rheumatoid arthritis patients was 2 times higher than control group, in defense to the oxidative stress, reinforcing the vitality of Trx [125, 126].

Age-related neurodegenerative diseases such as Alzheimer's and Parkinson’s diseases are attributed to oxidative stress that causes necrosis of neurons and protein misfolding [127]. Aggregates of amyloid-β-peptide make up senile plaques causing oxidative stress on the brain tissue. Redox proteins like Trx-1 provide the first line of defense against oxidative stress, in an *in vitro* study, over expression of Trx-1 completely

protected neuron cells from amyloid-β-peptide toxicity [128], indicating a direct role of Trx-1 in preventing senile plaques.

Cystic fibrosis is a fatal genetic condition afflicted by mutation in the chloride receptor channel of mucosal membranes. Overcompensation in liquid adsorption, leads to concentration of mucosal proteins in the epithelial surface of the pancreases, intestines and lungs. Cellular secretions form a gel-like network with mucosal proteins, DNA and dead cells. The increased viscoelasticity of the bodily secretions, impair clearance, harboring infections that lead to mortality [129]. Similar to other inflammatory diseases, there exists an oxidative stress on pulmonary cells because of neutrophils secreting cytokines and ROS species. In patients, unmodulated amounts of neutrophil elastase, a serine protease is secreted, which degrades elastin, extracellular matrix proteins and up-regulates inflammatory cytokines, worsening cystic fibrosis symptoms. [130]. Trx mediates these symptoms by addressing multiple facets of the disease. Both *E. coli* and hTrx showed inhibition of elastase activity by directly disrupting the four disulfide bonds crucial for the elastase tertiary structure and activity [131]. Maximum of 60% elastase inhibition was achieved with 10 μM Trx, while chemical redox reagents such as dithiothreitol (DTT) required 8-times the concentration for the same inhibition [131]. Trx also increases the solubility of mucin glycoproteins and release liquid from sputum at 30 μM Trx [129]. The improvement to viscoelasticity of the fluid, enhances its clearance and alleviates cystic fibrosis symptoms.

Thioredoxin Isolation Processes

Thioredoxin is widely used as a solubility tag to avoid recombinant proteins accumulating in inclusion bodies. It is used in conjecture with an affinity tag such as 6x-His or glutathione S-transferase (GST), to purify the protein. Currently, there is no known affinity chromatography to isolate thioredoxin using its inherent properties.

The following processes have been reported which purify human thioredoxin from *E. coli*. They consist of multiple unit operations with repetitive steps that decrease the productivity/efficiency. The earliest report of human thioredoxin purified from *E. coli* is from Wollman et al. [132]. The biomass was homogenized at 125 MPa for 2 passes in 100 mM Tris/HCl, (pH 8.0), 5 mM benzamidine HC1, 1.0 mM EDTA, 0.25 mM DDT, and 1.0 mM sodium azide buffer. After cell debris removal by centrifugation, the conductivity was decreased by diluting the lysate 3-fold in 50 mM Tris/HCl pH 7.7. Then the lysate was loaded on DEAE-sepharose column and bound proteins eluted with a 0-500 mM NaCl gradient. Thioredoxin was present in the 200 mM NaCl elution, which was then dialyzed into 25 mM piperazine HCl (pH 5.7) buffer. A second DEAE sepharose anion exchange chromatography was employed with a 0 to 250 mM NaCl elution gradient. Thioredoxin eluted in the 125-150 mM NaCl, then it was captured and concentrated. The third chromatography step of size exclusion by Ultrogel AcA54 was performed in 100 mM Tris/HCl, 2 mM sodium azide. This process is reported to have a 40% protein recovery and high purity as observed by a SDS-PAGE. Stein et al., 1995,[133] elaborates on the process for isolating *C. reinhardtii* thioredoxin expressed in *E. coli* cells. The proteins were released in Tris-HC1 30 mM, pH 7.9 buffer by high pressure homogenization at 100

MPa for 3 passes. After removal of cell debris, the lysate was heated to 70°C for 10 mins to denature and remove the precipitated proteins. A second pretreatment of fractional salting-out was applied, the thioredoxin precipitating between 40-90% ammonium sulfate concentrations was collected. The precipitate suspended in lysis buffer was separated by gravity-flow size exclusion chromatography with Sephadex G50 resin. The fractions with thioredoxin activity were further dialyzed to remove NaCl and subjected to anion exchange chromatography on DEAE sephacel column. The bound proteins were eluted with a 0-0.4 M NaCl linear gradient to obtain purified thioredoxin. The percent recovery and purity of thioredoxin from the process was not mentioned, an SDS-PAGE image showed no host cell protein impurities. Multiple publications by the same research group describe expressing and purifying thioredoxin in different systems using this process [134, 135]. The most recent process reported is by Harris et al., 2012 [136]. The cells were disrupted in 10 mM Tris, 5 mM DTT, pH 7.4 buffer. Lysate was pretreated with ammonium sulfate precipitation and hydrophobic interaction chromatography column was used to capture the proteins at 2 M ammonium sulfate concentration. Thioredoxin eluted from hydrophobic interaction chromatography was then desalted. Intermediate anion exchange chromatography with Source Q resin was employed. A linear 500 mM NaCl gradient was used to elute thioredoxin. Further, size exclusion chromatography was performed to obtain hTrx at a high purity with <0.01% HCPs and 50% protein recovery.

In summary, the processes in place for isolating thioredoxin involve at least 1 pretreatment unit operation, followed by 3 chromatography steps. Often, these chromatography operations have low efficiency since they are repeated in succession. For

orthogonal chromatography steps, there are conditioning unit operations required in between. The maximum recovery achieved is only 50% of the initial thioredoxin. The current processes, are not scalable to efficiently produce the required kilogram quantities of hTrx required for cystic fibrosis treatment, therefore alternative processes need to be explored.

1.3 Objectives and Dissertation Organization

The objective of this study was to understand and evaluate the application of mixed-mode resins as it pertains to recombinant proteins with challenging downstream processing requirements. The impact of several factors including expression level, starting purity, expression system, post-translational modification were explored. This dissertation is organized as follows-

Chapter I provides a general introduction of the biotherapeutics market and the necessity to explore technological advancements in downstream processing of recombinant proteins. The prospects of mixed-mode resins with the current knowledge of their applicability and persistent questions are presented. This chapter further introduces the two case studies employed to understand the versatility of mixed-mode resins. Literature review and insights into the two recombinant proteins, their therapeutic applications and respective bioprocessing challenges are provided.

Chapters II, III and IV contain individual studies of mixed-mode resins and are organized similar to a scientific publication. Each chapter further provides an introduction into the details of the study, followed by the methods undertaken. The results of the each

study are presented, followed by discussion of the findings and a chapter-specific conclusion.

Chapter II entitled "Isolation of phosphorylated osteopontin from transgenic *Chlamydomonas reinhardtii* using ceramic hydroxyapatite resin" is a study on the application of mixed-mode resin ceramic hydroxyapatite, to separate phosphorylated proteins. The specific objectives of this study were to -

i. Evaluate the selectivity of CHT resin to capture phosphorylated proteins and explore its multiple interaction mechanisms to improve selectivity
ii. Study the ability of mixed-mode resins to capture recombinant proteins expressed in very low starting purity, distinguish isoforms and separate them from host cell proteins that have similar properties
iii. Recover at least 30% osteopontin by orthogonal batch chromatography at > 90% purity by employing mixed-mode resin

Chapter III, "Exploring the separation power of mixed-modal resins for purification of recombinant osteopontin from clarified *Escherichia coli* lysates", discusses osteopontin isolation in the absence of protein phosphorylation. Several mixed-mode resins were tested and compared to single mode resins for protein purification and recovery. The specific objectives were to-

i. Evaluate isolation of osteopontin and the binding conditions for several mixed-mode by high-throughput screening and batch chromatography studies
ii. Isolate osteopontin in an efficient process at 95% purity and maximum possible yield

Chapter IV “High-throughput screening of mixed-mode resins and investigation of interaction mechanism with human thioredoxin”, explores a hybrid approach to process development combining high-throughput screening and molecular modelling to optimize protein separation from HEA HyperCel resin. The specific objectives were to-

i. Evaluate the direct capture and flexibility in loading conditions offered by mixed-mode resins compared to single-mode resins
ii. Understand the underlying protein-ligand interaction mechanism and the mode of action of elution buffer components
iii. Obtain active hTrx at > 95% purity and > 50% recovery using mixed-mode resins

Finally, Chapter V summarizes the major findings and contributions of this dissertation, concluding with recommendations for future work.

CHAPTER II

ISOLATION OF PHOSPHORYLATED OSTEOPONTIN FROM TRANSGENIC *Chlamydomonas reinhardtii* USING CERAMIC HYDROXYAPATITE RESIN*

2.1 Introduction

The workhorse of complex protein production for nearly 56% of recombinant proteins is the mammalian Chinese hamster ovary (CHO) cell line [137]. The ability of mammalian cells to properly fold and perform post-translational modifications (PTMs) of proteins, out-weighs the high cultivation costs and potential viral contamination issues. *Escherichia coli* is also extensively employed to produce recombinant proteins and does so at a fraction of the CHO cost but the resultant proteins often lack proper folding, PTMs and are prone to endotoxin contamination [138]. To overcome the disadvantages of mammalian and bacterial expression, the unicellular microalga *Chlamydomonas reinhardtii* has been explored as an alternative protein production platform. Specifically, the chloroplast of *C. reinhardtii* has been utilized for the production of difficult-to-express proteins that require specific folding and PTMs to exhibit biological function [139-143].

---

*Part of this chapter is reprinted from Ravi A, Guo S, Rasala B, Tran M, Mayfield S, Nikolov ZL. Separation Options for Phosphorylated Osteopontin from Transgenic Microalgae *Chlamydomonas reinhardtii*. *International Journal of Molecular Sciences.* 2018;19(2):585. Copyright 2018, with permission from authors.

One such mammalian protein is osteopontin (OPN), also called bone sialoprotein-1 (BSP1), which is present in milk, bodily fluids and is responsible for bone development and regeneration. Other crucial functions of OPN include prevention of renal calcifications, protecting cells from apoptosis [144] and cytokine activity that differentially regulates inflammatory and immune response to allergic reactions [145]. The native mammalian form of OPN is an acidic, glycosylated sialoprotein, rich in aspartic acid, glutamic acid and serine residues [56]. Nascent bovine OPN is a ~34 kDa (~300 amino acid) protein, with an isoelectric point (pI) of 4.3, an arginine-glycine-aspartic acid (RGD) motif, a thrombin cleavage site, a polyaspartate domain and multiple calcium binding sites. In addition, twenty-eight potential phosphorylation sites and 3 glycosylation sites have been identified in the structure of OPN [58, 67]. OPN's phosphorylation apparently provides a stabilizing effect on the bond between calcium and hydroxyapatite in bones [73], regulates the interaction of OPN with integrins during signaling in CD44 mediated immune responses [72] and is vital for inhibiting vascular calcification in smooth muscle cells [74]. Therefore, to take advantage of the diverse beneficial activities of OPN, a potential recombinant protein production system should also be able to deliver optimal in vivo OPN phosphorylation.

Despite the immense potential of OPN in the healthcare industry, reports dealing with recovery, purification and commercial applications have been relatively few. Attempts at purifying OPN from tissues and bones have been confined to affinity-tag chromatography [98, 99, 146, 147], which only allows the production of limited amounts for OPN characterization and functionality assays.

Most of the methods employed to purify larger quantities of OPN, relied on generic protein properties such as hydrophobicity and ionic charge. Early reports with human milk employ weak anion exchange chromatography followed by several low capacity processing steps that resulted in low OPN yields due to losses from the multiple purification steps [92, 94]. Currently, the primary source of OPN is bovine milk whey, which is processed by two consecutive anion exchange chromatography steps or anion exchange chromatography followed by two consecutive hydrophobic interaction chromatography steps [57, 93]. Understandably, anion exchange adsorption is the default choice for capture and concentration of acidic OPN. It appears that consideration of other resin chemistries to increase process selectivity and yield warrants further investigation. The question to ask is whether the polyaspartate cluster (88–93 AA) and multiple phosphorylation sites in OPN can be exploited to achieve a more specific interaction with chromatographic adsorbents carrying transition metals and Ca^{2+} ions.

Therefore, the specific objectives of this study were (1) to assess the feasibility of chloroplast of the microalgae *C. reinhardtii* to produce phosphorylated OPN and (2) to evaluate OPN recovery and adsorption chromatography options that could take advantage of phosphorylation and/or polyaspartate sequences in the OPN structure. To evaluate the performance of algal-produced OPN, *E. coli* transformed with same OPN gene construct was used as benchmark.

2.2 Materials and Methods

2.2.1 Cultivation of Recombinant Chlamydomonas reinhardtii Strain Expressing Bovine OPN

The chloroplast genome of *C. reinhardtii* strain cc1670 was modified to express bovine OPN by California Center of Algae Biotechnology, UCSD [148]. The *psbA* gene was replaced with cDNA for bovine OPN (GenBank accession number NP_776612.1) by homologous recombination. The modified strain was rescued by re-insertion of the *psbA* gene at a different location in the genome. A 1×-FLAG epitope tag (DYKDDDDKS) was inserted at the N-terminal of OPN sequence for identification and quantification, with an enterokinase cleavage site to facilitate removal after OPN purification.

Recombinant algal cells were grown on 15% Tris-Acetate-Phosphate (TAP) agar plates at room temperature. The colonies were transferred into TAP media containing 0.1% Hutner's trace solution (*C. reinhardtii* research center) and 150 µg/mL ampicillin [149, 150]. The cells were grown in sterile conditions with constant 125 rpm shaking, 200–300 µmols $m^{-2} \cdot s^{-1}$ of cool white light at room temperature. They were harvested in mid-log phase at OD_{750} = 0.5 by centrifugation at 3500 rpm and 4 °C (Allegra 25R, Beckman Coulter, Brea, CA, USA). The wet biomass was stored at −80 °C.

2.2.2 Recombinant E. coli Strain and Cultivation

E. coli strain BL21 was modified to express bovine OPN with an *N*-terminal FLAG sequence for OPN identification and quantification similar to *C. reinhardtii* by California

Center of Algae Biotechnology, UCSD. The recombinant strain was ampicillin resistant and OPN expression was controlled by the arabinose promotor.

1 mL glycerol stock of the recombinant strain was used to grow overnight inoculum (5 mL) in Luria-Bertani (LB) media (150 µg/mL ampicillin) at 37 °C and 200 rpm. The overnight inoculum was transferred to 1 L Terrific Broth (Sigma-Aldrich, St. Louis, MO, USA, Cat # T0918) and *E. coli* cells were grown at 37 °C, 200 rpm to OD_{600} = 0.8. OPN expression was induced overnight with 0.2% (*w*/*v*) arabinose at 37 °C and 200 rpm. The wet biomass was harvested by centrifugation and stored at −80 °C.

2.2.3 Batch Adsorption Chromatography and Purification Studies

Frozen biomass was thawed to room temperature and suspended in 1 g biomass:10 mL lysis buffer (50 mM Tris, 150 mM NaCl, 1 mM EDTA, pH 7.4) containing protease and phosphatase inhibitor cocktail pills (Roche, Mannheim, Germany). Cells were lysed by sonication (15 min for *C. reinhardtii* and 5 min for *E. coli*) in 30 s on/off intervals at 4 °C using a sonicator (Sonifier 250, Branson, Danbury, CT, USA) at 30% output control and 30% duty cycle with a micro probe (1/8" micro tip A3-561 Branson, Danbury, CT, USA). Cell lysates were centrifuged (10,000× *g* for 20 min at 4 °C, Allegra 25R centrifuge, Beckman Coulter, Brea, CA, USA) and cell-free supernatants were filtered through 0.22 µm sterile polyethersulfone membrane syringe filter (30 mm diameter, Genesee Scientific, San Diego, CA, USA) and this was considered the clarified lysate for chromatography experiments. Protease and phosphatase inhibitor cocktail pills (Roche, Mannheim, Germany) in their recommended concentrations were added to all buffers used in the chromatography experiments.

FLAG-affinity chromatography- FLAG-affinity purification was used to obtain highly purified recombinant OPN for analysis. 1 mL of anti-FLAG affinity gel (Sigma-Aldrich, St. Louis, MO, USA, Cat # A4596) was equilibrated in lysis buffer for 30 CV and mixed with 5 mL of *C. reinhardtii* clarified lysate or 1 mL of *E. coli* clarified lysate. Incubation of resin and lysate was carried out for 2 h at 4 °C with continuous end-over-end mixing in a Glas-Col rotor (Glas-Col LLC, Terre Haute, IN, USA) at ~33 rpm (40% speed control). The resin was separated from the clarified lysate by centrifuging at 6000× *g* for 5 min and the resin was loaded on a Bio Spin disposable chromatography column (Bio-Rad, Hercules, CA, USA, Cat # 732-6008). Non-specifically bound proteins were removed by washing with 10 CV of 50 mM Tris, 150 mM NaCl, 1 mM EDTA, pH 7.4. Proteins bound to resin were eluted using 5 CV of 100 mM Glycine, 400 mM NaCl, pH 3.5. The pH of the eluted proteins was immediately raised to 8.0 by adding 50 µL of 1 M Tris-HCl, to avoid protein denaturation at low pH.

Ceramic hydroxyapatite chromatography- Clarified lysates were dialyzed against 5 mM sodium phosphate (NaP) pH 6.8 for 2 h at 4 °C using snake-skin membrane (3.5 kDa molecular weight cut-off, Thermo Fisher Scientific, Waltham, MA, USA, Cat #68035). The clarified lysate (2.5 mL of *C. reinhardtii* clarified lysate, 0.66 mL of *E. coli* clarified lysate) was incubated for 1 h at room temperature by end-over-end mixing with 0.5 mL of ceramic hydroxyapatite resin (Bio-Rad, Hercules, CA, USA, Cat # 1584000) pre-equilibrated in 5 mM NaP pH 6.8 and resin was loaded on a chromatography column. The resin was washed with 10 CV of 5 mM NaP pH 6.8 followed by protein elution using

a step-wise increasing concentration (100 mM, 250 mM, 500 mM, 1000 mM and 1500 mM) of NaP buffers at pH 6.8 with 5 CV of each buffer concentration.

Immobilized Metal Affinity Chromatography (IMAC)- Gallium chloride at 400 mM concentration was immobilized on Chelating Sepharose FF (GE Healthcare Life Sciences, Marlborough, MA, USA, Cat # 17-0575-01) as per manufacturer instructions and equilibrated with 50 mM MES, 500 mM NaCl pH 5.5. The *C. reinhardtii* and *E. coli* lysates were dialyzed against 50 mM MES, 500 mM NaCl pH 5.5 for 2 h at 4 °C using snake-skin membrane (3.5 kDa molecular weight cut-off). The dialyzed sample (2.5 mL of *C. reinhardtii* clarified lysate, 0.66 mL of *E. coli* clarified lysate) was incubated with 0.5 mL of Ga-IMAC resin for 1 h at room temperature and loaded on a chromatography column. The resin was washed with 10 CV of 50 mM MES, 0.5 M NaCl pH 5.5, followed by protein elution using a step-wise increasing concentration (100 mM, 250 mM, 500 mM, 1000 mM and 1500 mM) of NaP buffers with 5 CV of each buffer concentration.

Anion-exchange chromatography- The clarified lysates were dialyzed against 50 mM Tris pH 7.0 for 2 h at 4 °C using snake-skin membrane (3.5 kDa molecular weight cut-off), to bring the conductivity to 4 mS. The dialyzed samples (2.5 mL of *C. reinhardtii* clarified lysate, 0.66 mL of *E. coli* clarified lysate) were incubated for 1 h at room temperature by end-over-end mixing with 0.5 mL of Capto Q resin (GE Healthcare Life Sciences, Marlborough, MA, USA, Cat # 17-5316-10) equilibrated in 50 mM Tris pH 7.0. The resin was separated by centrifuging at 6000× *g* for 5 min and loaded on a chromatography column. The resin was washed with 10 CV of 50 mM Tris pH 7.0, followed by protein elution using a step-wise increasing concentration (100 mM, 200 mM,

300 mM, 500 mM, 1000 mM) of NaCl in 50 mM Tris pH 7.0 with 5 CV of each buffer concentration.

2.2.4 Analytical Methods

All total protein measurements were calculated using Bradford assay (Coomassie plus Assay kit, Thermo Fisher Scientific, Waltham, MA, USA, Cat #23236) on a microtiter plate format with bovine serum albumin (BSA) as standard. The absorption was measured at 595 nm using VersaMax microplate reader (Molecular Devices, San Jose, CA, USA).

Proteins in sample were visualized and quantified using SDS-PAGE under reducing conditions. Denatured protein sample was loaded on NuPAGE Novex 4-12% Bis-Tris pre-cast gradient gels (Thermo Fisher Scientific, Waltham, MA, USA, Cat # NP0335BOX). The proteins were separated by electrophoresis for 35 min at constant 200 V. All proteins were visualized by SimplyBlue SafeStain Coomassie G-250 stain (Thermo Fisher Scientific, Waltham, MA, USA, Cat # LC6065). ImageJ software (v.1.49, U. S. National Institutes of Health, Bethesda, MD, USA) was used to calculate purity of proteins in each sample lane.

Anti-FLAG western blots were prepared by transferring protein bands from SDS-PAGE gels onto a nitrocellulose membrane using iBLOT transfer kit (Thermo Fisher Scientific, Waltham, MA, USA, Cat # IB401002) for 7 min. The membrane was blocked with 2.5% non-fat milk in 0.05% TBS-T for 1 h and washed 3× with 0.05% TBS-T. The blocked membrane was then incubated with anti-FLAG M2 alkaline phosphatase conjugated antibody solution (Sigma-Aldrich, St. Louis, MO, USA, Cat # A9469) diluted

1:2000 in 0.05% TBS-T for 1 h at room temperature on a gel rocker. The antibody solution was washed 3× with 0.05% TBS-T and developed for 2 min using a solution of NBT/BCIP developer pills (Sigma-Aldrich, St. Louis, MO, USA, Cat # B5655) dissolved in 10 mL of distilled water. Standard curves with FLAG-affinity purified OPN were used to estimate OPN concentrations when necessary. ImageJ software (v.1.49, National Institutes of Health, Bethesda, Maryland, MD, USA) was used to calculate relative amounts (%) of OPN in the fractions generated during adsorption chromatography experiments, normalized by the amount of OPN in the lysate. The 45 kDa and fragments of OPN were all included in calculating the amount of OPN in each fraction. Rubisco subunits were confirmed using similar western blotting protocol. Anti-Rubisco large and small subunit polyclonal antibodies (Agrisera antibodies, Vännäs, Sweden) were used as primary antibodies (1:5000) and anti-rabbit-alkaline phosphatase (Sigma-Aldrich, St. Louis, MO, USA) as secondary antibody (1:5000).

Direct ELISA was used to determine OPN concentration in *E. coli* samples using FLAG-BAP (Sigma-Aldrich, St. Louis, MO, USA, Cat # P7582) as standards. Samples were diluted in phosphate buffer saline (PBS) and incubated overnight at 4 °C on Nunc immunosorbent 96-well plates. After 3 washes with PBS-T, blocking solution of 0.3% BSA in PBS was added to the 96-will plate and incubated for 2 h at 37 °C followed by similar wash and incubation with anti-FLAG M2 antibody conjugated with horse radish peroxidase (Sigma-Aldrich, St. Louis, MO, USA, Cat # A8592) diluted 1:5000 in PBS. TMB developer (Sigma-Aldrich, St. Louis, MO, USA, Cat # T0440) was used to develop the reaction and stopped with 2 M HCl, the absorbance was read at 450 nm.

FLAG-affinity purified OPN samples at 50 µg/mL concentration were analyzed for their pI and molecular weight using 2D gel electrophoresis performed by Protein Chemistry Lab, Texas A&M University, USA. pI resolution was performed with immobilized pH gradient technology (IPG Dry Strip, GE Healthcare Life Sciences, Marlborough, MA, USA) followed by electrophoresis on GE Healthcare Tall Mighty Small system (8 × 10 cm). The resolved gel was silver stained to visualize OPN and specificity was confirmed by anti-FLAG western blot. The pI values of OPN were estimated using the standard curve established by the IPG Dry Strip manufacturer.

Phosphostaining was performed on FLAG-affinity purified OPN samples that were de-salted and de-lipidated by chloroform-methanol precipitation [151]. SDS-PAGE was performed as above and the gel was incubated in fixing solution (50% methanol, 10% acetic acid and 40% MilliQ water) overnight at room temperature on the gel rocker. The gel was washed 3× with MilliQ water and stained with Pro-Q diamond phosphostain (Thermo Fisher Scientific, Waltham, MA, USA, Cat # MPP33301) for 90 min in the dark. Destaining solution (20% acetonitrile in 50 mM sodium acetate pH 4.0) was added 3× with 30 min incubation each and the gel was finally washed 4× with MilliQ water. Gel imaging was performed on Typhoon Trio fluorescent imaging system (GE Healthcare Life Sciences, Marlborough, MA, USA) at excitation 532 nm green and 560 nm bandpass emission filter.

2.3 Results and Discussion

2.3.1 Expression and Characterization of Recombinant Osteopontin in C. reinhardtii and E. coli

The transgenic cells of *C. reinhardtii* and *E. coli* expressing OPN were created by Mayfield's group at California Center of Algae Biotechnology, University of California San Diego (UCSD) [148] and biomass was grown at Texas A&M University. Quantification of OPN concentration in *C. reinhardtii* lysates was difficult because of the low expression levels and interference of lysate components with enzyme-linked immunosorbent assay (ELISA). In the absence of a reliable quantification method, we relied on band density analysis of western blots with ImageJ software (v.1.49, U. S. National Institutes of Health, Bethesda, MD, USA), using FLAG-affinity purified OPN as a standard. *C. reinhardtii* OPN expression levels varied between biomass batches and was on average 4× lower than OPN in *E. coli* cells, as indicated by similar band densities of 4× and 16× diluted *C. reinhardtii* and *E. coli* cell lysates, respectively (Figure 2.1, lanes 2 & 3). In terms of initial OPN concentration expressed as a percent of total soluble protein (TSP), *E. coli* lysates contained 2.9% and algal lysates between 0.1% and 0.2% OPN.

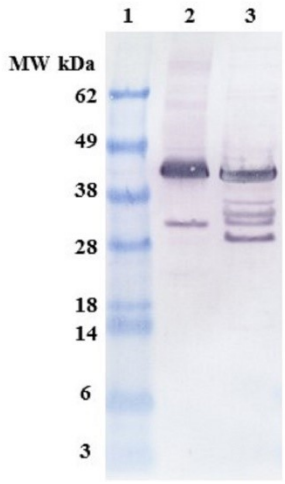

Figure 2.1 Anti-FLAG western blots showing N-terminal fragments of osteopontin (OPN). Lane 1. Molecular weight (MW) marker, lane 2. *C. reinhardtii* lysate diluted 4×, lane 3. *E. coli* lysate diluted 16×

Full-length recombinant OPN migrated to an apparent molecular weight of 45 kDa. This observation was consistent with the varied molecular weight (75–44 kDa) of OPN reported in literature and was attributed to the highly acidic nature of the protein [59, 76]. OPN expressed in the chloroplast of *C. reinhardtii* (Lane 2) consists of a major 45 kDa band and an *N*-terminal 35 kDa fragment. In addition to the 45 kDa band, *E. coli* lysate (Lane 3) contains several *N*-terminal fragments with apparent molecular weights corresponding to 40, 38, 35, 30 and 28 kDa. There were considerably fewer *N*-terminal fragments observed in algal lysates as compared to *E. coli*, suggesting that OPN is better protected from fragmentation in the chloroplast of *C. reinhardtii* than in the *E. coli* cytosol.

The FLAG-affinity-purified *E. coli* and *C. reinhardtii* OPNs were analyzed by 2D electrophoresis gel (Figure 2.2) to estimate pI of various OPN forms. The 45 kDa OPN from *C. reinhardtii* resolved in a *p*I range from pH 3.5 to pH 4.5. A similar streak of varying pI (pH ~3.5 to 4.0) was observed with the 35 kDa fragment. The observed streaks

suggest the presence of OPN isoforms that are likely due to heterogeneous post-translational phosphorylation and/or in vitro enzymatic de-phosphorylation. In contrast, *E. coli* 45 kDa OPN resolved into a spot localized at pH 4.5. The *E. coli* OPN fragments were also localized at approximately the same pH 4.5. Single spots instead of streaks of *E. coli* OPN is consistent with the expected lack of protein phosphorylation in *E. coli* [152-154]. Additional spots probably belonging to *E. coli* host protein were also detected on 2D gels.

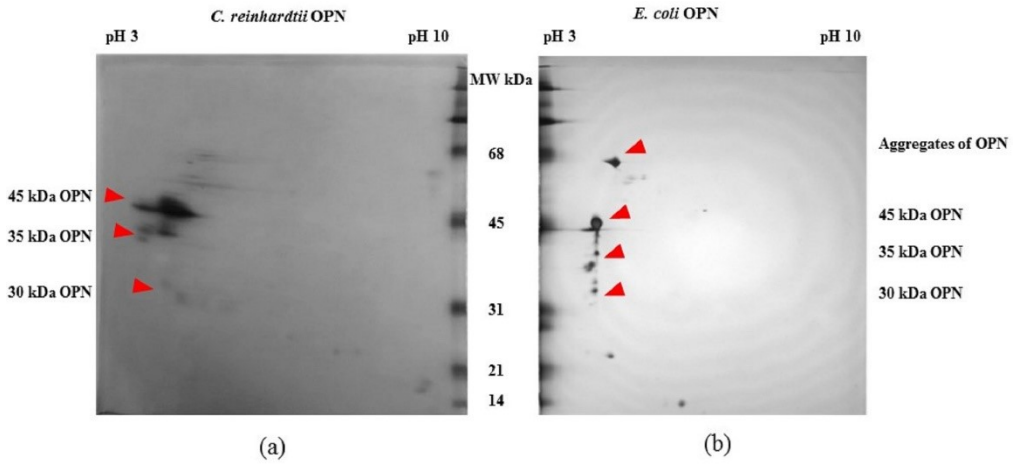

Figure 2.2 2D gel electrophoresis of OPN from transgenic (a) *C. reinhardtii* and (b) *E. coli* lysates obtained by FLAG-affinity purification

The presence or absence of phosphorylation on the recombinant OPN was detected by phosphostaining an SDS-PAGE gel (Figure 2.3). The stained band in lane 4 indicates that the FLAG-affinity purified 45 kDa OPN from *C. reinhardtii* is phosphorylated, while its counterpart from *E. coli* in lane 5 is not stained and, thus, not detectable. The phosphostained band in lane 1 belongs to 45 kDa ovalbumin, which served as a

phosphorylated protein marker. The absence of phosphostaining of the 35 kDa band may indicate little or no phosphorylation.

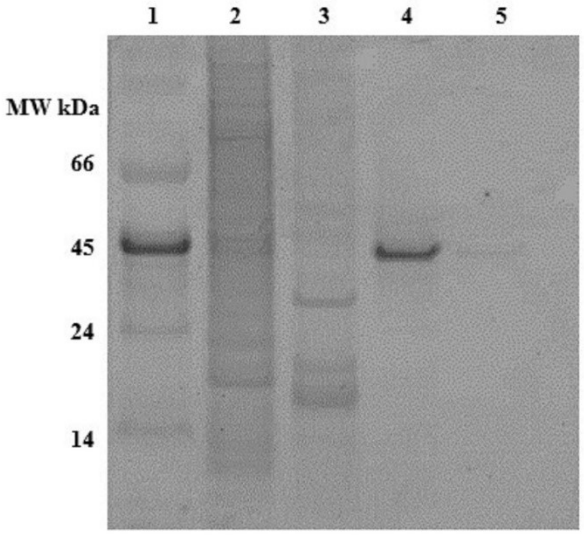

Figure 2.3 Pro-Q diamond phosphostained gel of OPN. Lane 1. MW marker, lane 2. *C. reinhardtii* lysate, lane 3. *E. coli* lysate, lane 4. Recombinant OPN purified from *C. reinhardtii*, lane 5. Recombinant OPN purified from *E. coli*. Each lane contains the same amount (~50 µg) of total soluble protein (TSP)

The detection of phosphorylated residues in algal 45 kDa OPN provided motivation to look into the specificity of algal OPN interaction with ceramic hydroxyapatite (CHT) and immobilized transition metal (Ga, Fe, Zn) resins.

2.3.2 Ceramic Hydroxyapatite Chromatography

The results from equilibrium adsorption of OPN to CHT resin from clarified *C. reinhardtii* and *E. coli* lysates are summarized in Figure 2.4.

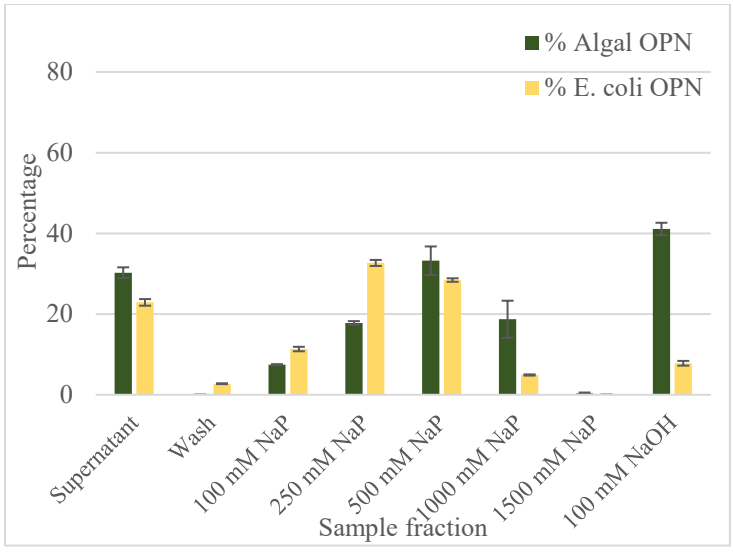

(a)

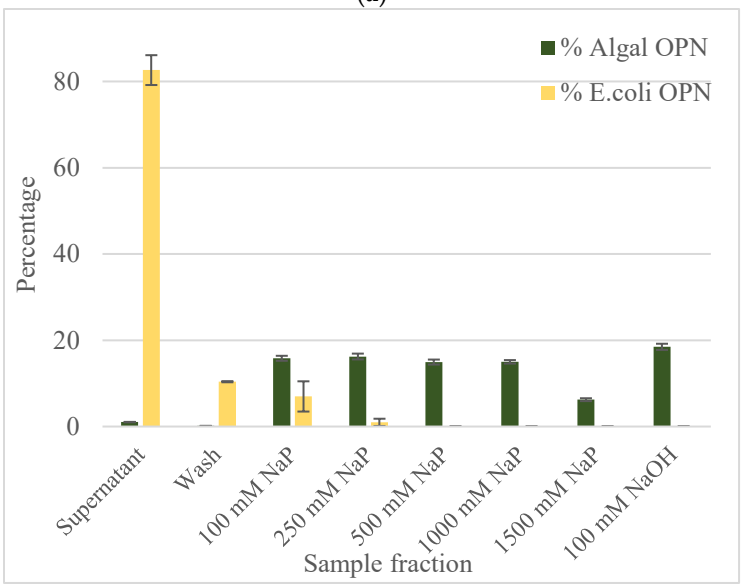

(b)

Figure 2.4 OPN distribution in fractions obtained with ceramic hydroxyapatite (CHT) resin (a) with no salt; (b) with 250 mM NaCl. Step elutions were performed with sodium phosphate (NaP) buffer, pH 6.8. Data (% OPN) were generated by ImageJ analysis of anti-FLAG western blots and normalized by the amount in the lysate. Error bars indicate standard deviation of triplicate ImageJ measurements

The adsorbed *E. coli* and *C. reinhardtii* OPN, respectively, were eluted using increasing strength (100 to 1500 mM) of NaP buffer. The bar graph in Figure 2.4a reveals that the majority (>70%) of OPN from both lysates was adsorbed to the CHT resin in the

absence of salt. The relatively low amount of *C. reinhardtii* OPN detected in the supernatant (30%) and its absence in the wash fractions indicates strong interactions between OPN and CHT. The bound *C. reinhardtii* OPN began to elute with 100 mM NaP and continued eluting through 1000 mM phosphate concentration. A significant fraction of adsorbed OPN eluted with the 250 mM (18%) and 500 mM NaP (33%) steps, respectively. Since we could not close the mass balance on OPN in the eluted fractions, even after 5 column volumes (CV) elution with 1500 mM NaP, we resorted to harsher desorption conditions using 100 mM NaOH. The strongly adsorbed OPN, estimated at 41% of initial OPN by ImageJ analysis, was completely eluted with 100 mM NaOH. Western blots (Figure 2.5b) show that the 35 kDa fraction was eluted with 100 mM NaP and that the 45 kDa form interacted even more strongly, requiring higher phosphate concertation >250 mM NaP and 100 mM NaOH for desorption.

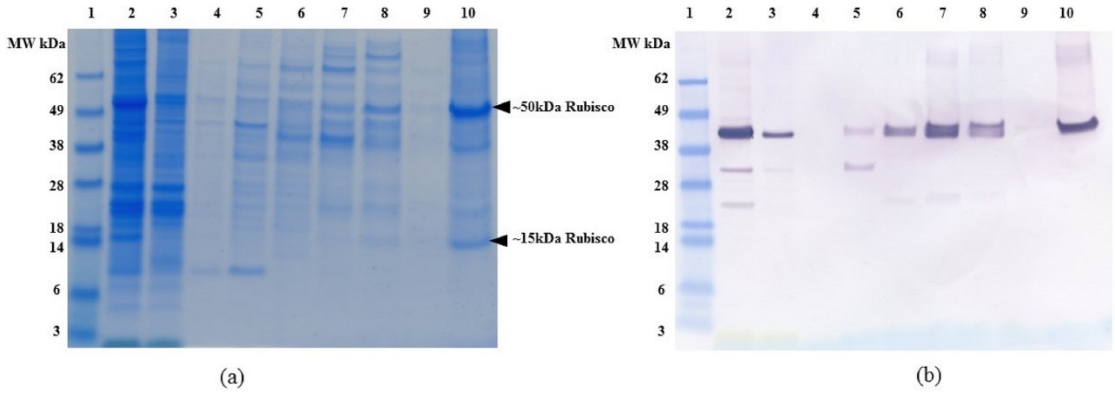

Figure 2.5 (a) SDS-PAGE and (b) Anti-FLAG western blot of *C. reinhardtii* lysate binding and elution profile from ceramic hydroxyapatite (CHT) resin without 250 mM NaCl. All samples diluted to <1 mg/mL TSP. Lane 1: MW marker, lane 2. Clarified lysate, lane 3. Supernatant, lane 4. Washes 3 column volumes (CV), lane 5. Elution with 100 mM NaP, lane 6. Elution with 250 mM NaP, lane 7. Elution with 500 mM NaP, lane 8. Elution with 1000 mM NaP, lane 9. Elution with 1500 mM NaP, lane 10. Elution with 100 mM NaOH. All elutions were performed with 5 CV of the respective buffer

As the bar graph in Figure 2.4a indicates, about 23% of *E. coli* OPN remained in the supernatant and 3% was found in the wash fractions. In contrast to *C. reinhardtii*, 72% of *E. coli* OPN eluted from hydroxyapatite resin in the 100-500 mM phosphate buffer range. As expected from the mass balance of OPN fractions eluted with the three NaP steps changes, the application of 100 mM NaOH did not yield a significant amount of OPN (only 8% of initial amount). The significant difference in the amount of 45 kDa OPN eluted with 100 mM NaP (7% algal OPN consisting of mainly 35 kDa OPN vs. 11% of *E. coli* 45 kDa OPN) and 100 mM NaOH (41% algal OPN vs. 8% *E. coli* OPN) steps indicate that *E. coli* and *C. reinhardtii* OPN interact differently with heterogeneous binding sites of CHT resin.

To determine if the different interaction strengths of OPN with CHT were due to phosphorylation i.e. phosphorylated (*C. reinhardtii*) vs. non-phosphorylated (*E. coli*)

OPN, the adsorption and elution experiments were repeated in the presence of 250 mM NaCl (Appendix Figure A1). The inclusion of 250 mM NaCl in the adsorption and elution buffers was intended to reduce ionic interactions of amino acid side chains of OPN with Ca^{2+} and PO_4^{3-} sites on the CHT without disrupting the much stronger coordinate bonding between OPN's phosphoryl groups and Ca^{2+} on CHT surface. The results shown in Figure 2.4b clearly demonstrate a difference in the adsorption of *E. coli* and *C. reinhardtii* OPN in the presence of salt. About 83% of *E. coli* OPN remains in the supernatant at the end of the adsorption period compared to the barely detectable amount (~1%) OPN in *C. reinhardtii* supernatants. An additional 10% of *E. coli* OPN was removed in the wash step while none of *C. reinhardtii* OPN was desorbed during the washing. Comparison of the data presented in Figure 2.4 demonstrates that the adsorption of *E. coli* OPN to CHT was significantly weakened by 250 mM NaCl, whereas that of *C. reinhardtii* was not. The latter, somewhat atypical behavior of increased *C. reinhardtii* OPN binding, can be explained by NaCl suppression of electrostatic repulsions between phosphoryl groups on OPN and PO_4^{3-} sites on the CHT [155]. The suppression of electrostatic repulsions, results in enhanced interactions between algal OPN's phosphoryl groups with the Ca^{2+} on CHT surface.

Therefore, *E. coli* OPN probably binds to hydroxyapatite by electrostatic interactions as depicted in Figure 2.6 below. This observation is consistent with the reported multi-modal interaction of proteins with CHT via charge interactions between acidic and basic amino acid side chains with the Ca^{2+} and PO_4^{3-} moieties on CHT, respectively, which can be reversed by increasing the ionic strength of the buffer [40].

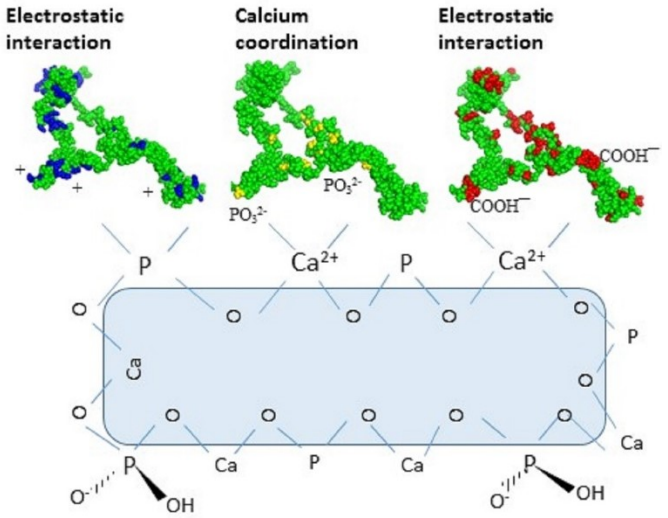

Figure 2.6 Putative multimodal interaction mechanisms of OPN with ceramic hydroxyapatite (CHT) resin at pH 6.8. Basic (arginine, histidine and lysine) amino acids of OPN are shown in blue, phosphoryl groups in yellow and acidic (aspartic and glutamic acid) in red

Based on these data, we believe that protein phosphorylation made a difference in the interaction of OPN with ceramic hydroxyapatite resin for the following reasons. First, compared to *E. coli* OPN, the addition of NaCl had a minimal or no measurable effect on *C. reinhardtii* OPN adsorption and elution from CHT (Figure 2.4). The presence of NaCl weakens *E. coli* OPN interaction with CHT as evidenced by 83% of OPN remaining unbound in supernatant and the residual 17% being desorbed during wash and first step 100 mM NaP step (Figure 2.4b). Second, the elution of *C. reinhardtii* OPN, irrespective of ionic strength, required displacement by increasing phosphate concentration and complete desorption of phosphorylated OPN by the application of 100 mM NaOH. This line of evidence suggests that *C. reinhardtii* OPN adsorption to CHT is mediated by the stronger Ca^{2+}–PO_3^{2-} coordinate binding rather than simple charge interactions. And, the unusually strong adsorption of the 45 kDa *C. reinhardtii* OPN form, which required 100

mM NaOH for elution (Figure 2.4b), is probably the result of interaction of multiple, closely positioned phosphoryl (PO_3^{2-}) groups on OPN molecule with calcium moieties (Ca^{2+}) of CHT resin.

To assess the specificity and purification capability of CHT, we compared host protein binding and elution by SDS-PAGE (Figure 2.5a). Data in Figure 2.5a indicate that a significant number of algal proteins would co-elute with OPN. The major OPN "competitor" appears to be acidic, phosphorylated chloroplast protein, Rubisco [156], as large (~50 kDa) and small subunit (~15 kDa) can be seen in 1000 mM NaP and 100 mM NaOH fractions (Figure 2.5a, lane 8 and 10 respectively). The identity of Rubisco was confirmed by western blots using anti-Rubisco large and small subunit antibodies (Appendix Figure A3). Thus, the presence of Rubisco in *C. reinhardtii* lysates would eventually reduce the resin breakthrough capacity and OPN purification fold, both of which are important factors in process scale-up. A possible solution to CHT application for OPN purification is to remove Rubisco and other interfering host protein impurities from the clarified lysates before OPN binding to CHT.

2.3.3 Gallium-Immobilized Metal Affinity Chromatography (Ga-IMAC)

Gallium, iron and zinc immobilized on Chelating Sepharose are known to bind phospho-peptides by coordinate bonds [157-159]. Gallium, having higher affinity than other metals for phosphorylated peptides [160], has been selected in this study to determine if differential interactions between Ga^{3+} and phosphorylated protein residues could be utilized for the separation of *C. reinhardtii* OPN from non-phosphorylated proteins. As before, *E. coli* OPN has been used to assess the specificity of OPN–Ga

interactions due to phosphorylation. To eliminate any ionic interactions between the protein and Ga-IMAC resin, OPN adsorption and elution was tested in the presence of 150 mM and 500 mM NaCl. Results from Ga-IMAC batch adsorption chromatography are shown in Figure 2.7. Approximately 20% of *C. reinhardtii* OPN remained unbound in the supernatant compared to only 7% of *E. coli* OPN. An additional 8% of algal OPN was removed during the resin wash step. The majority of the unbound and wash fractions contained 35 kDa form of algal OPN (Appendix Figure A2) which, as discussed above, did not bind strongly to CHT either. The adsorbed *C. reinhardtii* OPN started to elute with 100 mM NaP with 8-12% of 45 kDa OPN continuing to elute in each step elution up to 1000 mM NaP concentration. The major fraction (21%) of bound *E. coli* OPN was in the second step elution with 250 mM NaP (Figure 2.7). The remaining bound *E. coli* OPN was eluted with 500 and 1000 mM NaP.

The binding mechanism of *C. reinhardtii* OPN to Ga-IMAC apparently does not involve phosphorylated residues because non-phosphorylated *E. coli* OPN binds and elutes similarly to phosphorylated *C. reinhardtii* OPN (Figure 2.7). In addition, the similar binding and elution profiles observed with Fe-IMAC resin suggests that OPN interacts with Ga^{3+} and Fe^{3+} via the multiple carboxylic acidic containing amino acids occurring in close proximity (carboxyl clusters) present in both *E. coli* and C. *reinhardtii* OPN. Unfortunately, we could not confirm this hypothesis because adsorption at or below pH 4.5 (pKa of carboxyl groups) was not possible due to OPN precipitation at that pH range. Based on our data, it appears that protein interactions with transition metals (Ga^{3+} or Fe^{3+}) are not confined specifically to phosphorylated residues and, therefore, the application of

Ga-IMAC resin would not be useful for the separation of *C. reinhardtii* OPN from other acidic algae proteins present in the lysates.

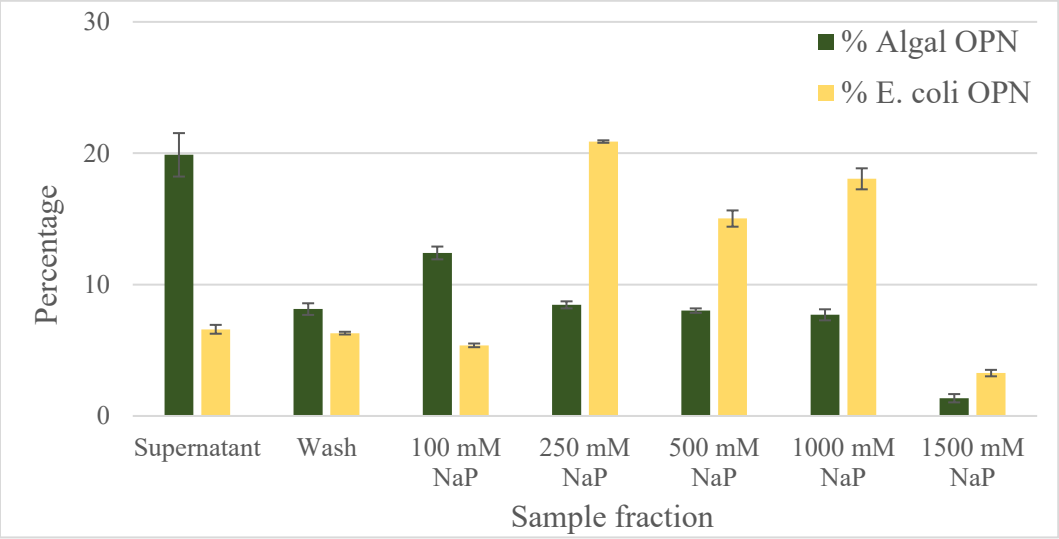

Figure 2.7 OPN distribution in fractions obtained with Ga-IMAC resin. Adsorption and elution was done in the presence of 500 mM NaCl. Step elutions were performed with sodium phosphate (NaP) buffer, pH 5.5. Data (% OPN) were generated by ImageJ analysis of anti-FLAG western blots and normalized by the amount in the lysate. Error bars indicate standard deviation of triplicate ImageJ measurements

2.3.4 Anion Exchange Chromatography

Previous studies with *E. coli* OPN have used anion exchange chromatography as one of the purification steps [96, 97]. The use of anion exchange adsorption is a natural choice for highly acidic proteins like OPN. We decided to compare the interaction of *C. reinhardtii* and *E. coli* OPN with a strong anion exchange resin (Capto Q, GE Healthcare Life Sciences, Marlborough, MA, USA). The analysis of binding and elution pools of OPN from both sources are summarized in the bar graph (Figure 2.8) and western blots

(Figure 2.9). When bound at pH 7.0 and a low conductivity of 4 mS, OPN bound strongly and specifically to the resin. No *C. reinhardtii* OPN (<1%) was detected by western blot in the supernatants and the washes (Figure 2.8). The majority of *C. reinhardtii* 35 kDa OPN fragment, which constitutes 11% total OPN was eluted with 100 mM NaCl (Figure 2.9a lane 5) suggesting weaker interaction with the quaternary amine than the intact 45 kDa form. The 45 kDa OPN from *C. reinhardtii* eluted in 200–500 mM NaCl range reaching a peak concentration in the 300 mM NaCl elution fraction. A faint band (~1.4%) was also observed with 1000 mM NaCl elution (Figure 2.9a lane 9). *E. coli* OPN also bound on anion exchange column strongly, demonstrated by the lack of a band in the supernatant and washes (Figure 2.9b lane 3 and 4). The elution of intact 45 kDa *E. coli* OPN starts earlier than algal OPN, with 16% in 100 mM NaCl elution (Figure 2.9b, lane 5) and elution continues till 500 mM NaCl with the highest concentration (37%) at 300 mM NaCl elution similar to *C. reinhardtii* OPN. The elution region for *E. coli* OPN is narrower under the same conditions with very little to no OPN over 500 mM NaCl elution. This observation corresponds to the 2D gel electrophoresis results, where *E. coli* OPN fragments were localized to spots, reflecting homogenous pI that should result in a uniform binding strength to the Capto Q resin. *C. reinhardtii* OPN had horizontal streaks on the 2D gel indicating a broader pI range of OPN due to heterogeneous phosphorylation. Hence, the elution profile of the adsorbed OPN would require a broader range of salt concentration to break the “heterogeneous” strength interactions with the resin. The ionic strength difference in the onset of 45 kDa OPN elution, 200 mM (*C. reinhardtii*) vs. 100

mM NaCl (*E. coli* OPN), probably reflects higher acidity of phosphorylated *C. reinhardtii* OPN.

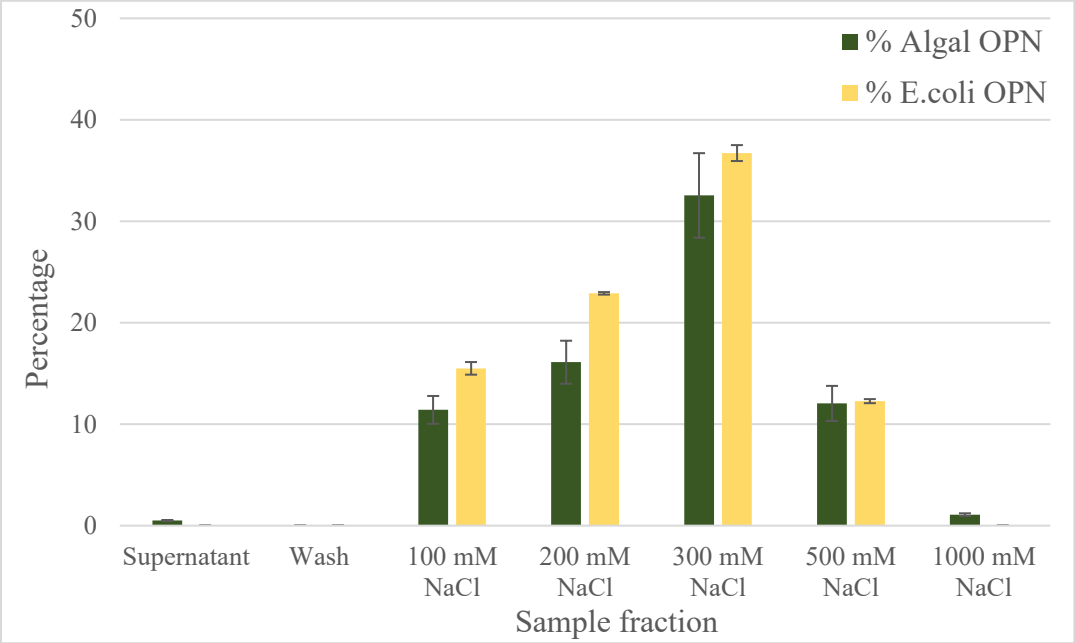

Figure 2.8 OPN distribution in fractions obtained with strong anion exchange resin (Capto Q). Step elutions were performed with sodium chloride in 50 mM Tris pH 7.0. Data (% OPN) were generated by ImageJ analysis of anti-FLAG western blots and normalized by the amount in the lysate. Error bars indicate standard deviation of triplicate ImageJ measurements

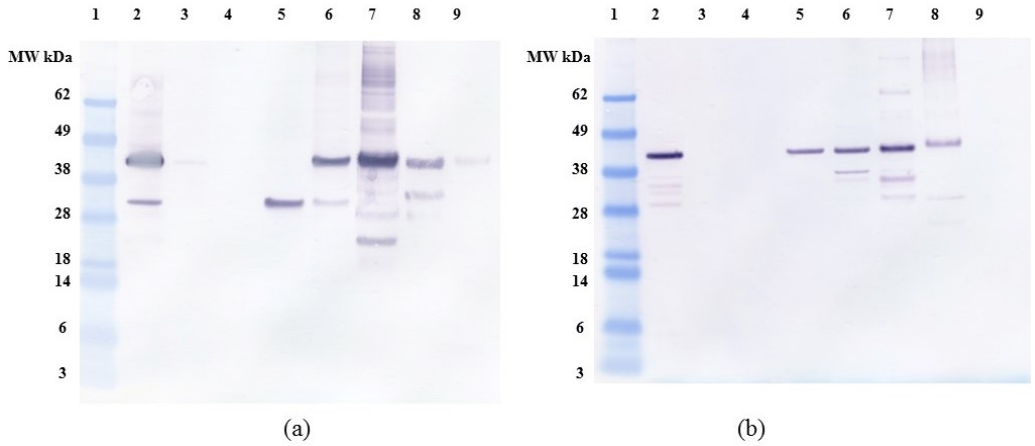

Figure 2.9 Anti-FLAG western blot of (a) *C. reinhardtii* (b) *E. coli* OPN binding and elution profile from Capto Q (strong anion exchange) resin. All samples diluted to <1 mg/mL TSP. Lane 1. MW marker, lane 2. Clarified lysate, lane 3. Supernatant, lane 4. Washes (3 CV), lane 5. Elution with 100 mM NaCl, lane 6. Elution with 200 mM NaCl, lane 7. Elution with 300 mM NaCl, lane 8. Elution with 500 mM NaCl, lane 9. Elution with 1000 mM NaCl. All elutions were performed with 5 CV of the respective buffer

SDS-PAGE (Figure 2.10) reveals that partial separation of OPN from *C. reinhardtii* host protein by anion exchange chromatography is possible. The majority (>99%) of recombinant algal OPN was adsorbed on the resin, about 49% of the host protein was present in the supernatant (lane 3) and wash fractions (lane 4) while the rest of the host protein was co-adsorbed with OPN. The majority of host protein was eluted in 100–300 mM NaCl fractions (lanes 5–7), whereas, OPN eluted in 200–500 mM NaCl fractions (lanes 6–8). Thus, by pooling 200 to 500 mM NaCl elution fractions at least forty-fold increase of OPN purity (from 0.2% to 8% TSP) and 80% recovery can be achieved by anion exchange chromatography. The anion exchange data also demonstrate that a substantial fraction of phosphorylated host protein (Rubisco), which was identified above as the major interfering host protein for OPN purification with CHT, can be partially

separated from OPN by excluding the 200 mM NaCl elution and pooling only the 300 and 500 mM fraction for further OPN isolation. In the latter case, OPN purity would increase to 20% at the expense of reduced recovery (~60%) as calculated from Figure 2.10.

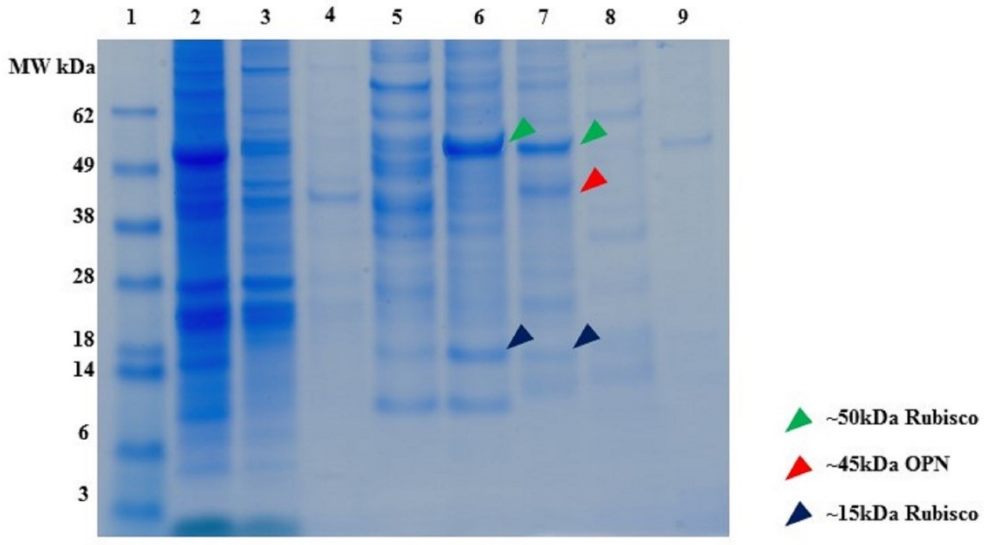

Figure 2.10 SDS-PAGE of *C. reinhardtii* lysate binding and elution profile from Capto Q (strong anion exchange) resin. All samples diluted to <1 mg/mL TSP. Lane 1. MW marker, lane 2. Clarified lysate, lane 3. Supernatant, lane 4. Washes (3 CV), lane 5. Elution with 100 mM NaCl, lane 6. Elution with 200 mM NaCl, lane 7. Elution with 300 mM NaCl, lane 8. Elution with 500 mM NaCl, lane 9. Elution with 1000 mM NaCl. All elutions were performed with 5 CV of the respective buffer

2.3.5 Two-Step Purification of OPN by Capto Q and CHT Chromatography

The proposed two-step process was tested by capturing OPN and removing *C. reinhardtii* impurity proteins using anion exchange, Capto Q resin followed by separation of phosphorylated osteopontin by mixed-mode CHT resin. Anion exchange chromatography did not completely eliminate impurity protein Rubisco, but majority of

both fragments were separated from OPN in the 200 mM NaCl. Resolving acidic host cell impurities from the OPN containing fractions, reduces the protein load on CHT chromatography and minimizes interference of acidic species with selectivity of phosphorylated proteins. Capto Q elution fractions containing OPN, 300 mM and 500 mM NaCl buffer eluates were pooled, they contained OPN at 23% purity and 63% yield (Figure 2.10). This elution pool was conditioned by dialysis and brought to the binding condition of pH 6.8 containing 250 mM NaCl. Batch chromatography with CHT resin was performed and OPN was eluted with increasing concentrations of NaP. Table 2.1 shows the distribution of OPN in the elution fractions, and the purity of each step elution. OPN was completely bound to CHT resin and 13% of OPN started eluting with 100 mM NaP buffer at 23% purity. Since this fraction purity was similar to the Capto Q elution pool purity (23%), it was not included in the CHT elution pool. Elutions fractions from 250 mM - 1000 mM NaP buffer contained 33% of OPN bound to CHT at a high purity of 75%. This was a remarkable 375-fold increase from the lysate purity of 0.2%. This increased selectivity of OPN was possible due to successful removal of interfering acidic impurities using Capto Q resin as the capture chromatography. The current recovery of 33% is not ideal, but the losses are exacerbated by the heterogeneous isoforms of OPN interacting with the ligand and eluting in a wide range of elution buffer concentration.

Table 2.1 Recovery and purity of OPN from two-step purification by Capto Q and CHT chromatography

Sample	Elution fraction	% Purity	% Recovery	% Purity of selected elution pool	% Recovery in selected elution pool
Clarified lysate		-	100		
Capto Q	300 mM–500 mM NaCl			23.5	61
CHT	100 mM NaP	22.7	13		
	250 mM NaP	68.7	13		
	500 mM NaP	58.3	12		
	1000 mM NaP	99	8	75	33%
	1500 mM NaP	-	0		
	100 mM NaOH	41.7	4		

2.4 Conclusions

Osteopontin was successfully expressed in the chloroplast of *C. reinhardtii*, a novel alternative platform for recombinant protein production, capable of performing phosphorylation as a post-translational modification. The *C. reinhardtii* strain expressed two major OPN isoforms (45 kDa and 35 kDa) with pI ranging from 3.5 to 4.5 due to heterogeneous post-translational phosphorylation.

Several chromatography resins were evaluated for isolating OPN by utilizing interactions with the phosphorylation and the unique polyaspartate sequence. Ceramic hydroxyapatite resin demonstrated affinity for acidic and phosphorylated proteins and adsorbed the phosphorylated OPN (45 kDa) isoform strongly. The adsorption and co-elution of phosphorylated host proteins like Rubisco along with *C. reinhardtii* OPN, reduced the purification efficiency of CHT resin. Since CHT could not distinguish

between major phosphorylated impurities (Rubisco) and OPN, it is not ideal for separation of phosphorylated recombinant proteins from *C. reinhardtii*.

Gallium-IMAC, did not exhibit a preferential binding of phosphorylated OPN. Both phosphorylated OPN from *C. reinhardtii* and non-phosphorylated OPN from *E. coli* appeared to have similar binding and elution behavior with Ga-IMAC. Our study suggests that Ga^{3+} interacts with multiple carboxyl groups of OPN and host proteins and has no specific preference for the phosphorylated algal OPN 45 kDa form. As such, Ga-IMAC resin does not offer any advantage over CHT as a potential purification method for phosphorylated OPN forms.

Anion exchange chromatography is a viable adsorption step for capturing OPN from both *E. coli* and *C. reinhardtii* clarified lysates. The anion exchange chromatography conducted under optimal adsorption, resin-wash and elution conditions removes as much as 50% of host protein while maintaining OPN recovery yield at 80%. Other anionic protein impurities bound to the resin can be partially separated from OPN based on their strength of charge interactions with the amine ligand resulting in a 20% pure OPN fraction.

The suggested purification process of anion exchange chromatography followed by mixed-mode CHT chromatography was performed and phosphorylated OPN at 75% purity was obtained. The process recovery was 33%, further efforts to increase the purity were not undertaken due quantification limitations that stem from poor expression titers.

Because of low accumulation levels in our current *C. reinhardtii* strain leading to low starting concentration of OPN in the clarified *C. reinhardtii* lysate (0.1–0.2% TSP),

the development of a scalable OPN purification train will probably require three or more chromatography steps.

CHAPTER III

EXPLORING THE SEPARATION POWER OF MIXED-MODAL RESINS FOR PURIFICATION OF RECOMBINANT OSTEOPONTIN FROM CLARIFIED *E. COLI* LYSATES*

3.1 Introduction

Osteopontin (OPN) is a structural protein essential for biomineralization process such as bone remodeling and kidney stone inhibition [161-164]. It is also recognized as a molecular marker for tissue disorders including cancer due to its role in cell signaling, adhesion, and migration in regular conditions and during stress responses [165, 166]. The prospective health benefit as a therapeutic as well as potential diagnostic and prognostic value have invigorated the development for an efficient and scalable downstream process.

Recombinant OPN is a single-chain polypeptide composed of about 300 amino acids and it is highly acidic with an isoelectric point of 4.3 [167]. OPN is often categorized as an Intrinsically Disordered Protein (IDP) which is biologically active in a flexible form lacking a well-defined secondary and tertiary structure [168, 169]. OPN's acidic isoelectric point, low expression level, flexible structure and the acidic nature of host cell proteins are challenges to the development of OPN purification methods that make the search for a suitable and efficient purification process vitally important.

---

*Reprinted from Guo, S., Ravi A, Mayfield S, Nikolov ZL. Exploring the separation power of mixed-modal resins for purification of recombinant osteopontin from clarified *Escherichia coli* lysates. *Biotechnology Progress*, 2018. Copyright 2018, with permission from Wiley.

Despite the lack of post-translational phosphorylation, recombinant OPN from *E. coli* has made major contributions to OPN related research as it shows biological functions such as cell adhesion enhancement, cell proliferation activities, and cell migration improvement activities [96, 99].

Various strategies have been attempted to purify OPN from recombinant *E. coli* lysates. Fusion tags such as Glutathione-S-transferase (GST) and Histidine (His) were widely applied for studying OPN biochemistry for their convenient purification by affinity chromatography [99, 147, 170]. These fusion protein methods produced micrograms of OPN for biochemical characterization without supplying data on yield and potential scalability. In general, tagged proteins are not desirable for manufacturing biotherapeutics as their removal increases regulatory burden, reduces process yield and results in higher operating cost.

Non-tag methods for OPN purification from recombinant *E. coli* as well as native sources such as milk were also reported. Anion exchange chromatography is often used as the default method for OPN purification as its low isoelectric point allows strong binding [57, 92, 94]. The recently reported purification of mouse OPN expressed in *E. coli* is probably the most relevant analog for our work [96]. The cell-free lysate was fractionated using a series of isoelectric precipitation steps (pH 6, 5, and 4.3) followed by 20% ammonium sulfate precipitation. The multiple precipitation steps increased OPN purity from 7% to 45%, but severely reduced OPN yield to 21%. A final OPN purity of 97% was achieved by processing the ammonium sulfate precipitate with anion exchange

followed by cation exchange chromatography. The overall OPN yield was a low 12.8% [96].

In our previous study focusing on microalgae-expressed OPN, we investigated the interaction of *E. coli*-expressed OPN and phosphorylated OPN from microalgae with ceramic hydroxyapatite (CHT, Bio-Rad) and strong anion exchange (Capto Q, GE Healthcare) resins [171]. Selectivity was observed when OPN bound to both resins from low-ionic strength lysates by charge interactions. At higher ionic strength (250 mM NaCl) only phosphorylated OPN bound to CHT presumably via (Ca^{2+} - PO_3^{2-}) coordinate binding. Our preliminary studies with microalgae-expression indicated that OPN suffered from stability issues when exposed to 1.5 M ammonium sulfate which was required for efficient binding by hydrophobic interaction to Phenyl Sepharose FF (high-sub, GE Healthcare).

The lack of orthogonality in reported processes and OPN's poor salt stability in our hands led us to search for more efficient and scalable OPN purification methods employing mixed-modal resins. Mixed-modal adsorbants have received attention from process developers for their wide variety of chemistries that provide unique advantages over traditional single-mode chromatography [172]. Several reports have shown the potential application of mixed-modal resins as capture chromatography step for recombinant proteins expressed in *E. coli*. A purification process using HEA HyperCel (Pall) efficiently separated recombinant human granulocyte colony stimulating factor from host cell proteins and product-related impurities, which otherwise required three traditional ion-exchange chromatography steps [20]. The salt-tolerant adsorption

properties of HEA and PPA HyperCel resins were successfully utilized to purify recombinant allergen (rBet v 1a) and achieve 9-fold purification from "physiological-like" crude extract [173]. In another example, the combined action of the same two resins was superior to affinity purification of maltose-binding fusions from *E. coli* extracts [174]. Due to complex interactions of proteins with mixed-modal ligands, the screening of a wide range of conditions is often required to comprehensively evaluate ligand-protein interaction and identify the design space for process development [26, 35, 54, 175].

In this study, we used high-throughput screening (HTS) and batch adsorption experiments to obtain a better understanding of OPN interaction with three mixed-modal resins (Capto adhere, HEA HyperCel and PPA HyperCel) and select optimal adsorption and elution conditions. The latter conditions allowed us to propose a two-step purification process that maximizes OPN recovery and purification factor.

3.2 Materials and Methods

3.2.1 E. coli Cell Cultivation and Harvest

The OPN recombinant *E. coli* strain was provided by Dr. Mayfield from University of California, San Diego. The construct was based on BL21-AI strain. The production of recombinant OPN was regulated by an arabinose inducible promotor. A FLAG fusion tag was added to the N-terminus of recombinant OPN for detection purposes. The construct contained an ampicillin resistance selective marker.

The strain was kept as frozen stock cell bank in 25% glycerol at -80°C for long term storage. To start new culture, 1 mL of frozen stock cell was inoculated in 25 mL

Miller's Luria Broth (LB medium, Miller's) (Sigma-Aldrich, L3522) with 150 μg/mL Ampicillin for plasmid selection and incubated at 37°C on an orbital shaker at 200 rpm for 5 hours as the seed culture. Five mL of the seed culture was then transferred to 1 L Terrific Broth (Sigma-Aldrich, T0918) with 50 μg/mL Ampicillin and incubated at 37°C and 200 rpm shaking until OD 600 reached 0.8. OPN protein production was induced by adding Arabinose to a final concentration of 0.2% (w/v). The cells were incubated on an orbital shaker at 37°C with 200 rpm overnight. The cells were harvested by centrifugation at 3,000 g for 10 minutes at 4°C. The harvested *E. coli* biomass was stored at -80°C until use.

3.2.2 Cell Lysis and Protein Extraction

The frozen biomass was suspended in lysis buffer (150 mM NaCl, 1 mM PMSF, 50 mM Tris, pH 7.4) at 1:10 (w/v) ratio and lysed by sonication (QSonica, Q55) at 40% amplitude of 30 seconds on/off cycle in ice bath for 5 cycles. The cell debris was removed by centrifugation at 15,000 g for 30 minutes at 4°C. The supernatant was collected and further clarified by syringe filter of 0.22 μm pore size as clarified cell lysate, which served as the starting material of the chromatography studies.

3.2.3 High-Throughput Screening (HTS) for Protein-Ligand Interaction Studies

HTS experiment was performed to study the interaction between OPN and mixed-modal ligands under different conditions. Salt concentration and pH were two factors to be tested and multiple levels of each factor were included in a full factorial design with 3 replicates. The specific conditions tested were discussed in results and discussion. The pH

of the clarified cell lysate was adjusted with 0.2 M HCl or 0.2 M NaOH and salt concentration by adding solid NaCl to the cell lysate followed by mixing end-over-end on a test tube rocker (Thermolyne speci-mix, ThermoFisher Scientific) for 15 minutes at room temperature. At the end of the mixing period, clarified lysate was centrifuged at 15,000 g for 30 minutes at 4°C to remove the precipitates.

The resin slurry (50%) was dispensed in a 96-well filter plate (3M Empore), 0.05 mL resin for each well. Storage buffer was removed by centrifugation at 300 g for 7 minutes. Resin equilibration was achieved by adding 4 column volumes (0.2 mL each well) of loading buffer of designed adsorption conditions to the sorbents respectively, mixing gently for 10 minutes and then removed by centrifugation at 300 g for 7 minutes. The equilibration process was done twice before sample application. Conditioned cell lysate was loaded to the equilibrated resins (0.2 mL of lysate for each well) and the plate was sealed. The lysate-resin mixture was incubated with gentle vortex ensuring no visual settling of the resins for 1 hour at room temperature. The unbound sample was collected for analysis by centrifugation.

3.2.4 Batch Adsorption Experiments for Resin Performance Evaluation

Mixed-modal resins used in this study were Capto adhere purchased from GE Healthcare (Marlborough, MA, USA), HEA and PPA HyperCel from Pall (Port Washington, NY, USA). The ligand structure and primary adsorption chemistry are listed in Table 3.1.

Table 3.1 List of candidate mixed-mode resins for OPN purification

Resin	Vendor	Adsorption chemistry	Ligand structure	Matrix
HEA HyperCel	Pall	Hydrophobic interaction; Electrostatic interaction	Hexylamine 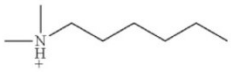	Cellulose
PPA HyperCel	Pall	Hydrophobic interaction; Electrostatic interaction	Phenylpropylamine 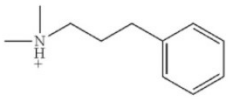	Cellulose
Capto adhere	GE	Electrostatic interaction; Hydrophobic Interaction	N-benzyl-n-methyl ethanolamine 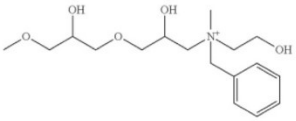	Agarose matrix with dextran surface extender

The general procedure of batch adsorption experiment was as follows: Conditioned cell lysates were incubated with pre-equilibrated resins for 1 hour with end-over-end mixing at room temperature. The loading volume was set at 6 column volumes (CV; 1.2 mL conditioned lysate load to 0.2 mL resin) for all the resins tested, equivalent to feeding about 30 mg total protein/mL resin. The lysate-resin mixture was then loaded on a PolyPrep column (Bio-Rad) and the unbound protein was collected by gravity as "Flowthrough". The resin was washed with 10 CV of loading buffer. Adsorbed proteins were eluted using 10 CV of the appropriate elution buffer. All the samples were collected by gravity for analysis. The average gravity-driven linear velocity during elution was about 100 cm/h. The specific protocols designed for individual resins are listed below.

HEA HyperCel low-salt batch adsorption and elution- HEA HyperCel low-salt binding condition was the same as the lysate condition (150 mM NaCl, 50 mM Tris, pH

7). No additional conditioning step was required. The clarified lysate was incubated with HEA HyperCel resin pre-equilibrated with binding buffer (150 mM NaCl, 50 mM Tris, pH 7) for 1 hour at room temperature. The lysate-resin mixture was then transferred into a PolyPrep Column and the flowthrough sample was collected by gravity. The resin then was washed by 20 CV binding buffer and the wash sample was also collected for further analysis. Protein elution was designed to be a 3-step process with 10 CV of each elution buffer. The first elution was achieved using 1 M NaCl, 50 mM Tris pH 7 buffer. The second elution was 1 M NaCl, 100 mM sodium acetate (NaAc) pH 5 buffer. The third elution buffer was 100mM sodium citrate buffer at pH 3 with no NaCl addition.

HEA HyperCel high-salt batch adsorption and elution- A second binding condition tested for HEA HyperCel resin was at high salt concentration. Solid NaCl was added into clarified lysate to reach a final NaCl concentration of 3 M. After 15 minutes of end-over-end mixing, the lysate was centrifuged at 15,000 g for 30 minutes to remove any precipitates. The conditioned lysate was then incubated for 1 hour at room temperature with pre-equilibrate HEA HyperCel resin by the high salt binding buffer (3 M NaCl, 50 mM Tris, pH 7). The lysate-resin mixture was then transferred into a PolyPrep Column and the flowthrough sample was collected by gravity. The wash and elution procedure following HEA high salt batch adsorption was exactly the same as HEA low salt batch adsorption.

PPA HyperCel low-salt batch adsorption and elution- The PPA low salt batch adsorption and elution experiment followed the same protocol as HEA low salt batch adsorption and elution experiment.

PPA HyperCel high-salt batch adsorption and elution- Similarly, the PPA low salt batch adsorption and elution experiment followed the same protocol as HEA high salt batch adsorption and elution experiment.

Capto adhere batch adsorption and elution- The clarified lysate was conditioned by dialysis against 50 mM Tris buffer (pH 7) overnight at 4°C for salt removal using SnakeSkin dialysis tubing (MWCO = 3.5 kDa, ThermoFisher Scientific). The conditioned lysate was incubated with Capto adhere resin for 1 hour at room temperature by end-over-end mixing. The lysate-resin mixture was then transferred to PolyPrep column (Bio-Rad) and the "flowthrough" sample was collected by gravity. The resin was washed by 20 CV of 50 mM Tris pH 7 binding buffer. Elution was designed to have 3 stages of descending pH change (pH 5, 4, and 3). All elution buffers were 0.1 M citrate-phosphate buffer with no extra salt addition.

Capto Q (strong anion exchange) batch adsorption and elution- The experiments with Capto Q were performed using the same binding conditions and lysate conditioning used with Capto adhere resin. The resin was washed by 20 CV of 50 mM Tris pH 7 binding buffer. The elution was achieved in 3 steps with 50 mM Tris pH 7 buffer containing 0.2 M NaCl, 0.5 M NaCl, and 1 M NaCl.

3.2.5 Packed-Bed Purification of OPN

Packed-bed chromatography and process optimization was performed using ÄKTA Purifier (GE Healthcare Life Sciences), and the top two resin performers, PRC HEA HyperCel and HiTrap Capto Q, were evaluated in prepacked column format. PRC HEA HyperCel (1 mL) was purchased from Pall and HiTrap Capto Q (1 mL) from GE

Healthcare. The same feed composition and load volume as used in batch adsorption experiment was used on prepacked columns to allow for verification and comparison between batch adsorption and packed-bed chromatography trials.

The general protocols for packed-bed chromatography in this research are as follows. The volumetric flow rate was controlled at 0.2 mL/min to ensure 5 minutes residence time during sample loading. The same linear velocity was used for the wash and elution steps. Protein concentration during chromatography and ionic strength of elution buffers was monitored continually by absorbance reading at 280 nm and conductivity measurement, respectively. Eluted fractions (1 mL) were collected in fraction collector (Frac-950, GE Healthcare Life Sciences) and analyzed for total protein by Bradford assay and OPN content by ELISA. The elution process was the subject to change and optimization on packed-bed chromatography.

HEA HyperCel resin performance verification on prepacked column- Clarified lysate (in 150 mM NaCl, 50 mM Tris, pH 7 condition) was loaded onto the equilibrated PRC HEA HyperCel column (1 mL) and washed with 20 CV of binding buffer. Linear NaCl gradient (0.15 to 1.5 M NaCl over 20 CV) in 50 mM Tris pH 7 was applied as the elution process. The flow rate was controlled at 0.2 mL/min to ensure a 5 minute residence time for binding, and kept constant through wash and elution steps.

Two-step purification of OPN by HEA HyperCel and Capto Q- Clarified lysate (150 mM NaCl, 50 mM Tris, pH 7 buffer) was directly loaded onto the equilibrated PRC HEA HyperCel column and washed with 20 CV of binding buffer. A single step change elution was used for OPN recovery from HEA. The elution buffer was 50 mM Tris pH 7

buffer containing 1 M NaCl. The first 8 CV of elution fraction was collected as the HEA purified pool. The partially purified OPN from HEA HyperCel elute was dialyzed against 50 mM Tris pH 7 buffer overnight at 4°C for salt removal. Dialyzed HEA eluate (conductivity < 5 mS), was loaded on HiTrap Capto Q (1 mL) as previous protocols, washed with 20 CV of the binding buffer (50 mM Tris pH 7, 4 mS). After the wash procedure, 0–1 M NaCl linear gradient elution (20 CV) was applied to Capto Q for OPN elution.

3.2.6 Analytical Methods

Bradford assay for total protein determination- Total soluble protein was determined by Bradford assay in 96-well plates with bovine serum albumin (BSA) standards (Pierce™ Coomassie Plus (Bradford) Assay Kit, ThermoFisher Scientific) [176].

ELISA (enzyme-linked immunosorbent assay) for OPN quantification- The standards were prepared from FLAG-BAP (Sigma-Aldrich P7582) diluted in PBS. The samples were diluted in PBS and detected by anti-FLAG M2 antibody conjugated with HRP (Sigma-Aldrich A8592).

SDS-PAGE and Western-blot for product quality measurement- The purified fractions were analyzed by SDS-PAGE (Invitrogen NuPAGE 4- 12% Bis-Tris Gel). The gels were stained for 3 hours (SimpleBlue^{TM} Safe Stain, Novex). For Western-blotting, the protein was transferred to PVDF membrane (Invitrogen iBlot Gel Transfer Stacks, PVDF, mini) and detected by anti-FLAG M2 antibody conjugated with alkaline phosphatase (Sigma- Aldrich A9469).

Resin performances evaluation- The OPN capture performances of candidate resins were evaluated by two major parameters—purification factor and OPN recovery. The fractions collected from batch adsorption and elution experiments were analyzed by Bradford assay for total protein concentration and ELISA for OPN concentration. The purity of clarified lysate and fractions from batch adsorption and elution experiments were calculated by the equation below.

$$Purity = \frac{OPN\ (\frac{mg}{mL})}{TP\ \left(\frac{mg}{mL}\right)} \times 100\%$$

Because Bradford assay responds differently to proteins with different amino acid compositions, it was less reliable for highly purified OPN samples where only a handful of protein species existed. Therefore, the purity of purified OPN after two-step purification was determined by analyzing the SDS-PAGE image with ImageJ software [177].

The recovery of each candidate resin was calculated by dividing the amount of OPN (mg) from the elution fraction with the majority of OPN by the amount of OPN from the conditioned cell lysate (feed).

$$Recovery = \frac{OPN\ (mg)\ in\ the\ OPN\ elution\ fraction}{OPN\ (mg)\ in\ the\ feed} \times 100$$

Purification factor of each candidate resin was defined as the ratio of purity of the elution fraction with the majority of OPN and the purity of the feed.

$$Purification\ factor = \frac{Purity\ of\ the\ OPN\ elution\ fraction}{Purity\ of\ the\ feed} \times 100\%$$

3.2.7 Statistical Analysis

Statistical analysis was performed by JMP Pro 12 software. Response surface analysis was used to generate the prediction profiles of OPN and total protein adsorption to mixed-modal sorbents in response to pH and NaCl concentration. One-way ANOVA in JMP Pro was used on data from batch adsorption experiments to test the effects of resin types on OPN recoveries and purification factors. After confirming that resin types led to significantly different purification outcomes, a Tukey-Kramer HSD analysis was performed at $\alpha = 0.05$ level to compare between resins [178, 179].

3.3 Results and Discussion

3.3.1 OPN Adsorption Studies

The acidic and hydrophobic nature of OPN prompted us to test mixed-modal resins with anion exchange and hydrophobic interaction capabilities. HEA HyperCel, PPA HyperCel and Capto adhere resins are commercially available resins having both anionic and hydrophobic properties. Plate-based HTS was used to study the interaction between proteins and ligands under varying conditions to design bind and elute processes for OPN purification. Batch adsorption experiments were used as a rapid scale-down platform for resin performance evaluation.

3.3.1.1 HEA HyperCel Adsorption Studies

HEA HyperCel has a cellulose-based matrix with hexylamine ligand (Table 3.1). This ligand has anionic (pKa ~ 8) and hydrophobic properties at neutral pH, which should provide sufficient strength for protein capture under physiological conditions[23].

To investigate the interaction between OPN and the HEA ligand, HTS experiments were conducted in the pH range from 5 to 9 and salt concentrations from 0 to 3 M NaCl. The unbound OPN and total protein (TP) after equilibrium adsorption were quantified by ELISA and Bradford assay respectively [176]. Response surface analysis and the prediction profiles of OPN and TP bound to HEA resin are shown as Figure 3.1.

The contour profile of OPN adsorption (Figure 3.1a) shows that at any particular salt concentration within the tested range, OPN adsorption increased in pH 5 to 9 range. Salt concentrations of highest interest relevant to OPN capture are the two areas in contour plot where OPN adsorption was greater than 80%. These include the segments around pH 7 and salt concentrations below 0.3 M and above 2.7 M, respectively. In the lower concentration salt range (0 - 0.3 M) the majority of OPN was apparently adsorbed primarily by electrostatic interactions and as the salt concentration increased to 1 M NaCl these interactions were substantially weakened resulting in reduced OPN adsorption by as much as 50%. In the high-salt range (NaCl concentrations > 2.7 M) where hydrophobic interactions are expected to dominate, the adsorbed OPN fraction at pH 7 increased back to 80-90% level. The impact of pH and NaCl concentration on total protein (Figure 3.1b) was minimal as the most of host cell proteins were bound at greater than 80% level across the pH range. The latter outcome was not unexpected since the proteome of *E. coli* consists of array of proteins with a wide-range of charge and hydrophobic properties. The general observation is that a higher NaCl concentration led to a greater amount of protein adsorption (Figure 3.1b).

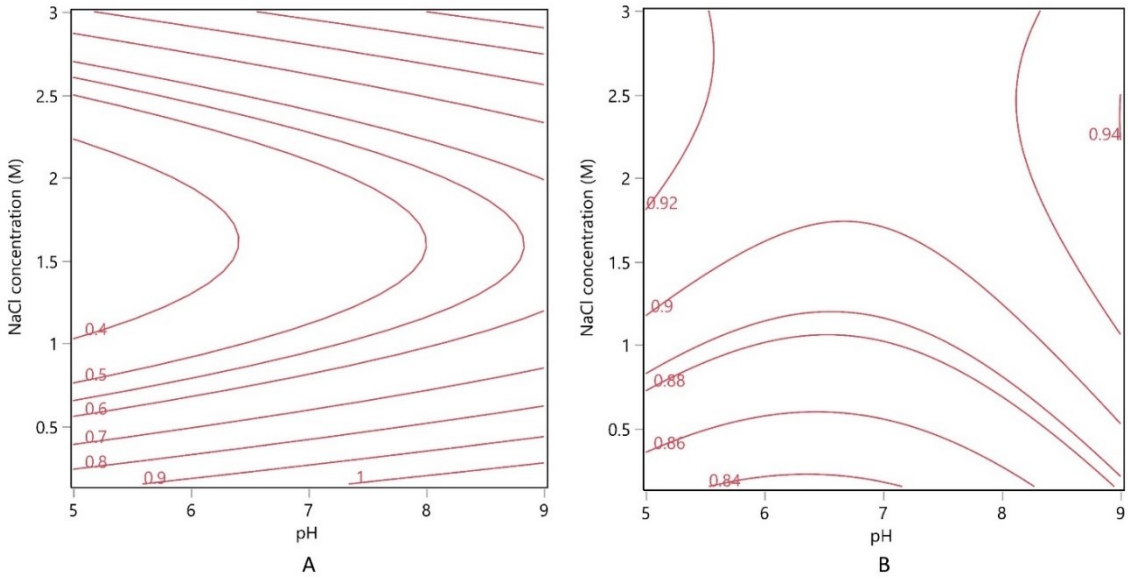

Figure 3.1 Contour profile of OPN (a) and total protein (b) bound to HEA HyperCel. Numbers on the contour grids represent the fraction of protein in the lysate that was adsorbed to HEA HyperCel

Per HTS results high-salt (3 M NaCl) and low-salt (0.15 M NaCl) adsorption conditions were selected for further investigation. For the batch adsorption under low salt condition, the clarified cell lysate was incubated directly with HEA resin for 1 hour at room temperature as described in Materials and Methods section. No resin conditioning was required as HTS results in Figure 3.1a predicted more than 90% of OPN would be bound at 150 mM NaCl, 50 mM Tris pH 7.

Based on the screening results in Figure 3.1, we designed a 3-step elution process for complete desorption of OPN using a combination of pH and salt concentration changes that gradually weakened hydrophobic and charge interactions and eventually led to electrostatic repulsion. The elution steps consisted of 1 M NaCl, 50 mM Tris buffer at pH 7, followed by 1 M NaCl, 0.1 M sodium acetate at pH 5 and 0.1 M sodium citrate at pH 3

without NaCl addition. The recovery of OPN and total soluble protein from the initial loading sample in each step are shown in Figure 3.2a.

As predicted by HTS data at pH 7, a very small amount of OPN (5%) was detected in the flowthrough fraction, whereas more than 40% of *E. coli* total protein did not bind to HEA and remained in the flowthrough. After resin washing with the binding buffer, NaCl concentration was increased to 1 M for the first elution step while keeping the pH at 7. Because the majority of bound OPN (76%) but only 6% of the bound *E. coli* protein was desorbed under those conditions, this step alone resulted in 14-fold purification of OPN. The rest of the adsorbed OPN was recovered in the subsequent elution steps.

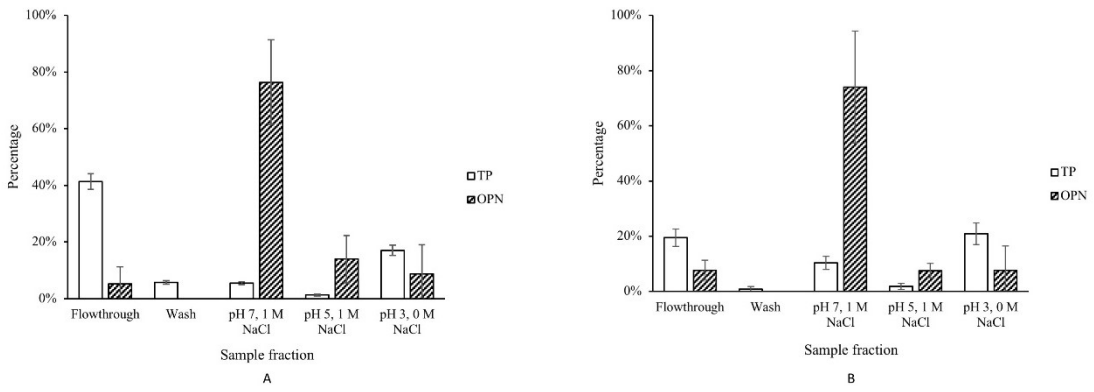

Figure 3.2 Batch adsorption and elution of OPN and *E. coli* total proteins using HEA HyperCel. (a) Low-salt adsorption: adsorption was performed from *E. coli* clarified lysate containing 150 mM NaCl at pH 7. (b) High-salt adsorption: Adsorption was performed from conditioned *E. coli* clarified lysate with 3 M NaCl in 50 mM Tris, pH7. Elution steps following for both adsorption conditions: 1 M NaCl, 50 mM Tris, pH 7; 1 M NaCl, 0.1 M sodium acetate, pH 5; 0.1 M sodium citrate pH 3 with no NaCl.

For adsorption experiments at high-salt, the resin was equilibrated with the binding buffer (3.0 M NaCl, 50 mM Tris, pH 7) and clarified lysate (pH 7) was adjusted to 3.0 M

NaCl concentration before incubation. The same elution steps and conditions as in the low salt adsorption experiments were applied (Figure 3.2b).

Under high salt conditions, hydrophobic interactions were apparently the dominating factor. More than 80% of *E. coli* proteins and 92% OPN were bound to HEA resin. After resin wash with 10 CV of binding buffer, the first elution step was done with 1 M NaCl in 50 mM Tris pH 7. The majority of OPN (74%) and 10% of total protein were desorbed in the first elution step achieving 7-fold purification of OPN in a single step. The rest of the bound OPN was recovered in the two subsequent elution steps (Figure 3.2b).

3.3.1.2 PPA HyperCel Adsorption Studies

PPA HyperCel is another mixed-modal adsorbent with phenylpropylamine ligand (Table 3.1). The same set of HTS experiments was performed with PPA as previously with the HEA HyperCel resin. The prediction contour profile of OPN amount adsorbed to the PPA HyperCel is shown in Figure 3.3a.

The adsorption behavior of total protein with PPA HyperCel (Figure 3.3b) was similar to HEA HyperCel resin reflecting the similarity of ligand structures. However, PPA HyperCel adsorbed the majority (>90%) of OPN over the whole range of pH and salt conditions. This different OPN adsorption outcome indicates that the aromatic ring in the PPA ligand had a greater impact on OPN adsorption than the aliphatic group in HEA.

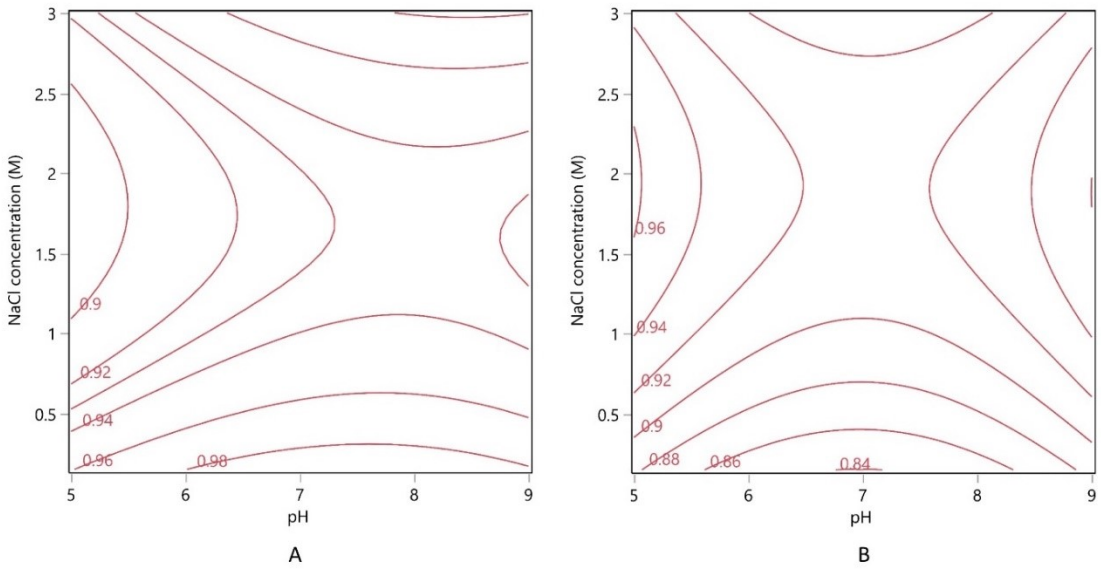

Figure 3.3 Contour profile of the proportion of OPN (a) and total protein (b) bound to PPA HyperCel. Numbers on the contour grids represent the fraction of protein in the lysate that was adsorbed to PPA HyperCel

The elution of adsorbed proteins from PPA resins was tested using the same pH and salt conditions as with HEA. As predicted by HTS, the *E. coli* proteins behaved similarly on both PPA and HEA HyperCel resins, but the OPN distribution in the eluted fractions was different (Figure 3.4a). A small fraction of OPN was recovered in the first elution step (1 M NaCl, pH 7) and almost none in the second. The majority of OPN (60%) was desorbed from PPA HyperCel at pH 3. Unfortunately, the pH 3 elution fraction also contained a significant amount of *E. coli* host cell proteins, which led to lower purification factors (3-fold purification for low-salt binding conditions and 2.5-fold for high salt binding). No significant difference in the adsorption and elution profiles of OPN and total protein was observed between low salt (Figure 3.4a) and high salt binding concentrations (Figure 3.4b).

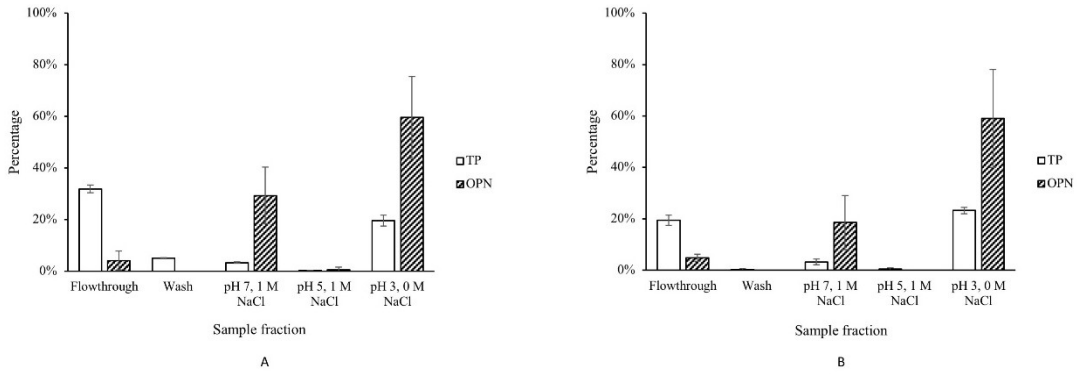

Figure 3.4 Batch adsorption and elution of OPN and *E. coli* total proteins using PPA HyperCel. (a) Low-salt adsorption: adsorption was performed from *E. coli* clarified lysate containing 150 mM NaCl at pH 7. (b) High-salt adsorption: Adsorption was performed from conditioned *E. coli* clarified lysate with 3 M NaCl in 50 mM Tris, pH7. Elution steps following for both adsorption conditions: 1 M NaCl, 50 mM Tris, pH 7; 1 M NaCl, 0.1 M sodium acetate, pH 5; 0.1 M sodium citrate pH 3 with no NaCl

3.3.1.3 Capto Adhere Adsorption Studies

Capto adhere is a strong mixed-modal anion exchange resin derivatized with N-benzyl-n-methyl ethanolamine and designed to bind proteins via electrostatic interaction, hydrogen bonding, and hydrophobic interactions. The hydrophobicity of Capto adhere ligand is reported to be reduced by the presence of multiple hydroxyl groups (Table 3.1) [54]. HTS of OPN and Capto adhere interactions (Figure 3.5) were carried out similarly to those for HEA and PPA resin screening. As shown in Figure 3.5, the NaCl concentration had a significant impact on OPN and total protein adsorption to Capto adhere. The fraction of adsorbed OPN decreased with increasing NaCl concentration, indicating that the predominant interactions between OPN and Capto adhere ligands were ionic (Figure 3.5). OPN adsorption with Capto adhere in high-salt buffer (3 M NaCl, pH 7) was also tested. Unlike HEA HyperCel, hydrophobic interactions, apparently, were not sufficiently strong

even in the presence of 3 M NaCl and more than 70% of OPN remained in the flowthrough fraction (data not shown).

Because a low conductivity condition was the only viable option for capturing OPN by Capto adhere, batch OPN adsorption experiments were preformed from dialyzed lysates (< 4 mS) at pH 7.

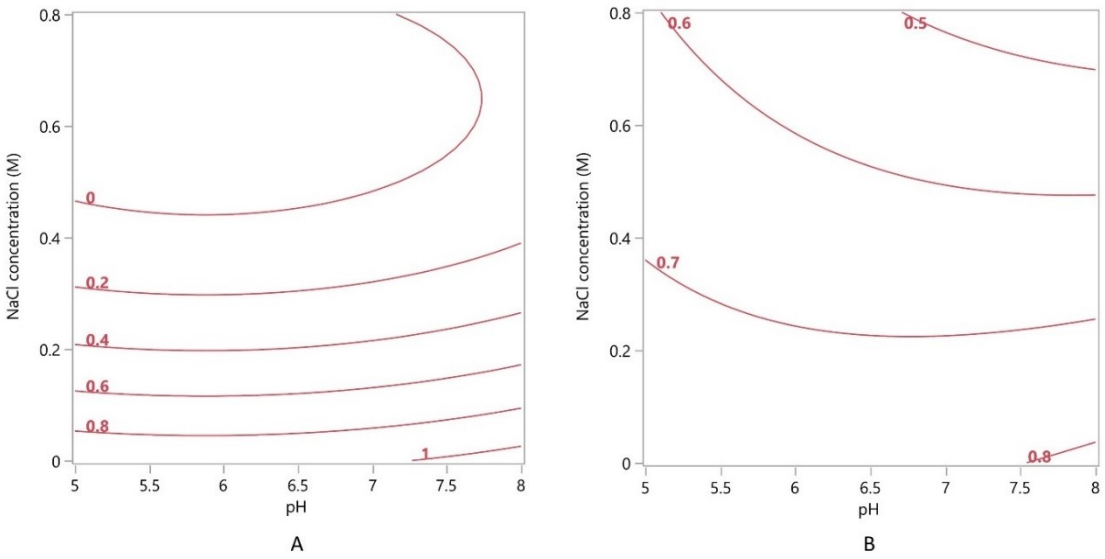

Figure 3.5 Contour profile of the proportion of OPN (a) and total protein (b) bound to Capto adhere. Numbers on the contour grids represent the fraction of protein in the lysate bound to the Capto adhere

Batch adsorption experiments were carried out using dialyzed cell lysates (pH 7). Preliminary elution data established that stepwise protein desorption with a descending pH buffer (0.1 M citrate-phosphate buffer at pH 5, 4 and 3), as suggested by the resin vendor, was optimal for the purification of OPN. Around 8% of OPN and 30% of host cell protein remained in the flowthrough (Figure 3.6a). After the wash step with the binding buffer, an additional 16% of host cell proteins were removed by pH 5 and pH 4 elution

steps with less than 2% of OPN lost at pH 4. The majority of OPN (78%) was recovered in the third elution step when the buffer pH was lowered to 3, a pH below OPN's pI. During this last stage about 17% of *E. coli* total protein co-eluted with OPN, which resulted in 4.6-fold OPN purification.

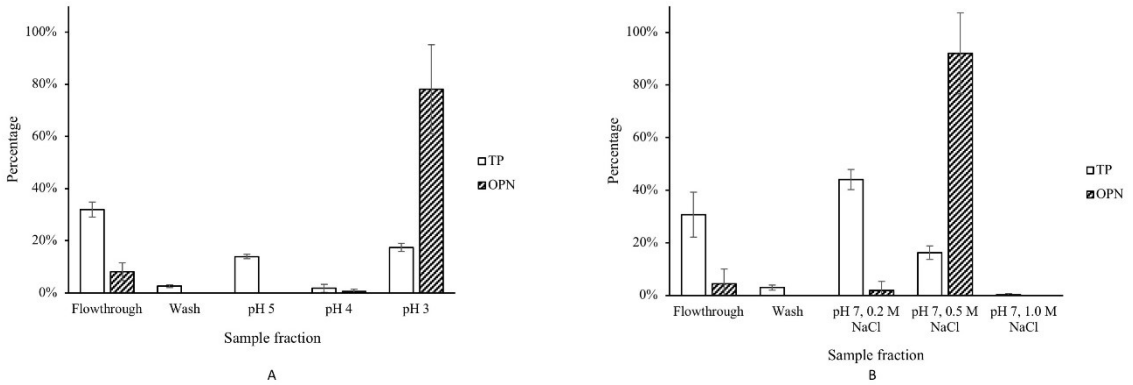

Figure 3.6 Batch adsorption and elution of OPN and *E. coli* total soluble protein with Capto adhere (a) and Capto Q (b). (a) Capto adhere adsorption: *E. coli* clarified lysate was dialyzed to remove salt before adsorption. Binding condition: pH 7, 50 mM Tris buffer. Elution steps: 0.1 M citrate-phosphate buffer pH 5, pH 4, and pH 3, respectively. (b) Capto Q Adsorption conditions: 50 mM Tris, pH 7 at < 5 mS/cm. Elution steps: 50 mM Tris, pH 7 containing 0.2 M, 0.5 M, and 1 M NaCl, respectively

3.3.1.4 Anion Exchange (Capto Q) Adsorption Studies

The strong anion exchange resin Capto Q was tested with the same batch adsorption protocols as the mixed-modal resins. Our preliminary adsorption data using clarified *E. coli* lysates indicated that OPN binds efficiently in the pH range between 6 and 8. However, significantly more *E. coli* total proteins were bound to Capto Q at pH 8 than at pH 6 and 7. Because pH 7 was the optimal condition of OPN extraction, protein adsorption to Capto Q was done from dialyzed lysate (< 5 mS/cm) at pH 7. Capto Q

adsorbed OPN effectively under those conditions. Following the washing step with binding buffer, OPN was eluted stepwise from the resin using 0.2 M, 0.5 M, and 1 M NaCl solution buffered by 50 mM Tris at pH 7. The relative total protein (TP) and OPN amounts in each fraction are plotted in Figure 3.6b. The flowthrough contained 31% of total protein and less than 5% of OPN. The first elution step (0.2 M NaCl) removed the bulk of adsorbed *E. coli* total protein (44% of the total protein in the feed) with about 2% loss of OPN. The second elution step eluted almost all of the bound OPN (92%) and residual *E. coli* proteins (16%). The elution process resulted in a six-fold increase in OPN purity (from 4% to 23%) and 92% OPN recovery.

3.3.2 Resin Performance Evaluation and Comparison

All the batch adsorption experiments were conducted in triplicate with similar loading volumes and total protein concentration (30 mg TP/mL resin). The binding and eluting conditions, purification factors, and OPN recoveries are summarized in Table 3.2 and are based on a single OPN elution fraction with the highest OPN recovery and not necessarily in the highest purification factor. OPN recoveries from the resins did not significantly differ because bind/elute process in batch adsorption experiments were designed to maximize OPN recovery in a single elution fraction. The resins in the summary table were ranked by the purification factors achieved.

One-way ANOVA test on the effect of resin type on OPN purification factor resulted in a P-value less than 0.0001, indicating that tested resins and conditions produced significantly different purification outcomes. Tukey-Kramer HSD analysis indicated that the OPN purification factor achieved using HEA HyperCel at low-salt condition was

significantly higher than the rest of the candidate resin ($\alpha = 0.05$). Besides the highest purification factor, HEA HyperCel also demonstrated a salt-tolerant protein adsorption, which allowed the direct capture of OPN from the cell lysate without additional conditioning step normally required by traditional ion exchange and hydrophobic interaction resins. The salt-tolerant adsorption feature of HEA HyperCel is important because a diafiltration or titration on crude lysate on a manufacturing scale would significantly increase processing time and potentially cause degradation. Despite the similarities to HEA HyperCel resin, PPA HyperCel and Capto adhere did not perform as well for OPN purification. The aromatic ring structure on the PPA ligand provided strong hydrophobic interaction capability with proteins which turned out not ideal for OPN purification. PPA HyperCel not only required multiple elution steps to recover OPN but did not achieve the separation HEA HyperCel did. Capto adhere, on the other hand, failed to provide the hydrophobic interaction needed for OPN capture and performed similar to traditional anion exchange resin for OPN capture and elution.

Table 3.2 A summary of OPN bind/elute conditions and respective purification factors and recoveries. Recoveries and purification factors are expressed as mean ± standard deviation

Resin	Binding Condition	OPN Elution Condition	Purification Factor	Recovery (%)
HEA HyperCel (Low-Salt)	50 mM Tris, pH 7, 0.15 M NaCl	50 mM Tris, pH 7, 1 M NaCl	14.0 ± 2.9	76.4 ± 15.0
HEA HyperCel (High-Salt)	50 mM Tris, pH 7, 3 M NaCl	50 mM Tris, pH 7, 1 M NaCl	7.1 ± 3.0	74.1 ± 20.3
Capto Q	50 mM Tris pH 7	50 mM Tris pH 7, 0.5 M NaCl	5.9 ± 0.7	92.0 ± 15.4
Capto adhere	50 mM Tris pH 7	pH 3 citrate phosphate buffer	4.6 ± 0.7	78.1 ±17.0
PPA HyperCel (Low-Salt)	50 mM Tris, pH 7, 0.15 M NaCl	0.1 M sodium citrate, pH 3	3.1 ± 0.9	59.6 ± 15.9
PPA HyperCel (High-Salt)	50 mM Tris, pH 7, 3 M NaCl	0.1 M sodium citrate, pH 3	2.5 ± 1.2	59.1 ± 19.0

3.3.3 Verification of HEA HyperCel Performance in a Packed-Bed Column

To confirm the validity of HEA resin performance, the batch adsorption and elution process was repeated in a packed-bed configuration (1 mL prepacked PRC HEA HyperCel) using the same feed composition and load volume. The ÄKTA system allowed us to investigate if additional purification of OPN could be achieved by using a linear gradient instead of stepwise elution. The A280 trace, conductivity expressed as NaCl concentration, and OPN concentration in the collected fractions determined by ELISA are plotted in the chromatogram in Figure 3.7. OPN concentration followed the same trend as

the A280 curve, which reached its peak at 1 M NaCl. Fractions (36-50 mL) spanning the concentration gradient from 0.6 M to 1.1 M NaCl contained 97% of loaded OPN, which (as expected) was substantially greater than the 76.4 % observed from the equilibrium batch adsorption. The gradient elution of OPN from packed-bed HEA column resulted in 16-fold purification, a slightly higher value than 14-fold achieved by the 1 M NaCl step (Figure 3.2a). This discrepancy can be ascribed to the loosely packed resin and the gravity driven flow, which resulted in a varying flowrate and probably some axial dispersion due to back mixing.

The attempt to translate OPN adsorption to HEA HyperCel in high-salt (3M NaCl) conditions using packed-bed column resulted in a significant pressure build-up during simple loading. In spite of the DNase treatment and clarification of the conditioned lysate by centrifugation and filtration prior to loading, the pressure exceeded the resin's maximum pressure resistance of 0.3 MPa during the sample loading at 60 cm/h (0.2 mL/min). After two attempts with newly packed-bed resin, we concluded that the pressure build-up was caused by protein precipitation on the column and decided to not proceed with the development of OPN purification under high-salt (3 M NaCl) binding conditions. In spite of observed variability, we demonstrated that batch adsorption and elution experiments in conjunction with HTS were suitable as a low-cost process development method.

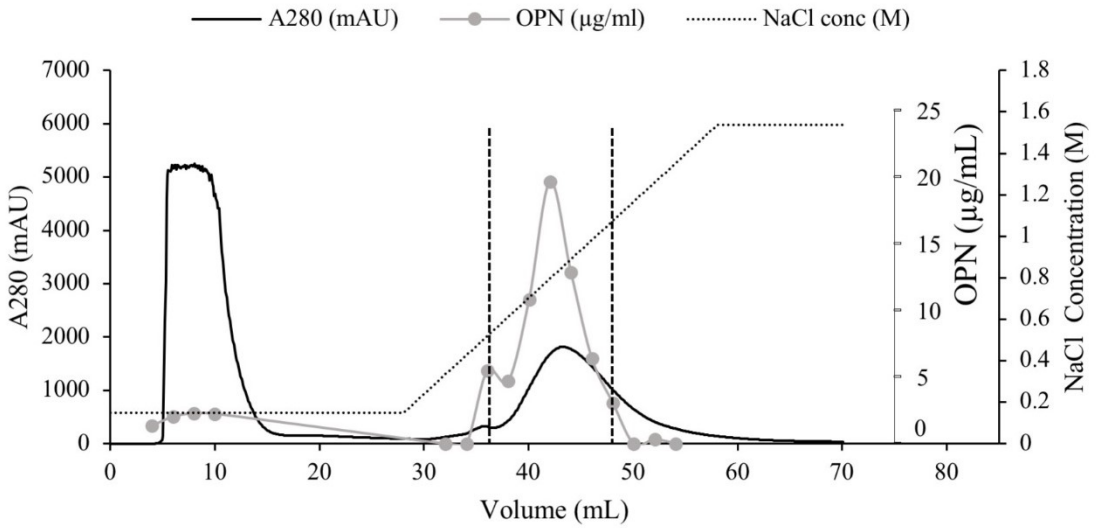

Figure 3.7 Chromatogram of HEA HyperCel low salt bind/elute operated by ÄKTA system. Clarified lysate was loaded onto the equilibrated PRC HEA HyperCel column (1 mL) at 0.2 mL/min to ensure 5 minutes residence time. The column was washed with 20 CV of binding buffer and eluted by linear NaCl gradient (0.15 to 1.5 M NaCl over 20 CV). OPN eluted in the peak around 1 M NaCl illustrated between the vertical dark broken lines. This experiment was duplicated and yielded reproducible results

3.3.4 Two-Step Purification of OPN by HEA and Capto Q Chromatography

The results in Figure 3.7 indicate that OPN should be easily eluted in a single step without affecting purification efficiency and yield. The step elution of OPN with 50 mM Tris buffer, pH 7, containing 1 M NaCl is shown in Figure 3.8.

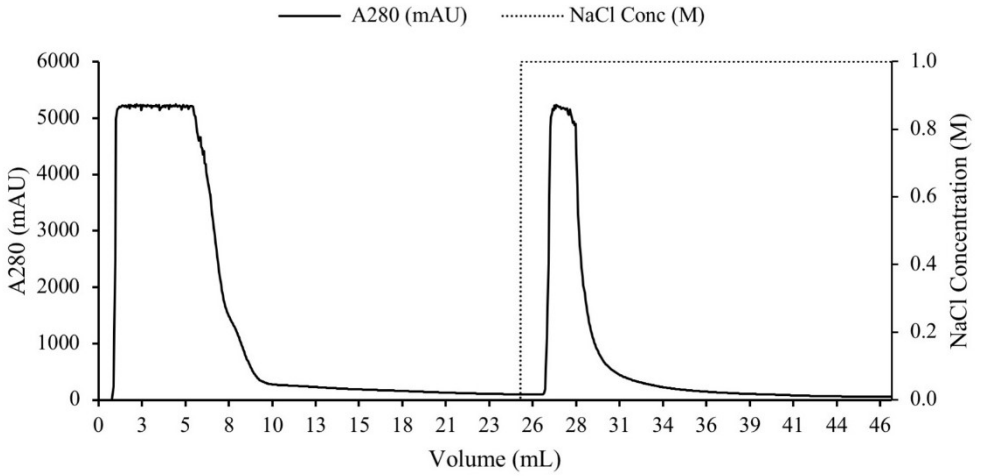

Figure 3.8 The chromatogram of OPN step elution from HEA HyperCel. Clarified lysate was loaded onto the equilibrated PRC HEA HyperCel column (1 mL) at 0.2 mL/min. The column was washed by 20CV binding buffer. Elution was achieved by 50 mM Tris buffer, pH 7, 1 M NaCl. The process was repeated twice and yielded reproducible results

The main motivation for choosing a step elution over gradient elution was to obtain a higher-protein concentration pool and reduce elution buffer volume, the latter being important at a manufacturing scale (Figure 3.8). The eluted OPN pool was loaded to HiTrap Capto Q column (1 mL) after salt removal by dialysis. A linear salt gradient (0-1.0 M NaCl) was used to achieve additional separation of OPN from *E. coli* proteins. The bound protein eluted in 3 major peaks (Figure 3.9), and OPN was recovered in the second peak (fractions 32.3 to 33.8 mL).

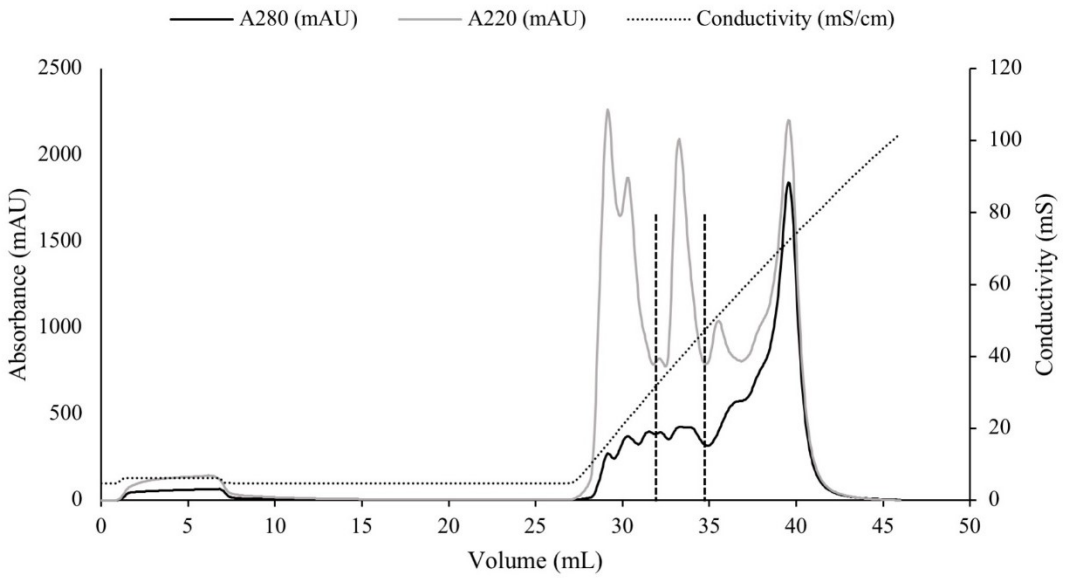

Figure 3.9 Chromatogram of OPN purification on Capto Q following the HEA HyperCel capture step. The eluted OPN pool was loaded to HiTrap Capto Q column (1 mL) at 0.2 mL/min flowrate after salt removal by dialysis. Linear ascending salt gradient (0-1.0 M NaCl) was used to further purify OPN from *E. coli* proteins. OPN eluted in the peak illustrated between the vertical dark broken lines (32.3 to 33.8 mL). The process was repeated twice and yielded reproducible results

The data of OPN purification process by HEA and Capto Q chromatography are summarized in Table 3.3 and Figure 3.10. The capture step by HEA HyperCel elevated OPN purity from 2% in the crude lysate to 29% resulting in a 15.6 purification factor. This step yielded 81% OPN recovery measured by ELISA. The subsequent dialysis of the OPN pool aimed at reducing the ionic strength to less than 5 mS/cm for optimal adsorption to Capto Q resin resulted in 61% OPN yield. The dialysis step, which was repeated several times with step-eluted OPN pools, resulted in 39 - 44% loss of OPN presumably due to OPN binding to the dialysis membrane. The latter assumption is based on the observation that the dialysis of the crude lysate under the same conditions for Capto Q adsorption

experiments (Figure 3.6b) did not result in a measurable OPN losses. Because no OPN was detected by ELISA in the dialysis buffer, we believe that low OPN concentration (67 μg/mL) in the pool of 233 μg/mL total protein was the reason for higher than expected OPN loss due to adsorption to the dialysis membrane. We expect this loss can be reduced once the process is scaled up, which would allow the use of tangential flow diafiltration. The shear force and higher membrane processing capacity enabled by tangential flow filtration on a large pool would help reduce protein adsorption to the membrane. By experimenting with key process parameters such as shear rate, protein concentration, and transmembrane pressure, an optimized tangential flow diafiltration process is expected to achieve higher yield during buffer exchange.

The second purification step, Capto Q packed-bed column, provided the necessary orthogonality to HEA and delivered additional 3-fold OPN purification at 90% recovery. Overall, the two-step purification process resulted in 44% OPN yield and 95% purity (Figure 3.10). The integration of orthogonal methods achieved OPN purification with higher purity in fewer unit operations compared to previously reported processes that relied on consecutive precipitation steps and non-orthogonal chromatography steps.

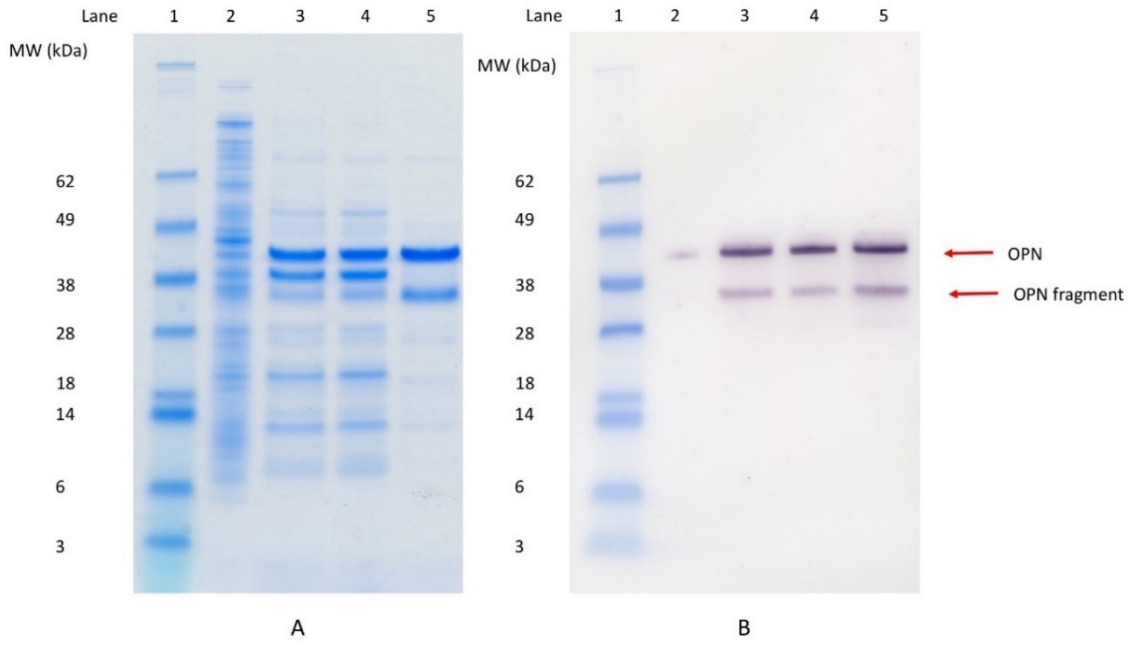

Figure 3.10 Purification of OPN by HEA and Capto Q two-step process. A: SDS-PAGE with Coomassie stain (SimpleBlue^{TM} SafeStain); B: Western-blot image. Both images are from the identical gel with the same sample loading in each lane. Lane 1: molecular weight markers; lane 2: *E. coli* clarified lysate; lane 3: Partially purified OPN fraction from HEA HyperCel elute; lane 4: Dialyzed HEA purified fraction as the feed for Capto Q chromatography; lane 5: Capto Q pool (fractions 32.3-33.8 mL). For lane 2-5, total protein loading was kept constant at 5 µg/lane

Table 3.3 Purification of OPN from *E. coli* lysate by a two-step process

Step	Volume (mL)	OPN (µg)	Purity (%)	Purification Factor	Step Recovery (%)	Overall Recovery (%)
Clarified Lysate feed	4.2	465.1	1.9	1.0	100	100
HEA HyperCel	5.6	378.2	29	15.6	81	81
Dialysis	6.0	228.8	20	0.7	61	49
Capto Q	1.50	202.8	95	3.5	89	44

3.4 Conclusion

The comprehensive investigation of three mixed-modal resins with hydrophobic and anionic characteristics revealed the effect of subtle ligand chemistries on the adsorption strength of OPN and *E. coli* proteins. The three mixed-modal resins responded to variation of pH and salt concentration in a dramatically different fashion. Capto adhere, often categorized as a mixed-modal anion exchanger, behaved as a traditional anion exchanger and required low conductivity for efficient OPN adsorption. HEA HyperCel proved to be mixed-modal resin with seemingly an optimal combination of hydrophobic interaction and anion exchanger properties for OPN purification. Protein adsorption occurred at both low-salt and high-salt concentration conditions. The hydrophobic arm of the ligand apparently helped achieving a salt-tolerant adsorption of OPN i.e. binding in the presence of 0.15 M NaCl. Interestingly, when the salt concentration in the adsorption buffer was greater than 2.7 M NaCl, the hydrophobic interactions became the dominating mechanism that resulted in greater adsorption of OPN. However, high-salt binding conditions were not conducive to OPN capture from clarified lysates using a packed-bed column because of pressure buildup. PPA HyperCel resin, a close sibling of HEA HyperCel, performed less efficiently as the aromatic ring on PPA ligand turned out to be too hydrophobic and OPN could not be easily eluted from PPA.

Different interaction chemistries of HEA HyperCel and Capto Q allowed the development of an orthogonal purification of OPN. The two-step process consisting of HEA followed by Capto Q achieved increase in OPN purity from 2% in the lysate to 95% in the Capto Q pool. The 44% overall yield is substantially higher than reported processes

and is achieved with fewer steps. The overall yield can be further improved when the process is optimized on a larger scale. The process described in this study took advantage of the salt-tolerant property of mixed-modal resin HEA HyperCel, which eliminated the need for dialysis/diafiltration of *E. coli* lysate before the capture chromatography step. This can be particularly beneficial when the process reaches large scale manufacturing in the future.

CHAPTER IV

HIGH-THROUGHPUT SCREENING OF MIXED-MODE RESINS AND INVESTIGATION OF INTERACTION MECHANISM WITH HUMAN THIOREDOXIN

4.1 Introduction

Protein isolation has traditionally used multiple chromatography operations in tandem, each selective to/targeting one property of the protein at a time. A class of chromatography resins that interact with multiple facets of the protein chemistry called mixed-mode resins is rapidly expanding. Their popularity is due to the unique selectivity that arises from combining interaction chemistries [172]. Enhanced selectivity, achieves the desired purification with reduced number of chromatography operation, avoiding the cost and product loss associated with additional unit operations, thereby improving process efficiency [23]. Mixed-mode resins provide protein binding in a range of salt-independent physiological conditions, eliminating the need for pretreatment or conditioning [33, 172]. They also have high binding capacity even in the salt-tolerant binding conditions [180, 181].

Several studies have shown potential for integrating mixed-mode resins as a part of the mAb purification platform, either as polishing chromatography or in some cases an alternative to Protein A affinity chromatography [24, 50]. The ability to separate mAb aggregates or fragments from monomers, improves the process efficiency and is a testament to the enhanced selectivity of mixed-mode resins [24, 182, 183]. Diverse biomolecules have been separated by mixed-mode resins including proteins, nucleic acids

and bio-polymers, demonstrating their versatile applications [23, 184]. The mechanism of interaction between the protein and ligand are complex, with multiple interaction mechanisms acting simultaneously often resulting in low protein recovery. To that end, additives to the elution buffer called modifiers have been investigated, for targeted reduction of each interacting mechanism. Murine antibodies bound to Capto MMC resin required a combination of 0.3 M arginine and 0.3 M NaCl in the elution buffer for > 80% recovery of mAb [185]. Fundamental understanding of the interaction mechanisms is vital for designing optimal adsorption and selective elution to successfully recover the target protein [54].

This study was designed to demonstrate the importance of understanding the interaction mechanism involved in adsorption and elution of a recombinant human thioredoxin (hTrx) from mixed-mode resins. Human thioredoxin-1, is a small 12 kDa protein, ubiquitous to all organisms. It has a redox active site responsible for maintaining a reduced cellular environment. hTrx has a highly ordered and conserved 4 α-helices, 5 β-sheet secondary structure resulting in thermal and pH stability. It is an acidic protein with a theoretical pI of 4.8 but has low net charge of -6.8 at pH 8, and hydrophathicity index of (- 0.096). Currently investigated applications include reducing the mucin network to alleviate symptoms of cystic fibrosis. Large dosage of 1.5 to 150 mmol/ kg of patient, translating to ~65 g per patient per year, would be needed for administering hTrx by aerosol inhalation [186]. Thus, a scalable and high yield process is required to deliver hTrx at a reasonable cost.

The processes used for purification and scale up of hTrx from *E. coli* have historically been tedious because it lacks distinctive ionic or hydrophobic surface properties to allow its efficient capture and purification. In previous reports, purification of hTrx starts with a pretreatment step, ammonium sulfate fractional precipitation or heat precipitation [133, 136]. The capture chromatography is either hydrophobic interaction chromatography or diafiltration followed by ion exchange chromatography. Elution is further purified by additional chromatography that are orthogonal and require a conditioning unit operation like diafiltration, or use the same capture chromatography, which is repetitive and decreases the efficiency of separation. Finally, all reported processes invariably use size-exclusion chromatography to obtain a purified 12 kDa hTrx [132, 133, 136]. The recovery of such a multi-chromatography operation is 40 - 50%. The enhanced selectivity offered by mixed-mode resins could be beneficial in improving the downstream processing efficiency of hTrx.

In this study, custom Prometic ligand library and commercial mixed-mode resins: Capto adhere, HEA HyperCel, Toyopearl NH_2-750F were tested. The total protein and hTrx binding were screened using high-throughput screening on a 96-well filter plate. The chromatography resin that showed most potential was selected for the capture of human thioredoxin directly from the *E. coli* cell lysate. The mechanism of interaction was studied by experimentally varying the binding and elution conditions. Several elution buffer modifiers were tested to disrupt the protein-ligand interactions and target specific modes of interaction. To explain experimental data and gain further insight into the interaction

mechanism between hTrx and mixed-mode ligand, molecular dynamics simulations using Desmond Schrödinger was employed.

The objectives of this study were to-

1. Demonstrate the versatility and separation efficiency of mixed-mode resins compared to single-mode reins
2. Explore the available interaction mechanisms on the mixed-mode resin experimentally and by molecular modelling
3. Optimize the binding and elution conditions by high-throughput screening to maximize thioredoxin recovery and purity

4.2 Materials and Methods

4.2.1 Recombinant Strain and Biomass

Recombinant *E. coli* BL-21 with a human thioredoxin-1 (accession number P10599) insert was provided by OrPro Therapeutics, Inc., California. Protein expression was controlled by a rhamnose inducible promoter and kanamycin selective marker.

E. coli cells were grown in LB media in a 4L New Brunswick bioreactor at National Center for Therapeutics Manufacturing, Texas A&M University. Cells were grown at 37°C for 5 h, then induced with 5 mM rhamnose at 32°C for 6 h, with pH and dissolved oxygen set at 7.0 and 40% respectively. The biomass accumulated was harvested by centrifugation 15,900xg for 15 min, stored at -80°C and used for experiments as required.

4.2.2 Lysate Preparation

Cells lysis was performed at 1g biomass in 10 mL buffer ratio. Cells were disrupted by sonication (QSonica, US) on ice at 40% amplitude, 30s on/off cycle for 5 min. The cell debris was removed by centrifugation at 10,000xg for 30 min at 4°C and the supernatant was sterile filtered to prepare the clarified lysate.

4.2.3 Lysis Buffer Optimization

The buffer pH and conductivity for cell lysis was optimized based on maximum hTrx recovery and starting purity. Triplicates of clarified lysate were prepared in different lysis buffer conditions (50 mM sodium citrate, 5 mM DTT pH 3.0; 50 mM sodium acetate, 5 mM DTT pH 5.0 and 50 mM Tris, 5 mM DTT pH 7.0) each with and without 500 mM NaCl. The optimized lysis buffer was then used to prepare the clarified lysate, which was the starting material for the rest of the experiments.

4.2.4 Selection of Capture Chromatography

Single-mode (Capto Q, Phenyl sepharose) and mixed-mode resins (Prometic ligand library, Capto adhere, HEA HyperCel, Toyopearl NH_2-750F) were purchased or donated from the manufacturers (Table 4.1). To select the ideal resin for capture chromatography, hTrx and host cell protein (HCP) binding were tested at different pH and conductivity (2 to 10 mS) conditions, using a high-throughput screening in a 96-well filter plate (Empore, 3M, US). Each well contained 50 µL of resin volume (CV) equilibrated to respective binding pH and conductivity, and incubated with 250 µL (5 CV) of clarified lysate at the corresponding binding pH and conductivity. Each binding condition was

performed in triplicate. Incubation was performed for 30 min by vortexing at room temperature. The filtrates from each well, that will be referred to as flow through were collected by centrifugation at 3000xg for 2 min or by applying vacuum. The collected flow through samples were analyzed for hTrx by ELISA and HCP by Bradford assay. To compare the adsorption preference of individual resins for hTrx relative to HCP, a relative binding ratio (k) defined as the ratio of % bound hTrx to % bound HCP was calculated for each pair of tested (pH and conductivity) conditions.

4.2.5 Optimization of Elution Conditions

The best performing resin and binding conditions was selected for elution optimization. Elution buffers 10 CV were tested by high-throughput screening on a 96-well filter plate as described above. Buffers containing arginine HCl, guanidine HCl and lysine HCl were also screened at varying concentrations of 0.1 – 0.5 M. The optimal elution buffer was selected based on maximum hTrx recovery and purity of the elution fraction.

4.2.6 Packed-Bed Chromatography

Twenty mL of the clarified lysate at optimized binding condition was loaded on 1 mL HEA PRC column attached to ÄKTA Purifier 10 at 0.25 mL/min. The column was washed with 10 CV of lysis at 0.5 mL/min. Bound proteins were eluted with a gradient of optimized elution buffer over 20 CV at 0.5 mL/min. Two mL fractions were collected and analyzed for hTrx recovery, purity and size distribution.

Table 4.1 Properties of the chromatography resins tested

Resin	**Manufacturer**	**Ligand**	**pKa**	**Types of interactions possible**	**Bead**
Capto Q	GE Healthcare Life Sciences	Quaternary amine $-N^+(CH_3)_3$ 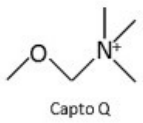 [182]	>10	Electrostatic interaction	7%cross-linked agarose
Phenyl sepharose	GE Healthcare Life Sciences	Phenyl 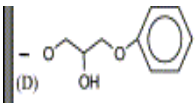 [187]	-	Hydrophobic interaction	6% cross-linked agarose
Capto adhere	GE Healthcare Life Sciences	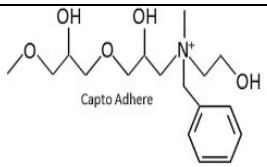 [182]	>11	Electrostatic interaction, hydrophobic interaction, hydrogen bonding	Highly cross-linked agarose
HEA HyperCel	Pall Life Sciences	$-\overset{+}{N}H\text{-}CH_2\text{-}(CH_2)_4\text{-}CH_3$ [182]	8	Electrostatic interaction, hydrophobic interaction, hydrogen bonding	Cross-linked cellulose
Toyopearl NH2-750F	Tosoh Biosciences	Proprietary polyamine 	8.5	Electrostatic interaction, hydrophobic interaction, hydrogen bonding	Methacrylic polymer (HW-75)

4.2.7 Analytical Techniques

The performance of chromatography resins were evaluated based of % protein recovery and % purity calculated as follows.

$$Percent\ product\ recovery\ (or)\ yield = \frac{(amount\ of\ product\ after\ unit\ operation)}{(amount\ of\ product\ before\ unit\ operation)} * 100$$

$$Percent\ purity = \frac{(amount\ of\ product)}{(amount\ of\ product + amount\ of\ total\ protein\ impurities)} * 100$$

$$Purification\ fold = \frac{(\%\ purity\ after\ unit\ operation)}{(\%\ starting\ purity)}$$

HCP concentration measurements were calculated using Bradford assay (Thermo Fisher Scientific, USA) on a microtiter plate format with BSA as standard [176]. The absorption was measured at 595 nm using VERSA Max microplate reader.

hTrx concentrations were measured by indirect ELISA. Protein samples were immobilized on a Nunc maxisorb plate and incubated with anti-thioredoxin monoclonal antibody (Abcam, USA) at 1:7500 dilution followed by anti-mouse polyclonal HRP at 1:10,000 dilution (Sigma, USA). The reaction was developed using TMB developer (Sigma, US) and stopped with 1 M HCl, absorbance at 450 nm was measured using VERSA Max plate reader.

Reducing/Denatured SDS-PAGE was used to visualize the protein makeup in a sample. Eight to twelve µg/well of denatured protein samples were loaded on NuPAGE Novex 4 - 12% Bis-Tris pre-cast gradient gels (Thermo Fisher Scientific, USA) and separated by electrophoresis for 35 min at constant 200 V. All proteins were visualized by

SimplyBlue SafeStain Coomassie G-250 stain (Thermo Fisher Scientific, USA) and analyzed against a SeeBlue Plus2 pre-stained protein standard (Thermo Fisher Scientific, USA). ImageJ v.1.49 software was used to calculate purity of proteins in each sample lane [177].

The size of hTrx was analyzed using TSK gel 2000 SWxL column (Tosoh, USA) connected to ÄKTA purifier 10 equipped with a fraction collector. Thirty microliters (30 μL) of concentrated sample (containing at least 1 mg/mL protein) was injected on the column and run at 1 mL/min for 15 min in 100 mM sodium phosphate, 5 mM DTT, pH 7.0.

Activity of hTrx was determined at pH 7 using a previously described method of insulin precipitation by thioredoxin [188]. Briefly, hTrx reduces the interchain disulfide bonds in insulin molecule resulting in precipitation which is monitored by the change in absorbance at 650 nm.

4.2.8 Statistical Analysis

All high-throughput screening experiments were conducted in triplicates. JMP Pro 12 software was used to for statistical analysis. Analysis of variance was performed and triplicates of the treatments were compared for significant difference using Tukey-Kramer HSD test at $\alpha = 0.05$.

4.2.9 Molecular Dynamics

Desmond Schrödinger software suite was used to perform the molecular modelling at the Lab for Molecular Simulations, Texas A&M University. The molecular simulation

process is briefly described schematically in Figure 4.1. PDB file (1ERT) of hTrx from X-ray crystallography was obtained and pre-processed to include polar hydrogens atoms and minimize molecular energy. The hexylamine (HEA) ligand was created using Maestro and 12 molecules of HEA were distributed randomly around 1 protein, to replicate the experimental ratio. All proteins, ligands and additives were protonated corresponding to pH 5.0 + 0.2 to emulate the experimental conditions. A solvation box of 55, 50, 50 Å size was created with water and neutralized with sodium chloride ions according to the TIP4P model [189]. Molecular dynamics was performed for 1.2 ns to relax the system and impart random starting orientations. Six frames of this run were used as starting points for molecular dynamics simulation, each for 40ns. These runs were under NPT conditions, for constant pressure under Optimized Potentials for Liquid Simulations (OPLS) force field. These were merged for a total trajectory of 240 ns and analyzed for interaction energies (Appendix Figure A4). Chimera was used to create the visual representations. The simulations were repeated with a dimer of hTrx (1ERT), in its oxidized form with a solvation box of 75, 55, 85 Å size.

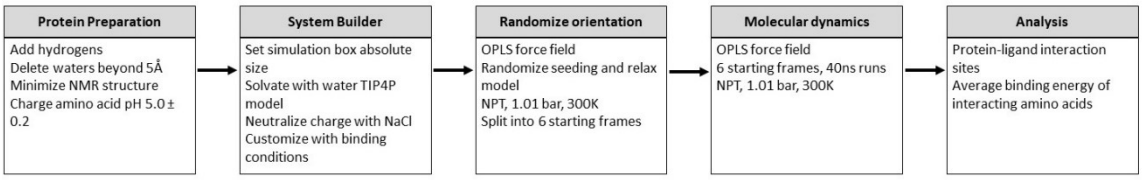

Figure 4.1 Detailed schematic of the steps involved in molecular modelling of hTrx interaction with HEA ligand

4.3 Results

4.3.1 Lysis Buffer Optimization

The first step in downstream process development is cell lysis. Starting off with the most hTrx recovery and higher purity is paramount to an efficient purification process. Varying buffer pH (7, 5, and 3) for cell lysis were tested. pH 7 and 3 were tested for being 2 points over and below the pI of the protein. pH 5 was tested because it was close to the pI of hTrx (4.8) but also close to the pI of other acidic protein impurities from *E. coli* cell. The impact of 500 mM NaCl to release any proteins bound electrostatically to the cell debris was also tested. The hTrx recovery and purity were measured by Bradford and ELISA assays and shown in Figure 4.2.

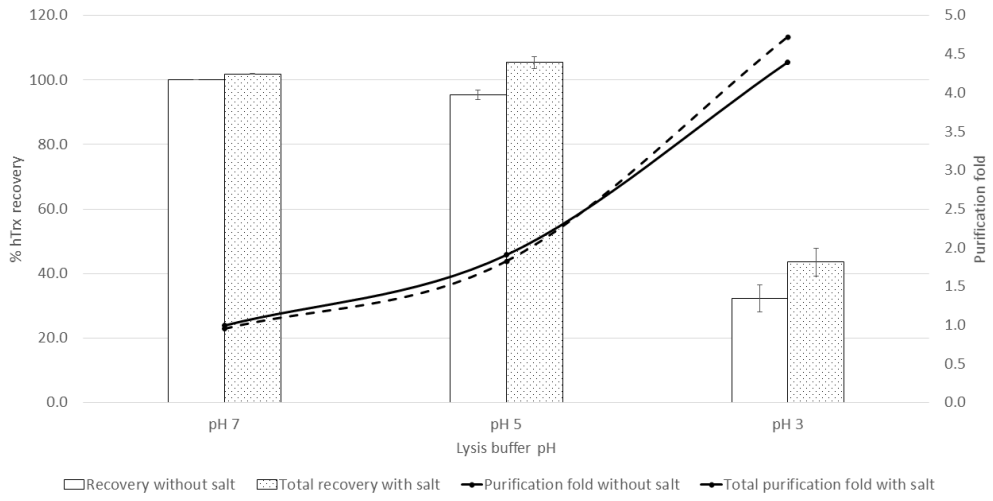

Figure 4.2 Impact of lysis buffer conditions of cell lysis. Error bars indicate standard deviation of triplicate measurements

Cell lysis at pH 3, resulted in poor recovery of hTrx. Since the addition of salt does not recover more than 45% of the hTrx, the reduced extractability is probably not due to electrostatic interaction with the cell debris. By crossing the isoelectric point to reach pH 3, hTrx solubility is affected, resulting in a lower extractability. Compared to pH 7, cell lysis at pH 5 released all of hTrx from the cell (95.4% recovery). The HCP content, however, was reduced significantly (2-fold) at pH 5, leading to an increase in hTrx purity by 1.9 fold. The differential solubility of hTrx and HCP at pH 5, despite being close to its pI, can be attributed to the highly ordered secondary structure of hTrx. The presence of NaCl in the lysis buffer did not have an effect on the hTrx recovery or on increasing lysate purity, and thus, was not included in the lysis buffer. The optimized lysis buffer consisted of 50 mM sodium acetate, 5 mM DTT at pH 5. DTT was present in all buffers used in this study to ensure reduced state of hTrx dithiols groups.

4.3.2 High-Throughput Resin Screening for Capture Chromatography

4.3.2.1 Single-Mode Resins

Equilibrium hTrx binding to traditional ion exchange resin, Capto Q, was tested at pH above the pI of the protein (pH 5, 7 and 9) to prevent hTrx precipitation and at varying conductivities (2, 5 and 10mS) by high throughput screening and the percent hTrx in flow through was analyzed (Figure 4.3a). Interaction between hTrx and Capto Q at lysate pH of 5, was poor. Since the binding pH is close to the pI of hTrx, the overall charge of the protein was insufficient for strong electrostatic interactions with the quaternary amine ligands of the Capto Q resin. At pH 5, very low conductivity < 2 mS/cm was necessary to

bind hTrx. As the conductivity increases beyond 2 mS, the binding of hTrx is deterred substantially. Increasing the binding pH to 7 or 9, improved hTrx binding, due to increase in the net negative surface charge of hTrx. However, at these conditions (pH 7 or 9), the HCPs were also more negatively charged, resulting in more bound HCP (Figure 4.3b) and lower adsorption selectivity. Due to the small size and low surface charge of the protein, hTrx binding to Capto Q resin was highly sensitive to the conductivity.

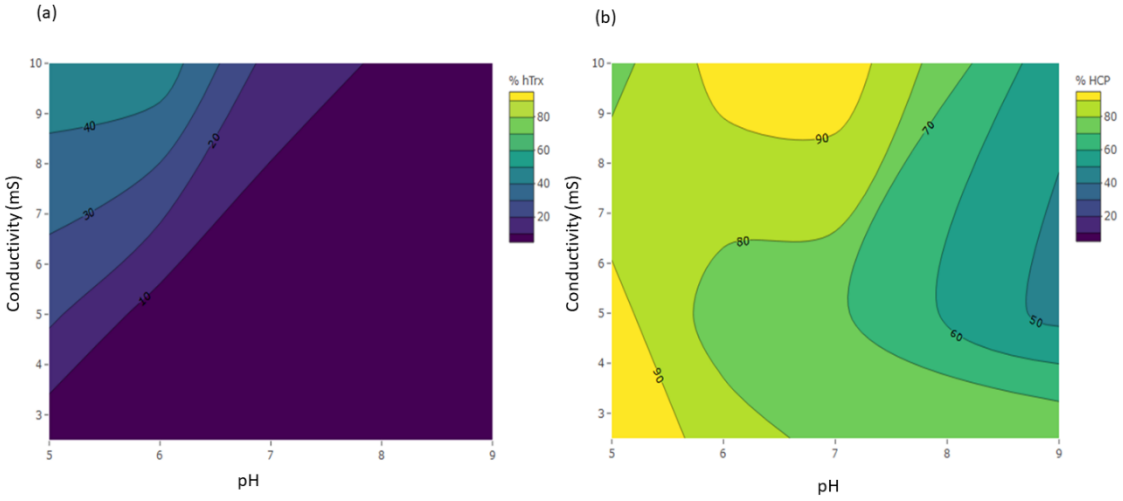

Figure 4.3 High throughput screening of (a) percent hTrx and (b) HCP in Capto Q resin flow through across pH 5, 7 and 9 over 2 to 10 mS conductivity

Hydrophobic interaction chromatography of hTrx with Phenyl Sepharose resin was also tested by high-throughput screening at pH 5, 7 and 9 and ammonium sulfate concentration ranging from 1 to 3 M (Figure 4.4). Data in Figure 4.4 indicate that high concentrations of ammonium sulfate (>2 M) would be required for complete binding of hTrx to the chromatography resin irrespective of the binding pH. Despite the high salt, the binding to the resin was weak, and hTrx was lost in the washes, further 30% loss of hTrx was observed due to salting-out (data not shown). In general, high salt concentrations are

not favorable as they increase the buffer viscosity and promote protein aggregation, hTrx aggregates have decreased activity and should be avoided [190].

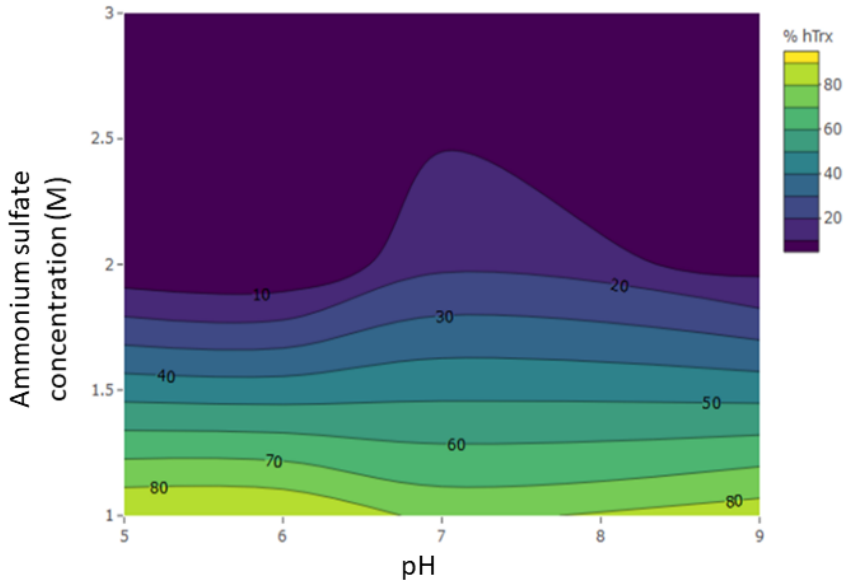

Figure 4.4 High throughput screening of percent hTrx in Phenyl Sepharose resin flowthrough across pH 5, 7 and 9 over 1 to 3 M ammonium sulfate concentrations

In conclusion, the two commonly used single-mode chromatography resins would not be optimal for direct capture of hTrx from clarified lysates, and search for alternative adsorption resins with different chemistries seems warranted.

4.3.2.2 Mixed-Mode Resins

Prometic Ligand Library

Ninety six different ligands were provided in a microtiter filter plate by Prometic ligand library. Each well was a unique combination of ligands connected by a triazine linker to agarose beads, imparting the mixed mode interaction properties. Cell lysate at

pH 5 and 2 mS was loaded to zone 1 (anion exchanger), zone 2 and 4 (corresponding to anion exchange with aliphatic and aromatic hydrophobic ligands respectively). The flow through was analyzed for HCP and hTrx and the 8 best performing resins were selected for further evaluation (data not shown). These 8 resins, were tested for salt-tolerant binding at conductivity of 2, 5 and 10 mS, and pH 7 or 8. The relative binding ratio (k) was calculated by the ratio of % hTrx bound to the % HCP bound under each condition. Among the resins that displayed hTrx binding at moderate salt concentrations, the two resins that had the highest relative binding ratio, were D1 and D8. Resin D1 was a general ion-exchanger (zone 1), which has k = 2.8 at the optimized pH of 8.0 (Table 4.2). Resin D8 (zone 4) was a mixed-mode resin, which bound 91% of hTrx with relative binding ratio of 1.6 at the optimized pH of 8.0. D1 and D8 resins provided in bulk by Prometic Bioseparations were further evaluated by batch chromatography.

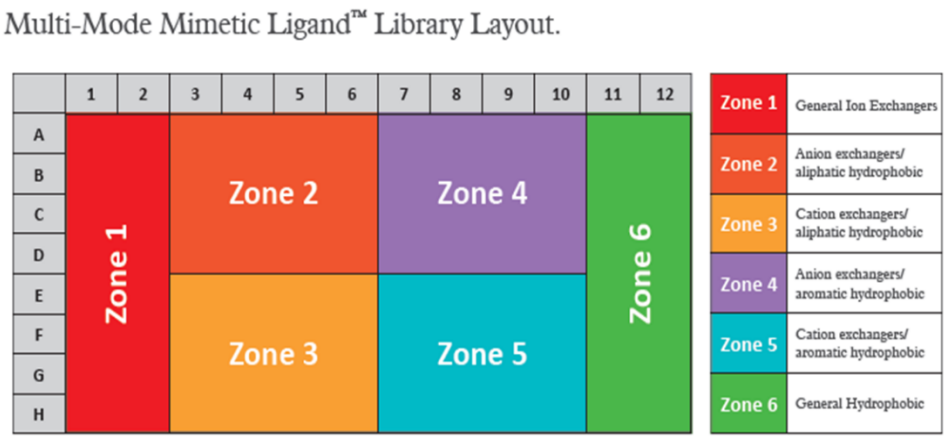

Figure 4.5 Prometic ligand library distribution on 96 well plate

Table 4.2 Relative binding ratio (k) for top 8 resin candidates at optimal binding pH and across conductivities of 2, 5 and 10 mS. Average of triplicate measurements are shown

Resin	Binding pH	Conductivity		
		2mS	5mS	10mS
B1	7	1.5	0.9	0.7
C1	8	1.7	0.6	-
D1	8	2.8	1.3	0.5
D2	8	1.5	1	0.3
D5	8	1.6	1	-
A7	8	2	-	-
D8	8	1.6	1.3	0.7
D9	8	1.8	1.3	0.8

Commercial Mixed-Mode Resins

Mixed-mode resins were tested in triplicates for equilibrium hTrx binding at pH 6, 7 and 8 and conductivities ranging from 2 to 10 mS (Figure 4.6). Toyopearl NH2-750F showed poor binding of hTrx throughout the binding conditions screened. Even at higher pH of 8, where hTrx has a relatively high negative net charge, and 2 mS conductivity, 80% of hTrx remained unbound in the flowthrough resulting in low relative binding ratio (k) of 0.4 (Table 4.3). Capto adhere bound hTrx in low to moderate conductivity range between 2 and 5 mS. Despite minimal net charge on the protein at pH 6, relative binding ratio of k=1.6 at 2 mS was achieved. At pH 7 and 8, where hTrx is negatively charged, complete protein adsorption occurred at moderate conductivities of 7.5 and 10 mS, respectively (Figure 4.6b). In spite of the relatively high k values ranging from 1.2 to 1.6 (Table 4.3), it should be noted that hTrx interaction with the Capto adhere was sensitive to conductivity. An extrapolation from the contour plot (Figure 4.6b) shows 20% of hTrx unbound at 6.5 mS, pH 6. The observed reduction in the adsorbed hTrx amounts as

function of ionic strength, indicates a decrease in the adsorption strength due to weaker charge interactions, albeit the binding was moderately salt-tolerant.

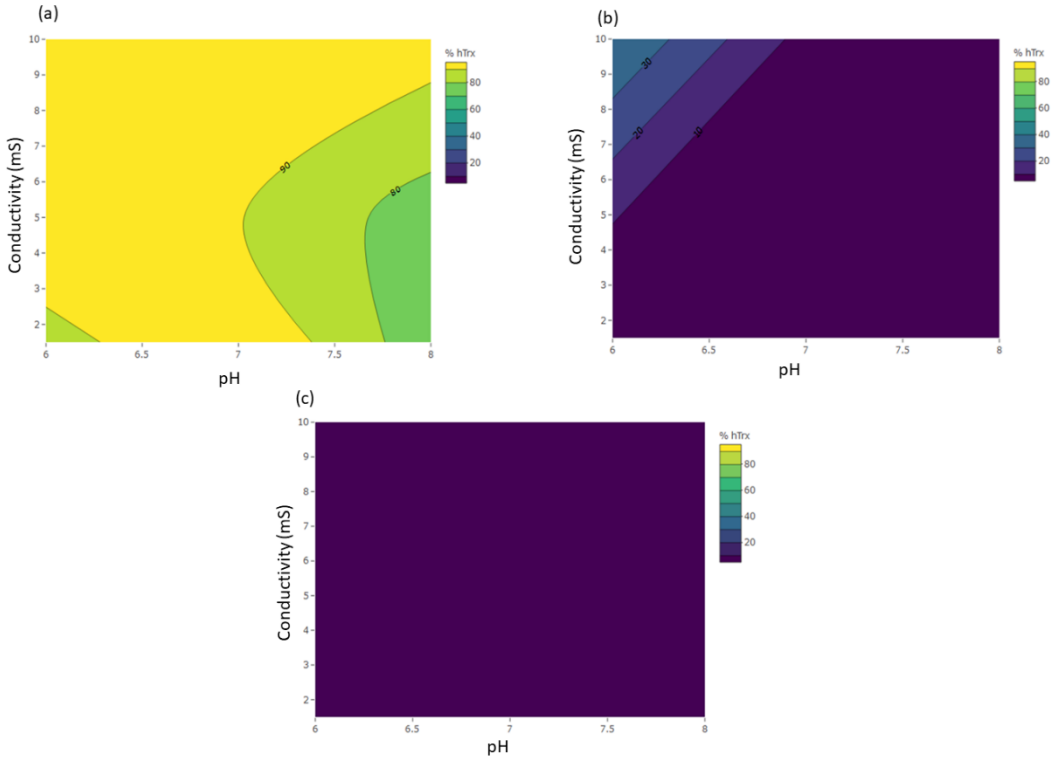

Figure 4.6 High throughput screening of percent hTrx in flowthrough of (a) Toyopearl NH2 750F (b) Capto adhere and (c) HEA HyperCel mixed mode resins across pH 6, 7 and 8 over 2 to 10 mS conductivities

Table 4.3 Relative binding ratio (k) for mixed-mode resins Toyopearl NH2 750F, Capto adhere and HEA HyperCel across pH 6, 7 and 8 over 2 to 10 mS conductivities. Average of triplicate measurements are shown

	Toyopearl NH2 750F			**Capto adhere**			**HEA HyperCel**		
	2 mS	5 mS	10 mS	2 mS	5 mS	10 mS	2 mS	5 mS	10 mS
pH 6	0.3	0.0	0.0	1.6	1.2	0.8	1.4	1.3	1.2
pH 7	0.0	0.2	0.0	1.6	1.3	1.2	1.4	1.3	1.3
pH 8	0.4	0.4	0.1	1.6	1.5	1.3	1.4	1.3	1.3

HEA HyperCel resin also displayed salt-tolerant binding with hTrx, across pH 6 to 8, consistently with k value ranging from 1.2 to 1.4 across all the screened binding conditions. At pH 7 and 8, complete binding of hTrx is observed (Figure 4.6c), even at 10 mS. At the pH 6, hTrx still binds completely to HEA HyperCel at 6.5 mS, when compared to Capto adhere which had a predicted 20% hTrx in the flow through under the same conditions (Figure 4.6). Similar to Capto adhere, hTrx binding to HEA HyperCel was gradually weakened by increase in conductivity, reflected in the decrease in relative binding ratio (Table 4.3), indicating that electrostatic interactions are playing a role in the protein adsorption to HEA.

Capto adhere and HEA HyperCel along with chromatography resins D1 and D8 from Prometic ligand library were further evaluated by batch chromatography experiments to determine their recovery and purification potential.

4.3.3 Testing the Recovery and Purity of Selected Mixed-Mode Resin Candidates

Batch chromatography was performed on 0.5 mL gravity flow columns, with direct loading at the clarified lysate conditions (pH 5, 5 mS) and adsorbed proteins were eluted stepwise with increasing NaCl concentrations in acetate buffer. Percent purity and recovery of hTrx in the elution fractions were determined and listed in Table 4.4.

The criteria for selecting resins that could be used for capture chromatography were set to at least 50% purity and 80% recovery of hTrx to improve on the processes reported in the literature.

Data in the Table 4.4 demonstrate that the Prometic resin D1, a general ion exchanger, adsorbed 71.6% of the initial hTrx and released the adsorbed protein at a rather low ionic strength (100 mM) elution conditions indicating weak electrostatic interaction between the ligand and hTrx. The purity of the eluted hTrx was 33.5%. Resin D8 under tested conditions (pH 5, 5 mS) adsorbed only 13.3% of the loaded amount of hTrx. Majority of hTrx was lost in the flow through. Neither Prometic chromatography resins met the purity criterion and they were eliminated from further consideration.

Table 4.4 Analysis of hTrx purity and recovery from batch chromatography on mixed-mode resins

	Prometic ligand library resin D1		**Prometic ligand library resin D8**		**Capto adhere**		**HEA HyperCel**	
	Purity %	Recovery %	Purity %	Recovery %	Purity %	Recovery %	Purity %	Recovery %
Clarified lysate	24.8	100	24.8	100	17.5	100	30.4	100
Elution 0.1 M NaCl	33.5	71.6	16.8	12.7	42.2	58.2	41.3	16.3
Elution 0.25 M NaCl	0	0	3.4	0.6	25.2	15.6	63.6	9.6
Elution 0.5 M NaCl							70	9.7
Elution 1.0 M NaCl							86.5	7.6
Elution 1.5 M NaCl							71.9	1.9
Overall	33.5	71.6	10.1	13.3	33.8	73.8	66.6	45.1

GE Healthcare's Capto adhere resin, completely adsorbed hTrx at the clarified lysate conditions of pH 5 and 5 mS. Consistent with the high-throughput screening studies, the adsorption strength was low and 58% of adsorbed protein was desorbed with a relatively low ionic strength buffer containing 100 mM NaCl (Table 4.4). Although the achieved purity of 42% was better than that of D1 resin, the recovery of 58% is too low

for capture chromatography. The second elution pool of hTrx with 0.25 M NaCl generated additional 16% of hTrx at 25% purity. It is possible to select only the hTrx from 100 mM NaCl elution to maximize on the purity that can be achieved, but that would be at the expense of 16% hTrx from the 250 mM NaCl elution, and such a product loss in the first step of protein purification is not ideal. Combined hTrx pools had an average purity and recovery of 33.8% and 73.8%, respectively. Similarly to D1, the Capto adhere resin fell short of selection criteria threshold.

HEA HyperCel resin displayed complete hTrx binding at the clarified lysate conditions. High ionic strength buffers (> 1 M) desorbed hTrx at an average purity of 67% but the recovery of 45% was suboptimal. Although it did not reach the desirable 80% recovery benchmark, HEA HyperCel resin was the only mixed-mode resin that displayed salt-tolerant binding of hTrx and met the purity criteria. In spite of the suboptimal recovery level, HEA HyperCel was selected for further studies for the following reasons-

1. Binding conditions compatible with direct loading of clarified lysate with minimal or no conditioning
2. Strong adsorption should theoretically allow achieving higher resin loads (and greater breakthrough capacity)
3. Significantly higher purity than other resin candidates provides a wider window of opportunity for optimization of desorption conditions (pH, elution buffer additives, modifiers, and displacement agents) while maintaining greater than 50% purity.

The following section addresses the last reason (#3) and investigates elution conditions that would yield higher hTrx recovery while maintaining greater than 50% purity.

4.3.4 Optimization of Elution Buffer for Improving Recovery of Thioredoxin from HEA HyperCel

To address the suboptimal desorption hTrx, three alternate organic compound-based elution buffers were explored. The effect of 50 mM Tris, 5 mM DTT, pH 7.0 containing arginine HCl, guanidine HCl and lysine HCl on hTrx recovery from HEA HyperCel resin were tested by high-throughput screening and shown in Figure 4.7a. Arginine and guanidine HCl were chosen for their ability to disrupt electrostatic, hydrophobic and hydrogen bonding, while lysine HCl for the ability to break electrostatic and hydrogen bonding. The highest hTrx recovery of 47% was achieved using 0.25 M guanidine-HCl buffer, but it was not significantly ($\alpha = 0.05$) better than 33% recovery with 1 M NaCl containing buffer. Similarly, the hTrx recovery with a 0.25 M arginine or 0.25 M lysine containing buffer was not significantly different than the other elution buffers.

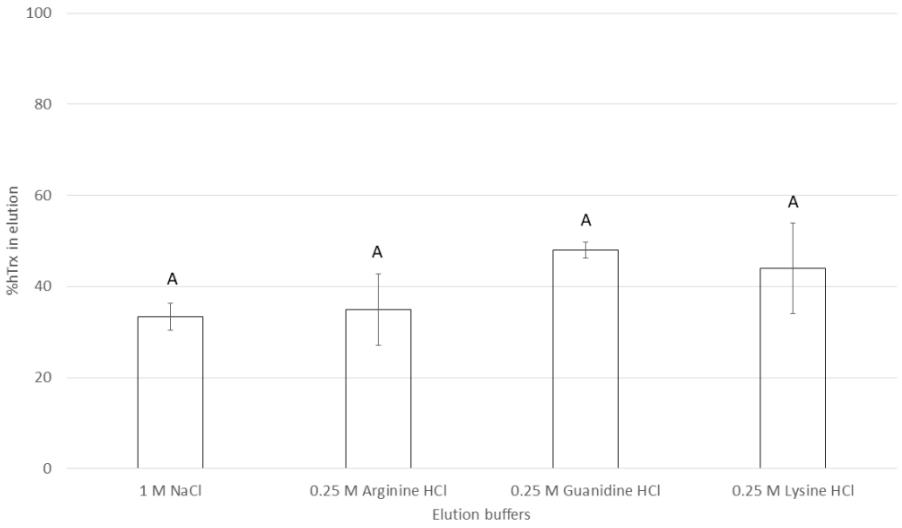

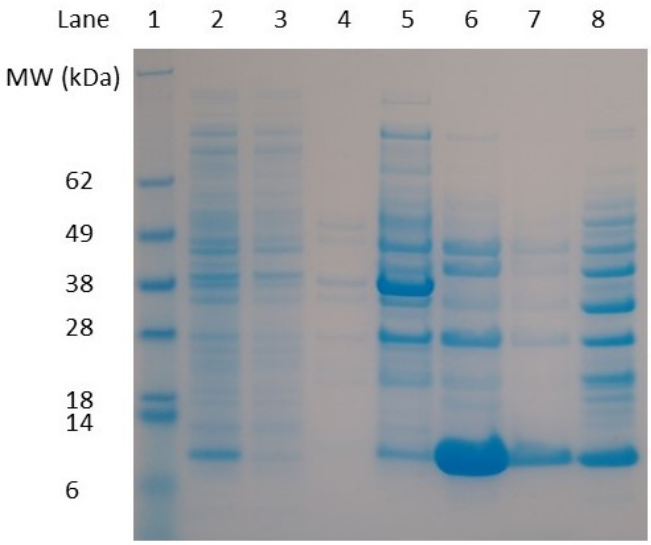

Figure 4.7 (a) hTrx recovery (%) from HEA HyperCel resin using different elution buffers. The effect of 50 mM Tris buffer containing 0.25 M Arginine, Lysine, or Guanidine were compared to the same buffer containing 1 M NaCl. Treatments sharing the same letter are not significantly different ($\alpha = 0.05$). Error bars indicate standard deviation of triplicate measurements (b) SDS-PAGE of *E. coli* lysate binding and elution profile from HEA HyperCel resin. All samples diluted to <1 mg/mL TSP. Lane 1. MW marker, lane 2. Clarified lysate, lane 3. Flow through, lane 4. Washes (3 CV), lane 5. Elution with 100 mM NaCl, lane 6. Elution with 1 M NaCl, lane 7. Elution with 250 mM arginine HCl (0-2 CV), lane 8. Elution with 250 mM arginine HCl (2-10 CV)

Figure 4.7a, demonstrate that each buffer contributes to the desorption of hTrx by breaking interactions between the protein and HEA ligand. Previous studies employing these buffers demonstrated that arginine and guanidine can affect electrostatic, hydrophobic and/or hydrogen-bond interactions, while NaCl disrupts primarily electrostatic interaction [35]. The specific desorption mechanism of lysine containing buffers has not been widely reported. Based on the molecular structure of lysine, one could safely assume interference with the same three types of molecular interactions as arginine.

The examination of SDS-PAGE eluted protein profiles (Figure 4.7b) shows that arginine elution buffer desorbed different host cell proteins than NaCl (Figure 4.7b lanes 6 and 8). These differences, although semi-quantitative in nature, confirm previous reports on desorption mechanism and let us hypothesize that the primary desorption mechanism of organic compound-based elution buffers and NaCl is different. Therefore, we next investigated the potential synergistic effect of combining organic compound-based buffers with NaCl buffer, aimed at increasing hTrx elution yield.

The elution buffers tested consisted of 0.1, 0.25 and 0.5 M arginine HCl, guanidine HCl or lysine HCl in 50 mM Tris, 5 mM DTT, pH 7.0 buffer containing 1 M NaCl. The data in Figure 4.8, summarize hTrx desorption yields (% recovery) using elution buffers that contained NaCl and one of the three organic modifiers. The combined effect salt and organic compound-based modifiers on recovery of hTrx from HEA HyperCel resin is compared to the protein recovery with only 1.0 M NaCl buffer in Figure 4.8.

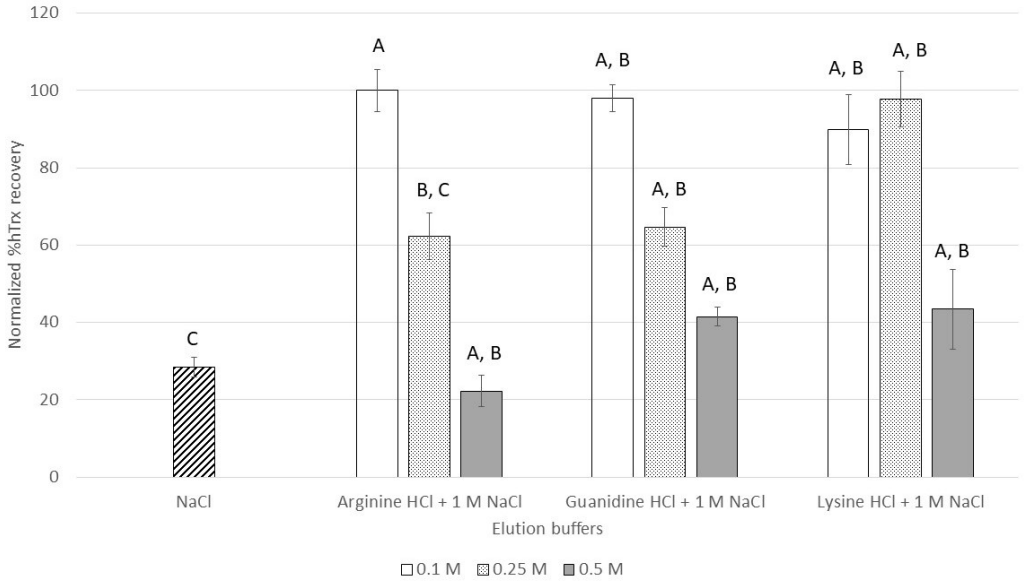

Figure 4.8 Effect of buffer modifiers on % hTrx recovery in elutions from HEA HyperCel chromatography resin. The elution buffers consisted of 0.1, 0.25 and 0.5 M arginine HCl, guanidine HCl or lysine HCl in 50 mM Tris, 5 mM DTT, pH 7.0 buffer containing 1 M NaCl. The %hTrx recovery values were normalized with the highest recovery as 100%. Treatments not sharing the same letter are significantly different (α = 0.05). Error bars indicate standard deviation of triplicate measurements

0.1 M of arginine, guanidine and lysine HCl combined with 1 M NaCl, efficiently eluted hTrx from HEA HyperCel completely (100%). The estimated recoveries were > 100% possibly due to margin of error in the analytical method to quantify hTrx, therefore the highest %hTrx recovery value was normalized to 100% in the figure. The complete hTrx recovery was a remarkable improvement compared to less than 50% recovery obtained with individual buffers (Figure 4.7), establishing that the combination of each buffer modifier at 0.1 M concentration with 1 M NaCl had a synergistic effect on the recovery of hTrx. Buffer containing 0.25 and 0.5 M of arginine HCl and guanidine HCl in 1 M NaCl appears to suppress the elution of hTrx, while with lysine HCl appears to exhibit

a similar suppression at 0.5 M concentration. The reason for recovery suppression is not clear and has not been reported before with any mixed-mode resins. In the absence of direct evidence and explanation of the suppression phenomenon, one could speculate that the higher concentrations of modifiers in elution buffer promotes rather than disrupts protein-ligand interactions similar to the "U-shaped" elution curve reported for some mixed mode resins.

Since any of the three organic modifies (arginine, guanidine, lysine) when combined with 1 M NaCl contributes to total hTrx recovery at 0.1 M concentration, we have chosen the arginine and NaCl combination to investigate and, if possible, to discern their impact on electrostatic, hydrophobic and hydrogen-bond interactions between hTrx and the HEA ligand. The main reason for selecting arginine over guanidine or lysine was the established body of evidence of using arginine as an elution buffer modifier known to preserve protein structural stability of complex therapeutics proteins such as monoclonal antibodies [35].

4.3.5 Modelling Thioredoxin Interaction with HEA HyperCel

Molecular modelling studies were performed on hTrx PDB structure (1ERT) to simulate interaction with free HEA ligand. The input on binding energies, interaction sites and mode of interaction are valuable information about the protein-ligand interaction that contribute to knowledge-based experimental design and targeted testing conditions. In this case, it was employed to gain an understanding of protein-ligand interaction mechanism and supplement experimental findings. Figure 4.9, shows the amino acid sites that interact with HEA ligand for greater than 25% time in the total 240 ns simulation. The color

gradient is based on the average interaction strength (kcal/mol) of two modes of interaction electrostatic and van der Waals (hydrogen bonding) interaction during the total simulation period. Under binding conditions of 0.05 M NaCl, pH 5.0, aspartic acids (16, 58, 60 and 61) and glutamic acids (13) bind with strong electrostatic energy to HEA ligand, the highest being asp 60 with -48.5 kcal/mol. Increasing the NaCl in the system to 1.0 M weakens the interactions of these amino acids but aspartic acid 16 and glutamic acids 13, 95 and 98 are still interacting with the ligand, consistent with the experimental results of partial hTrx elution from HEA HyperCel resin. In a system with only arginine of 0.2 M, a similar observation, aspartic acid 60 and glutamic acid 70 interact with moderate energies of -12.4 and -21.6 kcal/mol. Under the optimized elution condition of elution modifier (arginine) in the presence of 1.0 M NaCl, the interactions with ligand are broken with only aspartic acid 61 interacting weakly with -14.8 kcal/mol.

Molecular dynamics also was employed to test the theory that hTrx aggregates are retained stronger by the ligand. Dimers of hTrx with 2 intramolecular (cys 32- cys 35) and one intermolecular (cys 73- cys 73) disulfide bonds were subjected to the same simulation conditions. The average energies of interactions are shown in Table 4.5.

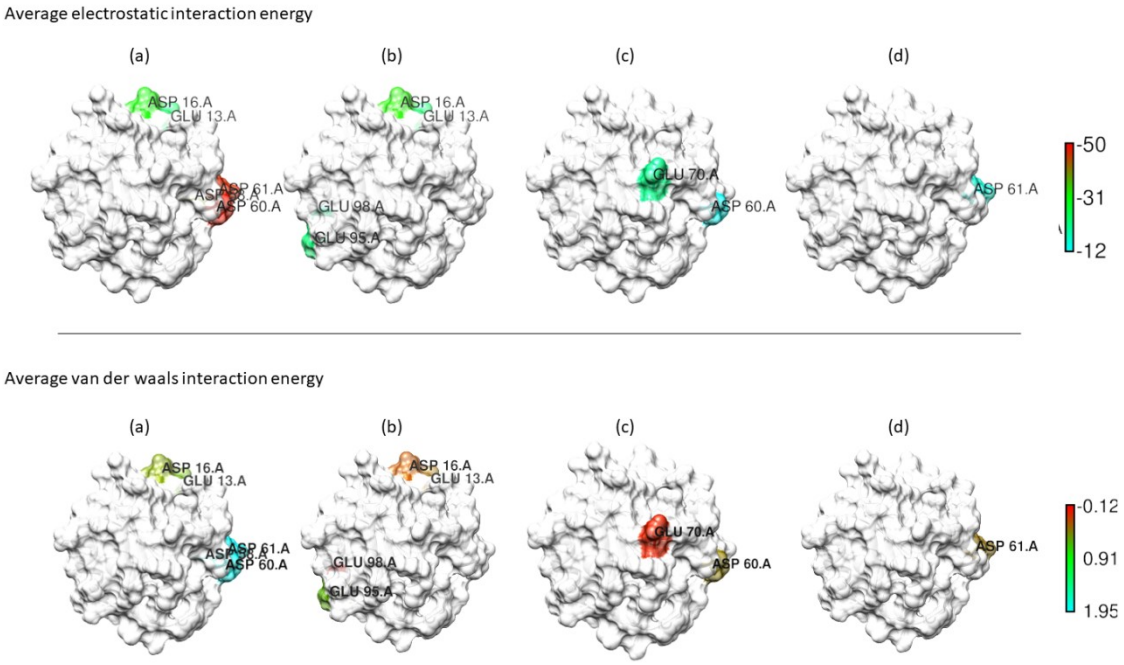

Figure 4.9 Analysis of molecular dynamics showing amino acids in hTrx interacting with HEA ligand shaded based on interaction energy (kcal/mol) under (a) 0.05 M NaCl; (b) 1.0 M NaCl; (c) 0.2 M arginine; (d) 1.0 M NaCl + 0.2 M arginine conditions

Dimers of hTrx also interact with the HEA ligand with the surface acidic amino acids aspartic and glutamic acids. Interestingly, the highest binding energies of dimers, -37.7 kcal/mol (electrostatic of asp 61.B) was lower than the binding energy of monomer -48.6 kcal/mol (electrostatic of asp 60). Additionally, phenylalanine 42 and 77 contribute to hydrophobic interactions that prevail in high salt conditions as well, but are reversed when arginine is introduced. However, the aspartic and glutamic acids still interact with the ligand and require the combination of NaCl and arginine to minimize electrostatic interaction and van der Waals interactions.

Table 4.5 Average energies of hTrx amino acids interacting with HEA ligand in the presence of arginine and NaCl molecules

	Monomer			Dimer		
Condition	Amino acid	Avg electrostatic energy (kcal/mol)	Avg van der Waals energy (kcal/mol)	Amino acid.chain name	Avg electrostatic energy (kcal/mol)	Avg van der Waals energy (kcal/mol)
0.05 M NACL	Glu13	-24.7	0.5	Asp26.A	-37.1	2.3
	Asp16	-32.0	0.5	Phe42.A	-0.7	-3.6
	Asp58	-38.7	1.8	Glu47.B	-17.0	0.8
	Asp60	-48.6	1.9	Glu56.A	-15.4	0.6
	Asp61	-47.1	2.6	Asp58.A	-36.0	0.4
				Asp58.B	-14.4	0.7
				Asp60.A	-23.6	1.0
				Asp61.B	-37.7	1.7
				Glu6.A	-15.1	-0.6
				Glu6.B	-25.8	0.5
				Phe77.A	0.2	-3.2
				Glu95.A	-21.8	0.4
				Glu95.B	-13.8	0.4
				Glu98.A	-23.2	-0.2

Table 4.5 Continued

	Monomer			Dimer		
Condition	Amino acid	Avg electrostatic energy (kcal/mol)	Avg van der Waals energy (kcal/mol)	Amino acid.chain name	Avg electrostatic energy (kcal/mol)	Avg van der Waals energy (kcal/mol)
	Asp16	-33.1	0.2	Phe42.A	0.1	-0.5
	Glu95	-23.0	0.6	Asp58.B	-21.2	1.2
	Glu98	-19.9	-0.1	Asp60.B	-22.3	1.3
				Asp61.B	-19.0	1.3
				Phe77.A	-1.0	-3.3
				Glu98.B	-19.0	0.1
0.2 M ARGININE	Asp60	-12.5	0.4	Glu13.A	-30.5	0.2
	Glu70	-21.4	0.0	Asp16.A	-18.2	0.1
				Asp58.B	-27.8	1.8
				Asp60.B	-14.4	0.5
				Asp61.B	-25.4	1.2
				Glu98.A	-32.8	0.8
1.0 M NACL + 0.2 M ARGININE	Asp61	-14.8	0.3	Asp58.A	-9.0	0.5

4.3.6 Packed-Bed HEA HyperCel Chromatography

To simplify the elution process and eliminate the need for pH adjustment after the binding of hTrx on the HEA packed-bed column, elution of hTrx using the same binding buffer (50 mM sodium acetate buffer, 5 mM DTT at pH 5.0) containing arginine and NaCl was tested. The amount of arginine required for optimal recovery of hTrx from a pH 5.0 elution buffer was re-examined using 0.025 to 0.5 M arginine concentration range and their effect on hTrx recovery is shown in Figure 4.10, and compared as before to 1 M NaCl control. Similar to previous pH 7.0 elution buffer composition, hTrx was completely (100%) eluted from HEA HyperCel resin with 0.1 M arginine in 1.0 M NaCl acetate buffer. Lower and higher than 0.1 M arginine concentrations resulted in an "U-shaped" elution recovery trend consistent with the previous data with mixed-mode resins [34, 191]. Therefore, to maximize hTrx recovery, the optimal composition of the pH 5.0 elution buffer consists of 50 mM sodium acetate, 5 mM DTT, 1.0 M NaCl, and 0.1 M arginine HCl.

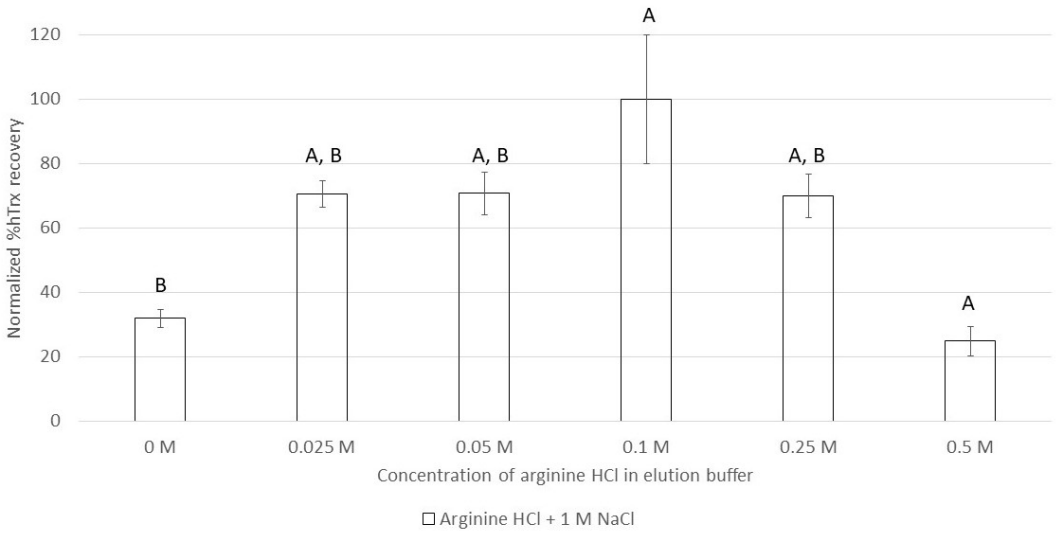

Figure 4.10 Optimization of arginine HCl concentration in 1 M NaCl in pH 5 acetate buffer for recovery of hTrx in HEA HyperCel elution. The %hTrx recovery values were normalized with the highest recovery as 100%. Treatments not sharing the same letter are significantly different ($\alpha = 0.05$). Error bars indicate standard deviation of triplicate measurements

The adsorption studies so far were performed essentially under equilibrium conditions, and packed-bed chromatography was investigated next. The aim was to confirm the strong adsorption of hTrx during a much shorter contact time of 5 min compared to 30 min in batch experiments and verify the effectiveness of optimized elution buffer conditions. The chromatogram from packed-bed chromatography is shown in Figure 4.11, with fractions containing hTrx highlighted within the vertical orange lines. The recovery and purity of hTrx in these fractions were measured, along with the size and activity, shown in Table 4.6.

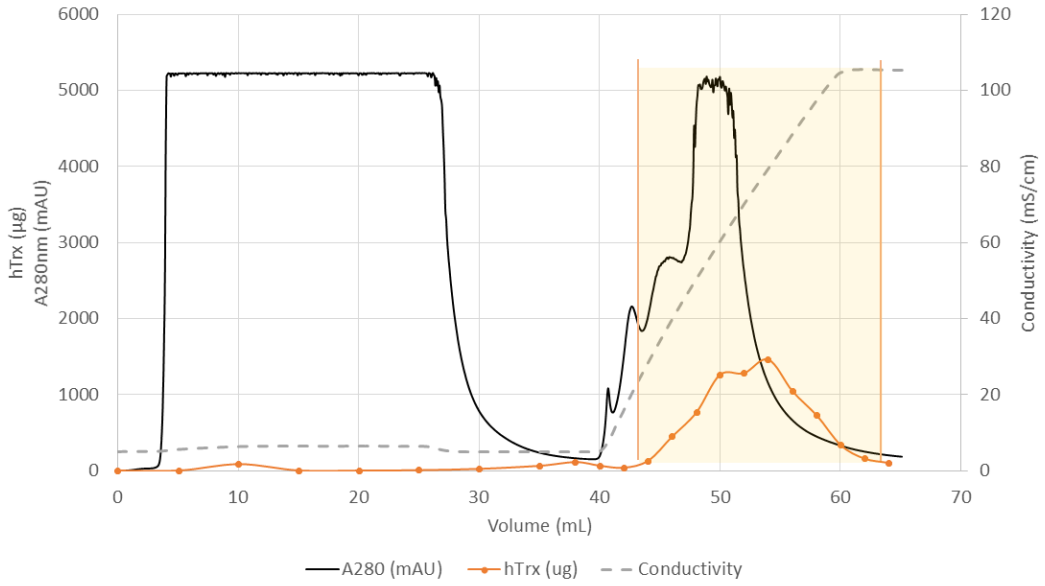

Figure 4.11 Chromatogram of hTrx purification by HEA HyperCel resin. Clarified lysate was loaded to PRC HEA column (1 mL) at 0.25 mL/min flowrate. Linear gradient of optimized elution buffer (0–1.0 M NaCl+ 0.1 M arginine HCl) at 0.5 mL/min was applied. hTrx eluted is shown as the shaded orange region between 43 - 65 mL

The HEA elutions contained hTrx at 52.3% purity, and the recovery was 100%. The use of optimized elution buffer containing 0.1 M arginine HCl and 1.0 M NaCl at pH 5 was effective in completely reversing the interactions and eluting hTrx bound to HEA HyperCel resin on a packed-bed column as well. The capture chromatography also reduced DNA content to 1.8×10^{11} µg, a 1-log reduction from the clarified lysate value. The turnover number, calculated from insulin reduction activity also increased to 7.1×10^{-5} min^{-1} due to the increase in purity.

Table 4.6 Purification table showing the capture of clarified lysate by HEA HyperCel chromatography

Step	Volume (mL)	HCP (mg)[a]	hTrx (mg)[b]	% Purity[c] (Purification fold)	% Recovery[d]	DNA (µg)[e]	Activity (min^{-1})[f]
Clarified Lysate	20	97.0	6.7	20.46 (1.0)	100	$9.0 * 10^{11}$	$5.2* 10^{-6}$
HEA elutions	18	4.3	7.4	52.3 (2.5)	100	$1.8 * 10^{11}$	$7.1* 10^{-5}$

a- Bradford
b-ELISA
c-SDS
d-ELISA
e-Picogreen assay
f-Insulin precipitation assay

4.3.7 Analysis of Human Thioredoxin in Elution Fractions

Another aspect to be analyzed to confirm multiple interaction mechanisms, is that the hTrx eluted by arginine and that by NaCl are the same isoform. Packed-bed chromatography was employed with first a gradient NaCl elution over 20 CV followed by 10 CV elution with 0.2 M arginine HCl (NaCl-Arg), similarly another experiment with the elution order reversed, 10 CV elution with 0.2 M arginine HCl then a 20 CV gradient NaCl elution (Arg-NaCl). The elution fractions were individually analyzed for size distribution, shown in Figure 4.12. Peak "1" in chromatograms (Figure 4.12a and 4.12b) corresponds to HCP impurities, confirmed by SDS-PAGE (data not shown) and arginine elution fractions contain peak "3" corresponding to the solvent absorbance in the dead-

volume. In both experiments, arginine and NaCl elution fractions contained 12 kDa hTrx eluting at 10.4 mL seen as peak "2". There were no hTrx aggregates observed in the elutions, and both NaCl and arginine HCl were eluting hTrx in its monomer form.

Insulin reduction activity is a characteristic of hTrx, and was used to confirm its identity (Figure 4.13a and 4.13b). In the case of NaCl-Arg, the two elutions also displayed insulin reduction activity with a turnover number of 7.7* 10^{-5} min^{-1} and 2.0* 10^{-5} min^{-1} respectively. Similarly, in the case of Arg-NaCl, the turnover number was 3.9* 10^{-5} min^{-1} and 1.3* 10^{-5} min^{-1} respectively. This established that both elution buffers removed hTrx of the same size from the column and the eluting fractions displayed hTrx activity.

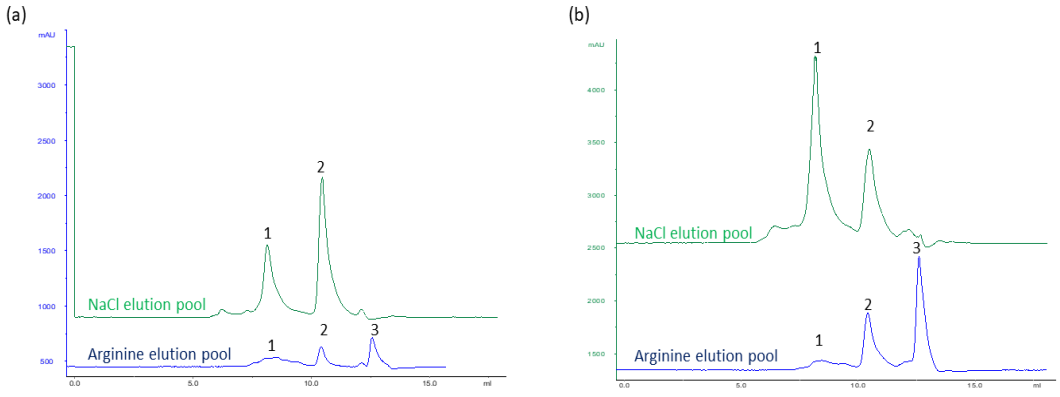

Figure 4.12 Analysis of size distribution using TSK gel 2000SWxL column for (a) NaCl-Arg elution pools and (b) Arg-NaCl elution pools

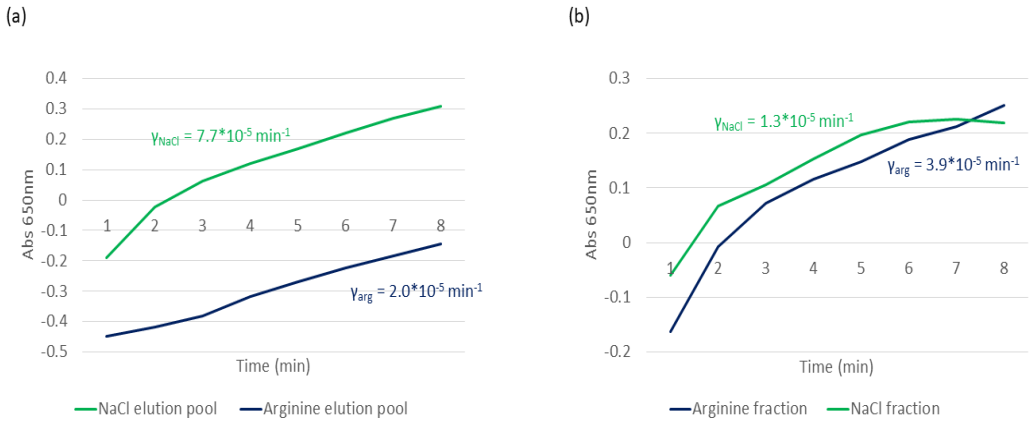

Figure 4.13 Insulin-reduction activity of hTrx in (a) NaCl-Arg elution pools and (b) Arg-NaCl elution pools

4.4 Discussion

Thioredoxin is a potent therapeutic molecule with anticipated use for cystic fibrosis treatment. Manufacturing the necessary quantities (estimated ~2000 kg/year) of hTrx would not be efficient with the current downstream processes in terms of overall product yield and likely to be cost prohibitive. Improving the efficiency of the isolation process will translate to lower manufacturing cost and affordability of the therapeutic product.

Current isolation processes for hTrx that employ anion exchange chromatography and hydrophobic interaction chromatography result in a significant (as much as 50%) loss in hTrx. Exploring single-mode resins shed light on the processing constraints of the current isolation methods. The main reasons for observed losses are related to inefficient adsorption resin capacity and adsorption strength that can be explained by the distribution

of charge and hydrophobic amino acids on the surface of hTrx. For example, adsorption of hTrx to Capto Q resin required unrealistically low conductivity range (0 to < 2 mS), since the protein has a minimal net charge (-0.6) at the optimized lysis pH. Clarified cell lysate is at pH 5 and conductivity of 5 mS would have to be either significantly diluted or diafiltered to facilitate electrostatic interaction with Capto Q resin. Either procedure is not ideal from a processing stand point; dilution would increase the processing time for loading larger lysate volumes onto Capto Q packed-bed columns whereas the diafiltration is an additional unit operation that would increasing the cost and processing time. The critical process weakness is the low binding strength of hTrx on the strong anion exchange resin making Capto Q resin unsuitable for capture step. Similarly, the low hydrophobicity of hTrx (GRAVY = - 0.096), required > 2 M ammonium sulfate to bind the protein to the strongest hydrophobic resin (phenyl ligand). The main deficiency associated with 2 M ammonium sulfate was the upfront 30 % loss of hTrx due to salting-out.

To overcome noted process constraints with Capto Q and hydrophobic interaction chromatography we resorted to mixed-mode adsorbents hoping to take advantages of dual adsorption mechanism to increase the protein binding capacity without the need for any substantial lysate conditioning (diafiltration or ammonium sulfate addition). Mixed-mode resin have not been extensively employed for direct capture from clarified lysates and thus, in the absence of data "brute-force" approach to select resins, i.e. high-throughput screening was undertaken. Mixed-mode resins were then explored for the benefits that could arise from multiple interaction chemistries. High-throughput screening was valuable in reducing the experimental time to attain reliable data on hTrx binding across pH and

conductivities. Of the resins screened several (Prometic ligands D1, D8, Capto adhere and HEA HyperCel) showed binding of hTrx under moderate salt-tolerant conditions (~5 mS). Amongst these resins, HEA HyperCel had consistently high relative binding ratio (k =1.2 to 1.4) even in moderate conductivities. hTrx interaction with the resin across pH 6 to 8 at conductivities up to 10 mS, was indicative of a strong interaction. The elution of adsorbed hTrx with a high ionic strength (75 mS) buffer containing 1 M NaCl was insufficient to fully recover hTrx. This indicated that hTrx-HEA ligand interactions were not solely electrostatic. To address the low yield required further high-throughput screening focusing on elution buffers that could disrupt other intermolecular interactions. This led us to investigate buffer additives containing arginine HCl, guanidine HCl and lysine HCl, which are known to have ability to break hydrogen bonds, and electrostatic and hydrophobic interactions. Individual organic elution buffers (Figure 4.7a) in the absence of NaCl, were not significantly different in increasing hTrx recovery than 1 M NaCl alone. Upon examination of eluted proteins by SDS-PAGE (Figure 4.7b), the difference in the profile of HCPs, led to the hypothesis that the desorption mechanism of organic modifiers and NaCl was different. This behavior is characteristic of mixed-mode resins where a protein can interact with the ligand through multiple modes of interaction. Therefore, to maximize the recovery yield these different interaction mechanism need to be tackled simultaneously during elution [23]. Consistent with that, synergistic behavior was observed when elution buffers combined these organic modifiers at an optimized concentration of 0.1 M with 1 M NaCl buffer, recovered 100% of hTrx from HEA HyperCel resin. Among the buffer modifiers, arginine HCl was chosen for further analysis for the following reasons.

Arginine HCl is known to preserve the structural stability of proteins. Protein denaturation in the presence of < 0.1 M guanidine HCl concentration was not expected hence was not the reason to exclude guanidine from further consideration, and actually guanidine could be an economically viable alternative to arginine. Comparing arginine and guanidine both of which share a guanidinium side chain, allows shedding light on the mechanism of hTrx. The guanidinium group present in both arginine and guanidine HCl, is electropositive and expected to reduce the electrostatic interaction. Arginine should have a stronger charge disruption effect because of its zwitter ionic property and steric hindrance from its alkyl group. Based on molecular modelling studies, both arginine and guanidine accumulate near the charged amino acids of proteins resulting in charge neutralization and desorption. They also promote hydrophobic interactions of the nearby amino acids with the resin. The enhancement of hydrophobic interactions with nearby amino acids would be more pronounced in the presence of guanidine HCl than arginine due to the steric hindrance effect of bulkier arginine molecule [192]. Hydrophobic interactions could also explain the "U-shaped" elution observed with > 0.1 M elution buffer modifiers when added to 1 M NaCl containing elution buffer (Figure 4.10).

Molecular simulation helped to better understand experimental observation. The primary mode of interaction at pH 5 is electrostatic and van der Waals (hydrogen bonding). Despite being close to the pI of the protein, the acidic residues (aspartic and glutamic acids) retain charge at pH 5 and interact with the HEA ligand. Simulation data confirm that NaCl and arginine are required to simultaneously break electrostatic and hydrogen

bonding with the aspartic and glutamic amino acids and completely reverse the interactions with the ligand.

Capture chromatography performed on 1 mL packed-bed column was consistent with the trend observed from high-throughput and equilibrium adsorption studies. The optimized elution buffer successfully recovered 100% of hTrx with a purity of 52.3%. The purity with packed-bed chromatography was lower than 67% achieved in batch chromatography experiments. The discrepancy can be attributed to a couple of reasons. First, due to inconsistencies in cell disruption by sonication, the starting purity of the lysate used in packed-bed chromatography was 20.5% (% HCP or TSP) compared to 30% used in the batch chromatography experiments. Second, there was a larger volume of clarified lysate loaded per ml of HEA HyperCel resin, which would increase the amount of impurities that bind and then co-elute with hTrx. There was no breakthrough of hTrx observed in the flow through, so the loading was within the binding capacity of the chromatography resin and there was no hTrx lost or unaccounted for in the mass balance. Clearly, there is room for further optimization of the HEA capture chromatography as further process development to reach the therapeutic standards of hTrx.

4.5 Conclusions

This study explored the pitfalls of using single-mode chromatography resins as it applies to hTrx isolation and the resulting product loss. Mixed-mode chromatography resins were explored to take advantage of better selectivity and direct loading in moderate salt concentrations.

Custom and commercial mixed mode resins displaying direct binding of hTrx from clarified lysate were narrowed down using high-throughput screening based on their selective binding of hTrx and HCPs. HEA HyperCel provided the maximum purity of 67% with a 45% recovery of hTrx by batch chromatography and was chosen as the capture chromatography because 1) allowed for direct binding of cell lysate without conditioning, 2) higher purity was obtained in the elutions 3) the interaction with HEA ligand was stronger and required higher NaCl concentrations to elute compared to other resins. Since recovery of high value therapeutic product is paramount for process efficiency, especially early in the isolation process, elution was optimized to improve recovery.

The optimized elution buffer of 50 mM sodium acetate, 1.0 M NaCl, 0.1 M arginine HCl, 5 mM DTT, pH 5 resulted in complete hTrx elution, while the individual buffer components could not elute all of the bound hTrx. Consequently, a true mixed-mode interaction exists where one isoform of hTrx interacts through multiple mechanisms with the HEA HyperCel resin. The nature of these interactions were determined by molecular modelling and discovered as electrostatic and van der Waals interactions (hydrogen bonding). More importantly, optimized concentration of buffer components was crucial in elution, since hTrx binding with the resin was promoted at > 0.1 M concentration of arginine HCl in the elution buffer. Packed-bed chromatography under direct loading and optimized elution conditions resulted in 52.3% purity and 100% hTrx recovery. Through understanding the mechanism of protein-ligand interaction, the recovery was significantly increased, while maintaining > 50% elution purity. With 100% recovery from the capture step, there is opportunity to further optimize the loading and

elution strategy to maximize the hTrx purity obtained from HEA HyperCel chromatography. The highly efficient capture chromatography alleviates the recovery burden on subsequent processing steps and sets precedent for a thoroughly optimized process.

The hTrx obtained from HEA HyperCel was confirmed to be biologically active with a turn over number of 7.1×10^{-5} min^{-1} and oxidized aggregates were not present in the elutions. Clearly, there is need for an additional chromatography or purification unit operation to reach the therapeutic standards of 99.9% purity and 125 ng DNA/ g of hTrx.

In summary, this study establishes that HEA HyperCel mixed-mode resins can be applied to crude lysate for direct capture of non-mAb therapeutic protein. Molecular modelling was applied to reveal the specific sites of protein-ligand interaction and its behavior under experimental conditions. The information gained bolstered the understanding of the process and reinforced the experimental findings. Scaled-down high-throughput screening was applied for binding and elution optimization, which successfully translated to packed-bed chromatography. Combining the knowledge from literature, computation modelling and high throughput screening, an active hTrx at 100% recovery and increased purity was obtained without aggregates.

CHAPTER V

CONCLUSION

Downstream processing contributes to 50-80% of the cost of therapeutic manufacturing. Mixed-mode resins are an emerging class of chromatographic stationary phase media, known for their high selectivity. Their application in purification of therapeutic proteins is still nascent. In this study, mixed-mode resins were applied to the downstream processing of two therapeutic proteins to gain insights into the challenges and benefits of mixed-mode resins. The two proteins studied suffered from multi-chromatography downstream process, due to processing difficulties arising from low expression titer, impurity profile, lack of charge or hydrophobic properties, etc. and stand to benefit from integrating mixed-mode resins in their downstream process. The following results and conclusions were made from each study.

5.1 Isolation of Osteopontin from *C. reinhardtii* Lysate Using CHT Resin

The ability of microalgae, *C. reinhardtii* to express OPN in its phosphorylated form was confirmed, although the starting purity was a low 0.1-0.2%. Additionally, multiple isoforms of pI ranging from 3.5 to 4.5 and fragments of 35 kDa were detected. Knowledge-based process development led to testing mixed-mode CHT resin to capture phosphorylated OPN. Direct capture of OPN from algal lysate, at pH 6.8 resulted in strong interactions of 70% of the OPN with mixed-mode CHT resin, requiring 1500 mM NaP followed by 100 mM NaOH to recover the bound OPN. The protein-ligand interaction was challenged by binding in the presence of 250 mM NaCl, which interestingly promoted phosphorylated OPN's binding, due to suppression of electrostatic repulsion between

negatively charged groups. Conversely, binding in 250 mM NaCl discouraged interaction of non-phosphorylated *E. coli* OPN, as 83% remained unbound. This confirmed that OPN's interaction with CHT resin was through multiple chemistries, the non-phosphorylated *E. coli* OPN interacted primarily through electrostatic interactions, while phosphorylated OPN necessitated NaP buffer to competitively elute the Ca^{2+}–PO_3^{2-} coordinate binding. However, CHT as the capture chromatography was ineffective in resolving phosphorylated algal impurities, such as Rubisco, from OPN. Therefore, alternate capture chromatography using anion exchanger, Capto Q resin was used, to separate Rubisco and before CHT chromatography. Such a two-step process resulted in 33% OPN recovery and 75% purity, which was a 375-fold increase from the lysate purity. In this case, a three-chromatography process would be necessary to obtain OPN in therapeutic specification. The low starting purity, combined with multiple isoforms were detrimental to protein recovery and quantification.

5.2 Application of HEA HyperCel Mixed-Mode Resin for the Capture of OPN from *E. coli* Lysate

Mixed-mode resins for the capture of osteopontin in the absence of phosphorylation were explored. Scaled-down, high-throughput screening studies predicted the binding chemistries offered. HEA HyperCel resin bound OPN at 150 mM NaCl and again at 3 M NaCl concentration, indicating a shift in retention modes from primarily electrostatic to hydrophobic binding based on salt conditions. PPA HyperCel, consistently bound OPN across the tested binding pH and conductivity, but the recovery with pH 3 elution buffer was a low 60%. Capto adhere resin was very sensitive to binding

pH and conductivity, offering no benefit in purity or recovery compared to single-mode anion exchange chromatography, Capto Q resin. Of the resins studied, binding to mixed-mode HEA HyperCel resin offered highest purification fold of 14, and recovery of 76%. Mixed-mode resins were a viable capture chromatography for OPN from *E. coli* lysate, increasing the purity of the lysate from 1.9% to 29%. After buffer exchange to reduce the conductivity, anion exchange chromatography was employed to increase the purity of the HEA elution to 95%. The typical 3 or more chromatography process used for purification of OPN was reduced to a 2-chromatography downstream process by using mixed-mode resins.

5.3 Mixed-Mode Resin Screening for the Capture and Recovery of Human Thioredoxin from *E. coli* Lysate

The downstream processing of human thioredoxin suffers from the lack of charge and hydrophobic properties, despite high expression titers. Direct comparisons between the limitations of single-mode resins were made with the possibilities offered by mixed-mode resins. Comparison of resin selectivity and salt-tolerant interactions were made possible by high-throughput screening. Mixed-mode HEA HyperCel resin had a consistently high relative binding ratio of 1.4 across pH and conductivities up to 10 mS. It offered direct capture of hTrx from clarified lysate and resulted in a 66.6% purity at 40 % recovery with 1 M NaCl elution. Molecular modeling revealed combined retention mode, electrostatic and hydrogen bonding between protein-ligand that required individual buffer components to address. The optimized concentration of organic buffer modifier, 0.1 M arginine HCl was added to 1 M NaCl elution buffer to completely recover hTrx

from the capture chromatography. Packed-bed chromatography under the optimized binding and elution conditions was used to confirm that biologically active hTrx at 52.3% purity and in monomer form was obtained from HEA HyperCel chromatography.

5.4 Recommendations for Further Process Development of Therapeutic Proteins

The following recommendations are to continue the study described in Chapter II-

i. Increasing OPN expression titers in *C. reinhardtii* is mandatory for further process development and scaling the suggested process to packed-bed chromatography
ii. Investigate the selectivity of CHT resin towards degree of phosphorylation in the phosphorylated OPN isoforms
iii. Explore other mixed-mode resins alternates to capture and resolve Rubisco from OPN. Followed by a comparison with single-mode anion exchange chromatography.

The following recommendations are to continue the study described in Chapter III-

i. Improve OPN recovery in the dialysis operation
ii. Determine the binding capacity to optimize OPN loading on packed-bed column.
iii. Characterize the OPN elutions for protein activity, isoforms and contaminant such as DNA, endotoxins

The following recommendations are to continue the study described in Chapter IV-

i. Explore pretreatment methods such as flocculation with charged polymers prior to capture chromatography, to reduce DNA, charged HCP impurities and improve hTrx binding capacity on HEA HyperCel resin.

ii. Optimize protein loading and wash to maximize elution purity achieved from HEA HyperCel chromatography

iii. Explore mixed-mode resins options for the next chromatography to achieve therapeutic purity and assemble the downstream process

iv. Perform molecular modelling at different organic modifier concentrations to understand the mechanism behind "U-shaped" elution behavior of hTrx from HEA HyperCel chromatography

v. Analyze the economic impact of mixed-mode resin on downstream processing cost

5.5 Mixed-Mode Resins Conclusion

The above cases are in no means exhaustive analysis on the capabilities of mixed-mode resins, but a representation to understand their performance under challenging processing situations of low starting purity, contrasting expression titers (0.1-0.2% vs 30%), varying impurity protein profile and specific challenges related to the expression hosts. The following conclusions can be drawn from the three studies regarding mixed-mode resins.

1. They were capable of handling complex lysates, from *C. reinhardtii* and *E. coli* cells and capture the therapeutic protein from it. Mixed-mode CHT resin was insensitive to low expression titers and starting purity, especially considering the pseudo-affinity binding with phosphoryl groups in OPN. Similarly, HEA

HyperCel resin also fared well at both 1.9% starting purity of OPN and high ~30% starting purity of human thioredoxin, enduring the large (> 30 mg/ml) protein load and still providing selectivity. Mixed-mode resins were versatile and could be used for direct capture from complex lysates as well as intermediate chromatography.

2. Mixed-mode resins offer wider range of compatible binding pH and salt concentration. Electrostatic interactions at low to moderate conductivities were crucial for direct lysate binding. Such functionalities overcome the need for conditioning operations like diafiltration, saving processing cost and time.
3. Mixed-mode resins offer multiple interactions, these can be individual interactions, based on binding condition or combined interactions, based on property of the protein. For example, HEA HyperCel resin, displayed individual electrostatic interaction with OPN at low salt concentration and shifted to hydrophobic interaction when bound at 3 M NaCl. In the case of hTrx, electrostatic and van der Waals interaction with the HEA ligand were simultaneous and resulted in strong interaction strength.
4. The protein-ligand interactions are driven by the properties of the protein. For example, the same HEA HyperCel resin interacted primarily by electrostatic interaction with OPN but through a combination of electrostatic and van der Waals interaction with hTrx. HEA HyperCel offers electrostatic, hydrogen bonding and hydrophobic interaction chemistry, but it is the property of the protein that dictates the binding mechanism. Therefore, a platform approach to binding and elution

conditions cannot be applied, but proven strategies to counteract the interaction mechanisms can be suggested.

Some of the challenges with mixed-mode resins were revealed during the course of this study are summarized below-

1. The complexities arising from combining multiple interactions make mixed-mode resins notorious for low product recovery. One has to recognize that multiple interactions while offering opportunity to achieve new enhanced separation selectivity, might not always be beneficial. For example, complete hTrx recovery demanded extensive buffer optimization studies and modelling protein-ligand interactions to develop a successful elution strategy. Another case that required intervention was phosphorylated OPN interacting with CHT resin. Apart from the simultaneous electrostatic and coordination bonding, there was undesirable electrostatic repulsion between phosphoryl groups in the protein and phosphate groups in the resin, which required suppression of electrostatic repulsions with 250 mM NaCl for complete binding
2. Thorough understanding of protein-ligand interaction mechanism and optimization of binding and elution conditions, is key to overcoming low protein recovery from some mixed-mode resins and achieving their potential. Knowledge-based approach presumes understanding of the process related impurities and protein-ligand interaction mechanism. In the cases of poorly understood systems, the experimental load could be immense and eventually result in an inefficient process. In our studies, hybrid approach combining scaled-down high-throughput

screening and molecular modelling were successfully employed to comprehensively understand the possible interactions with the resin and reduce the experimental trial-and-error required.

3. The presence of protein isoforms and impurities containing binding motifs similar to the target protein could defy the use of mixed-mode interactions. This challenge was encountered with CHT resin, where the selectivity of the mixed-mode resin was reduced in the presence of Rubisco, a host cell impurity protein that has similar properties to OPN. The poorly understood OPN structure limits our ability to further exploit the complex CHT chemistry and determine the capacity of CHT to resolve isoforms based on phosphorylation.

Recommendation for future work include-

1. Perform techno-economic analysis on using HEA HyperCel mixed-mode resins as capture chromatography
2. Future process development starting with modelling the protein-ligand interaction, followed by experimental optimization would be ideal for downstream process development efficiency
3. Expand the library of information on therapeutic proteins and their interaction with the most promising mixed-mode resins through molecular modelling
4. Explore new modalities of mixed-mode ligands that can overcome the current challenges

REFERENCES

1. Walsh, G., *Biopharmaceuticals: Biochemistry and Biotechnology*. 2013: John Wiley & Sons.

2. Zhong, X., et al., *Recent Advances in Biotherapeutics Drug Discovery and Development*, in *Drug Discovery and Development-Present and Future*. 2011, IntechOpen.

3. Walsh, G., *Biopharmaceutical Benchmarks 2018.* Nature Biotechnology, 2018. **36**: p. 1136-1145.

4. Jacoby, R., *Advanced Biopharmaceutical Manufacturing: An Evolution Underway.* Deloitte, May, 2015.

5. Sommerfeld, S. and J. Strube, *Challenges in Biotechnology Production—Generic Processes and Process Optimization for Monoclonal Antibodies.* Chemical Engineering and Processing: Process Intensification, 2005. **44**(10): p. 1123-1137.

6. Zhu, D., A.J. Saul, and A.P. Miles, *A Quantitative Slot Blot Assay for Host Cell Protein Impurities in Recombinant Proteins Expressed in E. coli.* Journal of Immunological Methods, 2005. **306**(1): p. 40-50.

7. Fahrner, R.L., et al., *Industrial Purification of Pharmaceutical Antibodies: Development, Operation, and Validation of Chromatography Processes.* Biotechnology and Genetic Engineering Reviews, 2001. **18**(1): p. 301-327.

8. Li, F., et al., *Current Therapeutic Antibody Production and Process Optimization.* BioProcessing Journal, 2007. **5**(4): p. 16.

9. Petsch, D. and F.B. Anspach, *Endotoxin Removal from Protein Solutions.* Journal of Biotechnology, 2000. **76**(2): p. 97-119.

10. Lowe, C.R., A.R. Lowe, and G. Gupta, *New Developments in Affinity Chromatography with Potential Application in the Production of Biopharmaceuticals.* Journal of Biochemical and Biophysical Methods, 2001. **49**(1): p. 561-574.

11. Jacquemart, R., et al., *A Single-Use Strategy to Enable Manufacturing of Affordable Biologics.* Computational and Structural Biotechnology Journal, 2016. **14**: p. 309-318.

12. Birch, J.R. and A.J. Racher, *Antibody Production.* Advanced Drug Delivery Reviews, 2006. **58**(5): p. 671-685.

13. Chon, J.H. and G. Zarbis-Papastoitsis, *Advances in the Production and Downstream Processing of Antibodies.* New Biotechnology, 2011. **28**(5): p. 458-463.

14. Demain, A.L. and P. Vaishnav, *Production of Recombinant Proteins by Microbes and Higher Organisms.* Biotechnology Advances, 2009. **27**(3): p. 297-306.

15. Jayapal, K.P., et al., *Recombinant Protein Therapeutics from Cho Cells-20 Years and Counting.* Chemical Engineering Progress, 2007. **103**(10): p. 40.

16. Przybycien, T.M., N.S. Pujar, and L.M. Steele, *Alternative Bioseparation Operations: Life Beyond Packed-Bed Chromatography.* Current Opinion in Biotechnology, 2004. **15**(5): p. 469-478.

17. Nfor, B.K., et al., *Rational and Systematic Protein Purification Process Development: The Next Generation.* Trends in Biotechnology, 2009. **27**(12): p. 673-679.

18. Mehta, A., *Downstream Processing for Biopharmaceuticals Recovery*, in *Pharmaceuticals from Microbes: The Bioengineering Perspective*, D. Arora, et al., Editors. 2019, Springer International Publishing: Cham. p. 163-190.

19. Rathore, A.S. and H. Winkle, *Quality by Design for Biopharmaceuticals.* Nature Biotechnology, 2009. **27**(1): p. 26.

20. Bhambure, R., K. Kumar, and A.S. Rathore, *High-Throughput Process Development for Biopharmaceutical Drug Substances.* Trends in Biotechnology, 2011. **29**(3): p. 127-135.

21. Hanke, A.T. and M. Ottens, *Purifying Biopharmaceuticals: Knowledge-Based Chromatographic Process Development.* Trends in Biotechnology, 2014. **32**(4): p. 210-220.

22. Kaleas, K.A., C.H. Schmelzer, and S.A. Pizarro, *Industrial Case Study: Evaluation of a Mixed-Mode Resin for Selective Capture of a Human Growth Factor Recombinantly Expressed in E. coli.* Journal of Chromatography A, 2010. **1217**(2): p. 235-242.

23. Yang, Y. and X. Geng, *Mixed-Mode Chromatography and Its Applications to Biopolymers.* Journal of Chromatography A, 2011. **1218**(49): p. 8813-8825.

24. Toueille, M., et al., *Designing New Monoclonal Antibody Purification Processes Using Mixed-Mode Chromatography Sorbents.* Journal of Chromatography B, 2011. **879**(13): p. 836-843.

25. Voitl, A., T. Müller-Späth, and M. Morbidelli, *Application of Mixed Mode Resins for the Purification of Antibodies.* Journal of Chromatography A, 2010. **1217**(37): p. 5753-5760.

26. Nfor, B.K., et al., *High-Throughput Isotherm Determination and Thermodynamic Modeling of Protein Adsorption on Mixed Mode Adsorbents.* Journal of Chromatography A, 2010. **1217**(44): p. 6829-6850.

27. Freed, A.S., S. Garde, and S.M. Cramer, *Molecular Simulations of Multimodal Ligand–Protein Binding: Elucidation of Binding Sites and Correlation with Experiments.* The Journal of Physical Chemistry B, 2011. **115**(45): p. 13320-13327.

28. Hou, Y. and S.M. Cramer, *Evaluation of Selectivity in Multimodal Anion Exchange Systems: A Priori Prediction of Protein Retention and Examination of Mobile Phase Modifier Effects.* Journal of Chromatography A, 2011. **1218**(43): p. 7813-7820.

29. Kallberg, K., H.O. Johansson, and L. Bulow, *Multimodal Chromatography: An Efficient Tool in Downstream Processing of Proteins.* Biotechnology Journal, 2012. **7**(12): p. 1485-1495.

30. Tiselius, A., S. Hjerten, and Ö. Levin, *Protein Chromatography on Calcium Phosphate Columns.* Archives of Biochemistry and Biophysics, 1956. **65**(1): p. 132-155.

31. Zhang, K. and X. Liu, *Mixed-Mode Chromatography in Pharmaceutical and Biopharmaceutical Applications.* Journal of Pharmaceutical and Biomedical Analysis, 2016. **128**: p. 73-88.

32. Burton, S., N. Haggarty, and D. Harding, *One Step Purification of Chymosin by Mixed Mode Chromatography.* Biotechnology and Bioengineering, 1997. **56**(1): p. 45-55.

33. Chen, J., et al., *The Distinctive Separation Attributes of Mixed-Mode Resins and Their Application in Monoclonal Antibody Downstream Purification Process.* Journal of Chromatography A, 2010. **1217**(2): p. 216-224.

34. Gao, D., D.-Q. Lin, and S.-J. Yao, *Patch Controlled Protein Adsorption in Mixed-Mode Chromatography with Benzylamine as Functional Ligand.* Biochemical Engineering Journal, 2008. **38**(3): p. 355-361.

35. Pezzini, J., et al., *A Comprehensive Evaluation of Mixed Mode Interactions of Hea and Ppa Hypercel™ Chromatographic Media.* Journal of Chromatography B, 2015. **976-977**: p. 68-77.

36. Holstein, M.A., et al., *Mobile Phase Modifier Effects in Multimodal Cation Exchange Chromatography.* Biotechnology and Bioengineering, 2012. **109**(1): p. 176-186.

37. Wang, R.-Z., et al., *Evaluation of Mixed-Mode Chromatographic Resins for Separating Igg from Serum Albumin Containing Feedstock.* Journal of Chromatography B, 2013. **936**: p. 33-41.

38. Gagnon, P., *Purification of Monoclonal Antibodies by Mixed-Mode Chromatography.* Process Scale Purification of Antibodies, 2009: p. 125-144.

39. Hilbrig, F. and R. Freitag, *Isolation and Purification of Recombinant Proteins, Antibodies and Plasmid DNA with Hydroxyapatite Chromatography.* Biotechnology Journal, 2012. **7**(1): p. 90-102.

40. Gagnon, P., *Monoclonal Antibody Purification with Hydroxyapatite.* New Biotechnology, 2009. **25**(5): p. 287-293.

41. Gorbunoff, M.J. and S.N. Timasheff, *The Interaction of Proteins with Hydroxyapatite: Iii. Mechanism.* Analytical Biochemistry, 1984. **136**(2): p. 440-445.

42. Gorbunoff, M.J., *The Interaction of Proteins with Hydroxyapatite: I. Role of Protein Charge and Structure.* Analytical Biochemistry, 1984. **136**(2): p. 425-432.

43. Zhang, X., T. Chen, and Y. Li, *A Parallel Demonstration of Different Resins' Antibody Aggregate Removing Capability by a Case Study.* Protein Expression and Purification, 2019. **153**: p. 59-69.

44. Gagnon, P.S., *Enhanced Purification of Antibodies and Antibody Fragments by Apatite Chromatography*. 2018, Google Patents.

45. Mamone, G., et al., *Hydroxyapatite Affinity Chromatography for the Highly Selective Enrichment of Mono-and Multi-Phosphorylated Peptides in Phosphoproteome Analysis.* Proteomics, 2010. **10**(3): p. 380-393.

46. Pinto, G., et al., *Fractionation of Complex Lipid Mixtures by Hydroxyapatite Chromatography for Lipidomic Purposes.* Journal of Chromatography A, 2014. **1360**: p. 82-92.

47. Bernardi, G. and T. Kawasaki, *Chromatography of Polypeptides and Proteins on Hydroxyapatite Columns.* Biochimica et Biophysica Acta (BBA) - Protein Structure, 1968. **160**(3): p. 301-310.

48. Bernardi, G., *[29] Chromatography of Proteins on Hydroxyapatite*, in *Methods in Enzymology*. 1971, Academic Press. p. 325-339.

49. Schwartz, W., et al., *Comparison of Hydrophobic Charge Induction Chromatography with Affinity Chromatography on Protein a for Harvest and Purification of Antibodies.* Journal of Chromatography A, 2001. **908**(1-2): p. 251-263.

50. Maria, S., et al., *Purification Process of Recombinant Monoclonal Antibodies with Mixed Mode Chromatography.* Journal of Chromatography A, 2015. **1393**: p. 57-64.

51. Lees, A., et al., *Purifying a Recalcitrant Therapeutic Recombinant Protein with a Mixed-Mode Chromatography Sorbent.* Bioprocess Int, 2009. **7**(2): p. 42-8.

52. Ravichandran, R., et al., *Studies on Recovery of Lactoferrin from Bovine Colostrum Whey Using Mercapto Ethyl Pyridine and Phenyl Propyl Amine Hypercel™ Mixed Mode Sorbents.* Biotechnology and Bioprocess Engineering, 2015. **20**(1): p. 148-156.

53. Chu, W.-N., et al., *High-Throughput Screening and Optimization of Mixed-Mode Resins for Human Serum Albumin Separation with Microtiter Filter Plate.* Biochemical Engineering Journal, 2018. **131**: p. 47-57.

54. Pezzini, J., et al., *Antibody Capture by Mixed-Mode Chromatography: A Comprehensive Study from Determination of Optimal Purification Conditions to Identification of Contaminating Host Cell Proteins.* Journal of Chromatography A, 2011. **1218**(45): p. 8197-8208.

55. Hirano, A., et al., *Mechanism of Protein Desorption from 4-Mercaptoethylpyridine Resins by Arginine Solutions.* Journal of Chromatography A, 2014. **1373**: p. 141-148.

56. Sodek, J., B. Ganss, and M.D. McKee, *Osteopontin.* Crit Rev Oral Biol Med, 2000. **11**(3): p. 279-303.

57. Azuma, N., et al., *A Rapid Method for Purifying Osteopontin from Bovine Milk and Interaction between Osteopontin and Other Milk Proteins.* International Dairy Journal, 2006. **16**(4): p. 370-378.

58. Kazanecki, C.C., D.J. Uzwiak, and D.T. Denhardt, *Control of Osteopontin Signaling and Function by Post-Translational Phosphorylation and Protein Folding.* Journal of Cellular Biochemistry, 2007. **102**(4): p. 912-924.

59. Denhardt, D.T. and X. Guo, *Osteopontin: A Protein with Diverse Functions.* The FASEB Journal, 1993. **7**(15): p. 1475-1482.

60. Butler, W.T., *The Nature and Significance of Osteopontin.* Connective Tissue Research, 1989. **23**(2-3): p. 123-136.

61. McKee, M.D., C.E. Pedraza, and M.T. Kaartinen, *Osteopontin and Wound Healing in Bone.* Cells Tissues Organs, 2011. **194**(2-4): p. 313-319.

62. Hoyer, J.R., J.R. Asplin, and L. Otvos, *Phosphorylated Osteopontin Peptides Suppress Crystallization by Inhibiting the Growth of Calcium Oxalate Crystals.* Kidney International, 2001. **60**(1): p. 77-82.

63. Patarca, R., R.A. Saavedra, and H. Cantor, *Molecular and Cellular Basis of Genetic Resistance to Bacterial Infection: The Role of the Early T-Lymphocyte Activation-1/Osteopontin Gene.* Critical Reviews in Immunology, 1992. **13**(3-4): p. 225-246.

64. Wang, K.X. and D.T. Denhardt, *Osteopontin: Role in Immune Regulation and Stress Responses.* Cytokine & Growth Factor Reviews, 2008. **19**(5): p. 333-345.

65. Prince, C.W., *Secondary Structure Predictions for Rat Osteopontin.* Connective Tissue Research, 1989. **21**(1-4): p. 15-20.

66. Fisher, L., et al., *Flexible Structures of Sibling Proteins, Bone Sialoprotein, and Osteopontin.* Biochemical and Biophysical Research Communications, 2001. **280**(2): p. 460-465.

67. Sørensen, E.S., T.E. Petersen, and P. Højrup, *Posttranslational Modifications of Bovine Osteopontin: Identification of Twenty-Eight Phosphorylation and Three O-Glycosylation Sites.* Protein Science, 1995. **4**(10): p. 2040-2049.

68. Kleinman, J.G., J.A. Wesson, and J. Hughes, *Osteopontin and Calcium Stone Formation.* Nephron Physiology, 2004. **98**(2): p. p43-p47.

69. Christensen, B., et al., *Post-Translationally Modified Residues of Native Human Osteopontin Are Located in Clusters: Identification of 36 Phosphorylation and Five O-Glycosylation Sites and Their Biological Implications.* Biochemical Journal, 2005. **390**(1): p. 285-292.

70. Singh, K., M.W. DeVouge, and B. Mukherjee, *Physiological Properties and Differential Glycosylation of Phosphorylated and Nonphosphorylated Forms of Osteopontin Secreted by Normal Rat Kidney Cells.* Journal of Biological Chemistry, 1990. **265**(30): p. 18696-18701.

71. Denhardt, D.T. and M. Noda, *Osteopontin Expression and Function: Role in Bone Remodeling.* J Cell Biochem Suppl, 1998. **30-31**: p. 92-102.

72. Weber, G.F., et al., *Phosphorylation-Dependent Interaction of Osteopontin with Its Receptors Regulates Macrophage Migration and Activation.* Journal of Leukocyte Biology, 2002. **72**(4): p. 752-761.

73. Gericke, A., et al., *Importance of Phosphorylation for Osteopontin Regulation of Biomineralization.* Calcified Tissue International, 2005. **77**(1): p. 45-54.

74. Jono, S., C. Peinado, and C.M. Giachelli, *Phosphorylation of Osteopontin Is Required for Inhibition of Vascular Smooth Muscle Cell Calcification.* Journal of Biological Chemistry, 2000. **275**(26): p. 20197-20203.

75. Kariya, Y., et al., *Osteopontin O-Glycosylation Contributes to Its Phosphorylation and Cell-Adhesion Properties.* Biochemical Journal, 2014. **463**(1): p. 93-102.

76. Gao, Y.A., et al., *Expression and Characterization of Recombinant Osteopontin Peptides Representing Matrix Metalloproteinase Proteolytic Fragments.* Matrix Biology, 2004. **23**(7): p. 457-466.

77. Yokosaki, Y., et al., *The Integrin A9β1 Binds to a Novel Recognition Sequence (Svvyglr) in the Thrombin-Cleaved Amino-Terminal Fragment of Osteopontin.* Journal of Biological Chemistry, 1999. **274**(51): p. 36328-36334.

78. Senger, D.R. and C.A. Perruzzi, *Cell Migration Promoted by a Potent Grgds-Containing Thrombin-Cleavage Fragment of Osteopontin.* Biochimica et Biophysica Acta (BBA) - Molecular Cell Research, 1996. **1314**(1): p. 13-24.

79. Scatena, M., L. Liaw, and C.M. Giachelli, *Osteopontin: A Multifunctional Molecule Regulating Chronic Inflammation and Vascular Disease.* Arteriosclerosis, Thrombosis, and Vascular Biology, 2007. **27**(11): p. 2302-2309.

80. Rittling, S.R., et al., *Mice Lacking Osteopontin Show Normal Development and Bone Structure but Display Altered Osteoclast Formation in Vitro.* Journal of Bone and Mineral Research, 1998. **13**(7): p. 1101-1111.

81. Chackalaparampil, I., et al., *Cells in Vivo and in Vitro from Osteopetrotic Mice Homozygous for C-Src Disruption Show Suppression of Synthesis of Osteopontin, a Multifunctional Extracellular Matrix Protein.* Oncogene, 1996. **12**(7): p. 1457-1467.

82. Wang, X., et al., *Delayed Expression of Osteopontin after Focal Stroke in the Rat.* Journal of Neuroscience, 1998. **18**(6): p. 2075-2083.

83. Meller, R., et al., *Neuroprotection by Osteopontin in Stroke.* Journal of Cerebral Blood Flow & Metabolism, 2005. **25**(2): p. 217-225.

84. Xie, Y., et al., *Expression of Osteopontin in Gentamicin-Induced Acute Tubular Necrosis and Its Recovery Process.* Kidney International. **59**(3): p. 959-974.

85. Persy, V.P., et al., *Differences in Osteopontin up-Regulation between Proximal and Distal Tubules after Renal Ischemia/Reperfusion.* Kidney International. **56**(2): p. 601-611.

86. Hur, E.M., et al., *Osteopontin-Induced Relapse and Progression of Autoimmune Brain Disease through Enhanced Survival of Activated T Cells.* Nature Immunology, 2007. **8**(1): p. 74-83.

87. Morimoto, J., et al., *Osteopontin; as a Target Molecule for the Treatment of Inflammatory Diseases.* Current Drug Targets, 2010. **11**(4): p. 494-505.

88. Singh, M., et al., *Osteopontin: A Novel Inflammatory Mediator of Cardiovascular Disease.* Front Biosci, 2007. **12**(1): p. 214-221.

89. Giachelli, C.M., et al., *Regulation of Vascular Calcification.* Roles of Phosphate and Osteopontin, 2005. **96**(7): p. 717-722.

90. Jahnen-Dechent, W., et al., *Mineral Chaperones: A Role for Fetuin-a and Osteopontin in the Inhibition and Regression of Pathologic Calcification.* Journal of Molecular Medicine, 2008. **86**(4): p. 379-389.

91. Zhao, H., et al., *The Role of Osteopontin in the Progression of Solid Organ Tumour.* Cell Death & Disease, 2018. **9**(3): p. 356.

92. Senger, D.R., et al., *Purification of a Human Milk Protein Closely Similar to Tumor-Secreted Phosphoproteins and Osteopontin.* Biochimica et Biophysica Acta (BBA)-Protein Structure and Molecular Enzymology, 1989. **996**(1-2): p. 43-48.

93. Bayless, K.J., G.E. Davis, and G.A. Meininger, *Isolation and Biological Properties of Osteopontin from Bovine Milk.* Protein Expression and Purification, 1997. **9**(3): p. 309-314.

94. Sørensen, S., S.J. Justesen, and A.H. Johnsen, *Purification and Characterization of Osteopontin from Human Milk.* Protein Expression and Purification, 2003. **30**(2): p. 238-245.

95. Christensen, B., T.E. Petersen, and E.S. Sørensen, *Post-Translational Modification and Proteolytic Processing of Urinary Osteopontin.* Biochemical Journal, 2008. **411**(1): p. 53-61.

96. Yuan, Y., et al., *Expression and Purification of Bioactive High-Purity Recombinant Mouse Spp1 in Escherichia coli.* Applied Biochemistry and Biotechnology, 2014. **173**(2): p. 421-432.

97. Weng, S.Y., et al., *High-Purity Recombinant Osteopontin N-Terminal Domain.* Acta Biochimica Et Biophysica Sinica, 2015. **47**(9): p. 758-760.

98. Ashkar, S., et al., *In Vitro Phosphorylation of Mouse Osteopontin Expressed in E. coli.* Biochemical and Biophysical Research Communications, 1993. **191**(1): p. 126-133.

99. Jang, J.-H. and J.-H. Kim, *Improved Cellular Response of Osteoblast Cells Using Recombinant Human Osteopontin Protein Produced by Escherichia coli.* Biotechnology Letters, 2005. **27**(22): p. 1767-1770.

100. Holmgren, A., *Thioredoxin Structure and Mechanism: Conformational Changes on Oxidation of the Active-Site Sulfhydryls to a Disulfide.* Structure, 1995. **3**(3): p. 239-243.

101. Nikitovic, D. and A. Holmgren, *S-Nitrosoglutathione Is Cleaved by the Thioredoxin System with Liberation of Glutathione and Redox Regulating Nitric Oxide.* J Biol Chem, 1996. **271**(32): p. 19180-5.

102. Zhang, R., et al., *Thioredoxin-2 Inhibits Mitochondria-Located Ask1-Mediated Apoptosis in a Jnk-Independent Manner.* Circulation Research, 2004. **94**(11): p. 1483-1491.

103. Arnér, E.S.J. and A. Holmgren, *Physiological Functions of Thioredoxin and Thioredoxin Reductase.* European Journal of Biochemistry, 2000. **267**(20): p. 6102-6109.

104. Zeller, T. and G. Klug, *Bacterial Thioredoxins-Genes and Regulation.* Genes, Genomes and Genomics. **1**(2): p. 226-232.

105. Zeller, T. and G. Klug, *Thioredoxins in Bacteria: Functions in Oxidative Stress Response and Regulation of Thioredoxin Genes.* Naturwissenschaften, 2006. **93**(6): p. 259-266.

106. Geck, M.K., F.W. Larimer, and F.C. Hartman, *Identification of Residues of Spinach Thioredoxin F That Influence Interactions with Target Enzymes.* Journal of Biological Chemistry, 1996. **271**(40): p. 24736-24740.

107. Watson, W.H., et al., *Thioredoxin and Its Role in Toxicology.* Toxicological Sciences, 2004. **78**(1): p. 3-14.

108. Tanaka, T., et al., *Thioredoxin-2 (Trx-2) Is an Essential Gene Regulating Mitochondria-Dependent Apoptosis.* The EMBO Journal, 2002. **21**(7): p. 1695-1703.

109. Matsui, M., et al., *Early Embryonic Lethality Caused by Targeted Disruption of the Mouse Thioredoxin Gene.* Developmental Biology, 1996. **178**(1): p. 179-185.

110. Nonn, L., et al., *The Absence of Mitochondrial Thioredoxin 2 Causes Massive Apoptosis, Exencephaly, and Early Embryonic Lethality in Homozygous Mice.* Molecular and Cellular Biology, 2003. **23**(3): p. 916-922.

111. Nakamura, H., et al., *Measurements of Plasma Glutaredoxin and Thioredoxin in Healthy Volunteers and During Open-Heart Surgery.* Free Radical Biology and Medicine, 1998. **24**(7): p. 1176-1186.

112. Watson, W.H., et al., *Redox Potential of Human Thioredoxin 1 and Identification of a Second Dithiol/Disulfide Motif.* Journal of Biological Chemistry, 2003. **278**(35): p. 33408-33415.

113. Holmgren, A., *Thioredoxin.* Annual Review of Biochemistry, 1985. **54**(1): p. 237-271.

114. LeMaster, D.M. and F.M. Richards, *Proton-Nitrogen-15 Heteronuclear Nmr Studies of Escherichia coli Thioredoxin in Samples Isotopically Labeled by Residue Type.* Biochemistry, 1985. **24**(25): p. 7263-7268.

115. Reutimann, H., et al., *A Conformational Study of Thioredoxin and Its Tryptic Fragments.* Journal of Biological Chemistry, 1981. **256**(13): p. 6796-6803.

116. Slaby, I. and A. Holmgren, *Reconstitution of Escherichia coli Thioredoxin from Complementing Peptide Fragments Obtained by Cleavage at Methionine-37 or Arginine-73.* Journal of Biological Chemistry, 1975. **250**(4): p. 1340-1347.

117. Haendeler, J., *Thioredoxin-1 and Posttranslational Modifications.* Antioxidants & Redox Signaling, 2006. **8**(9-10): p. 1723-1728.

118. Casagrande, S., et al., *Glutathionylation of Human Thioredoxin: A Possible Crosstalk between the Glutathione and Thioredoxin Systems.* Proceedings of the National Academy of Sciences, 2002. **99**(15): p. 9745-9749.

119. Mahmood, D.F.D., et al., *The Thioredoxin System as a Therapeutic Target in Human Health and Disease.* Antioxidants & Redox Signaling, 2013. **19**(11): p. 1266-1303.

120. Maulik, N. and D.K. Das, *Emerging Potential of Thioredoxin and Thioredoxin Interacting Proteins in Various Disease Conditions.* Biochimica et Biophysica Acta (BBA) - General Subjects, 2008. **1780**(11): p. 1368-1382.

121. Webb, C.R., et al., *Thioredoxin 1 Overexpression Extends Mainly the Earlier Part of Life Span in Mice.* The Journals of Gerontology: Series A, 2011. **66A**(12): p. 1286-1299.

122. Samuel, S.M., et al., *Clinical Perspective.* Circulation, 2010. **121**(10): p. 1244-1255.

123. Jikimoto, T., et al., *Thioredoxin as a Biomarker for Oxidative Stress in Patients with Rheumatoid Arthritis.* Molecular Immunology, 2002. **38**(10): p. 765-772.

124. Beech, D.J. and P. Sukumar, *Channel Regulation by Extracellular Redox Protein.* Channels, 2007. **1**(6): p. 400-403.

125. Tsuji, G., et al., *Thioredoxin Protects against Joint Destruction in a Murine Arthritis Model.* Free Radical Biology and Medicine, 2006. **40**(10): p. 1721-1731.

126. Maurice, M.M., et al., *Expression of the Thioredoxin–Thioredoxin Reductase System in the Inflamed Joints of Patients with Rheumatoid Arthritis.* Arthritis & Rheumatism, 1999. **42**(11): p. 2430-2439.

127. Ghosh, N., R. Ghosh, and S.C. Mandal, *Antioxidant Protection: A Promising Therapeutic Intervention in Neurodegenerative Disease.* Free Radical Research, 2011. **45**(8): p. 888-905.

128. Akterin, S., et al., *Involvement of Glutaredoxin-1 and Thioredoxin-1 in B-Amyloid Toxicity and Alzheimer's Disease.* Cell Death & Differentiation, 2006. **13**(9): p. 1454-1465.

129. Rancourt, R.C., et al., *Thioredoxin Liquefies and Decreases the Viscoelasticity of Cystic Fibrosis Sputum.* American Journal of Physiology-Lung Cellular and Molecular Physiology, 2004. **286**(5): p. L931-L938.

130. Kelly, E., C.M. Greene, and N.G. McElvaney, *Targeting Neutrophil Elastase in Cystic Fibrosis.* Expert Opinion on Therapeutic Targets, 2008. **12**(2): p. 145-157.

131. Lee, R.L., et al., *Thioredoxin and Dihydrolipoic Acid Inhibit Elastase Activity in Cystic Fibrosis Sputum.* American Journal of Physiology-Lung Cellular and Molecular Physiology, 2005. **289**(5): p. L875-L882.

132. Wollman, E., et al., *Cloning and Expression of a Cdna for Human Thioredoxin.* Journal of Biological Chemistry, 1988. **263**(30): p. 15506-15512.

133. Stein, M., et al., *Chlamydomonas reinhardtii Thioredoxins: Structure of the Genes Coding for the Chloroplastic M and Cytosolic H Isoforms; Expression in Escherichia coli of the Recombinant Proteins, Purification and Biochemical Properties.* Plant Molecular Biology, 1995. **28**(3): p. 487-503.

134. Gelhaye, E., et al., *Isolation and Characterization of an Extended Thioredoxin H from Poplar.* Physiologia Plantarum, 2002. **114**(2): p. 165-171.

135. Behm, M. and J.-P. Jacquot, *Isolation and Characterization of Thioredoxin H from Poplar Xylem.* Plant Physiology and Biochemistry, 2000. **38**(5): p. 363-369.

136. Harris, R.P., et al., *Determination and Control of Low-Level Amino Acid Misincorporation in Human Thioredoxin Protein Produced in a Recombinant Escherichia coli Production System.* Biotechnology and Bioengineering, 2012. **109**(8): p. 1987-1995.

137. Baeshen, N.A., et al., *Cell Factories for Insulin Production.* Microbial Cell Factories, 2014. **13**(1): p. 141.

138. Rosano, G.L. and E.A. Ceccarelli, *Recombinant Protein Expression in Escherichia coli: Advances and Challenges.* Frontiers in Microbiology, 2014. **5**: p. 172.

139. Rasala, B.A., et al., *Production of Therapeutic Proteins in Algae, Analysis of Expression of Seven Human Proteins in the Chloroplast of Chlamydomonas reinhardtii.* Plant Biotechnology Journal, 2010. **8**(6): p. 719-733.

140. Gong, Y., et al., *Microalgae as Platforms for Production of Recombinant Proteins and Valuable Compounds: Progress and Prospects.* Journal of Industrial Microbiology & Biotechnology, 2011. **38**(12): p. 1879-1890.

141. Specht, E., S. Miyake-Stoner, and S. Mayfield, *Micro-Algae Come of Age as a Platform for Recombinant Protein Production.* Biotechnology Letters, 2010. **32**(10): p. 1373-1383.

142. Munjal, N., et al., *Light-Induced Production of an Antibody Fragment and Malaria Vaccine Antigen from Chlamydomonas reinhardtii.* Processes, 2014. **2**(3): p. 625-638.

143. Sierra, L.S., C.K. Dixon, and L.R. Wilken, *Enzymatic Cell Disruption of the Microalgae Chlamydomonas reinhardtii for Lipid and Protein Extraction.* Algal Research, 2017. **25**: p. 149-159.

144. Mazzali, M., et al., *Osteopontin—a Molecule for All Seasons.* QJM, 2002. **95**(1): p. 3-13.

145. Xanthou, G., et al., *Osteopontin Has a Crucial Role in Allergic Airway Disease through Regulation of Dendritic Cell Subsets.* Nature Medicine, 2007. **13**(5): p. 570-578.

146. Stubbs, J.T., *Generation and Use of Recombinant Human Bone Sialoprotein and Osteopontin for Hydroxyapatite Studies.* Connective Tissue Research, 1996. **35**(1-4): p. 393-399.

147. Xuan, J.W., C. Hota, and A.F. Chambers, *Recombinant Gst-Human Osteopontin Fusion Protein Is Functional in Rgd-Dependent Cell Adhesion.* Journal of Cellular Biochemistry, 1994. **54**(2): p. 247-255.

148. Mayfield, S.P., et al., *Colostrum/Milk Protein Compositions*. 2015, Google Patents.

149. Hutner, S., et al., *Some Approaches to the Study of the Role of Metals in the Metabolism of Microorganisms.* Proceedings of the American Philosophical Society, 1950. **94**(2): p. 152-170.

150. Gorman, D.S. and R. Levine, *Cytochrome F and Plastocyanin: Their Sequence in the Photosynthetic Electron Transport Chain of Chlamydomonas reinhardi.* Proceedings of the National Academy of Sciences, 1965. **54**(6): p. 1665-1669.

151. Wessel, D. and U.I. Flügge, *A Method for the Quantitative Recovery of Protein in Dilute Solution in the Presence of Detergents and Lipids.* Analytical Biochemistry, 1984. **138**(1): p. 141-143.

152. Terpe, K., *Overview of Bacterial Expression Systems for Heterologous Protein Production: From Molecular and Biochemical Fundamentals to Commercial Systems.* Appl Microbiol Biotechnol, 2006. **72**(2): p. 211-22.

153. Ferrer-Miralles, N., et al., *Microbial Factories for Recombinant Pharmaceuticals.* Microbial Cell Factories, 2009. **8**(1): p. 17.

154. Fakruddin, M., et al., *Critical Factors Affecting the Success of Cloning, Expression, and Mass Production of Enzymes by Recombinant E. coli.* ISRN Biotechnology, 2013. **2013**: p. 7.

155. Gagnon, P., et al., *Igm Purification with Hydroxyapatite.*

156. Losh, J.L., J.N. Young, and F.M.M. Morel, *Rubisco Is a Small Fraction of Total Protein in Marine Phytoplankton.* New Phytologist, 2013. **198**(1): p. 52-58.

157. Aryal, U.K., D.J.H. Olson, and A.R.S. Ross, *Optimization of Immobilized Gallium (Iii) Ion Affinity Chromatography for Selective Binding and Recovery of Phosphopeptides from Protein Digests.* Journal of Biomolecular Techniques : JBT, 2008. **19**(5): p. 296-310.

158. Machida, M., et al., *Purification of Phosphoproteins by Immobilized Metal Affinity Chromatography and Its Application to Phosphoproteome Analysis.* FEBS Journal, 2007. **274**(6): p. 1576-1587.

159. Zhu, Y.S. and R.J. FitzGerald, *Caseinophosphopeptide Enrichment and Identification.* International Journal of Food Science & Technology, 2012. **47**(10): p. 2235-2242.

160. Biswas, S., A. Sarkar, and R. Misra, *Iron Affinity Gel and Gallium Immobilized Metal Affinity Chromatographic Technique for Phosphopeptide Enrichment: A Comparative Study.* Biotechnology & Biotechnological Equipment, 2017. **31**(3): p. 639-646.

161. Kitahara, K., et al., *Osteopontin Deficiency Induces Parathyroid Hormone Enhancement of Cortical Bone Formation.* Endocrinology, 2003. **144**(5): p. 2132-2140.

162. Kleinman, J.G., et al., *Expression of Osteopontin, a Urinary Inhibitor of Stone Mineral Crystal Growth, in Rat Kidney.* Kidney International, 1995. **47**(6): p. 1585-1596.

163. Worcester, E.M., et al., *The Calcium Oxalate Crystal Growth Inhibitor Protein Produced by Mouse Kidney Cortical Cells in Culture Is Osteopontin.* Journal of Bone and Mineral Research, 1992. **7**(9): p. 1029-1036.

164. Min, W., et al., *Quantitative Studies of Human Urinary Excretion of Uropontin.* Kidney International, 1998. **53**(1): p. 189-193.

165. Rangaswami, H., A. Bulbule, and G.C. Kundu, *Osteopontin: Role in Cell Signaling and Cancer Progression.* Trends in Cell Biology, 2006. **16**(2): p. 79-87.

166. Anborgh, P.H., et al., *Pre-and Post-Translational Regulation of Osteopontin in Cancer.* Journal of Cell Communication and Signaling, 2011. **5**(2): p. 111-122.

167. Senger, D.R., et al., *A Secreted Phosphoprotein Marker for Neoplastic Transformation of Both Epithelial and Fibroblastic Cells.* Nature, 1983. **302**(5910): p. 714.

168. Kurzbach, D., et al., *Cooperative Unfolding of Compact Conformations of the Intrinsically Disordered Protein Osteopontin.* Biochemistry, 2013. **52**(31): p. 5167-5175.

169. Fisher, L.W., et al., *Flexible Structures of Sibling Proteins, Bone Sialoprotein, and Osteopontin.* Biochemical and Biophysical Research Communications, 2001. **280**(2): p. 460-465.

170. Hwang, S.M., et al., *Osteopontin Inhibits Induction of Nitric Oxide Synthase Gene Expression by Inflammatory Mediators in Mouse Kidney Epithelial Cells.* Journal of Biological Chemistry, 1994. **269**(1): p. 711-715.

171. Ravi, A., et al., *Separation Options for Phosphorylated Osteopontin from Transgenic Microalgae Chlamydomonas reinhardtii.* International Journal of Molecular Sciences, 2018. **19**(2): p. 585.

172. Zhao, G., X.-Y. Dong, and Y. Sun, *Ligands for Mixed-Mode Protein Chromatography: Principles, Characteristics and Design.* Journal of Biotechnology, 2009. **144**(1): p. 3-11.

173. Brenac Brochier, V., et al., *High Throughput Screening of Mixed-Mode Sorbents and Optimisation Using Pre-Packed Lab-Scale Columns for the Purification of the Recombinant Allergen Rbet V 1a.* Journal of Chromatography B, 2009. **877**(24): p. 2420-2427.

174. Cabanne, C., et al., *Efficient Purification of Recombinant Proteins Fused to Maltose-Binding Protein by Mixed-Mode Chromatography.* Journal of Chromatography A, 2009. **1216**(20): p. 4451-4456.

175. Brenac Brochier, V. and V. Ravault, *High Throughput Development of a Non Protein a Monoclonal Antibody Purification Process Using Mini-Columns and Bio-Layer Interferometry.* Engineering in Life Sciences, 2016. **16**(2): p. 152-159.

176. Bradford, M.M., *A Rapid and Sensitive Method for the Quantitation of Microgram Quantities of Protein Utilizing the Principle of Protein-Dye Binding.* Analytical Biochemistry, 1976. **72**(1): p. 248-254.

177. Schneider, C.A., W.S. Rasband, and K.W. Eliceiri, *Nih Image to Imagej: 25 Years of Image Analysis.* Nature Methods, 2012. **9**(7): p. 671-675.

178. Kramer, C.Y., *Extension of Multiple Range Tests to Group Means with Unequal Numbers of Replications.* Biometrics, 1956. **12**(3): p. 307-310.

179. Tukey, J.W., *Comparing Individual Means in the Analysis of Variance.* Biometrics, 1949. **5**(2): p. 99-114.

180. Nogueira, R., M. Lämmerhofer, and W. Lindner, *Alternative High-Performance Liquid Chromatographic Peptide Separation and Purification Concept Using a New Mixed-Mode Reversed-Phase/Weak Anion-Exchange Type Stationary Phase.* Journal of Chromatography A, 2005. **1089**(1): p. 158-169.

181. Gao, D., D.-Q. Lin, and S.-J. Yao, *Mechanistic Analysis on the Effects of Salt Concentration and Ph on Protein Adsorption onto a Mixed-Mode Adsorbent with Cation Ligand.* Journal of Chromatography B, 2007. **859**(1): p. 16-23.

182. O'Connor, E., et al., *Monoclonal Antibody Fragment Removal Mediated by Mixed Mode Resins.* Journal of Chromatography A, 2017. **1499**: p. 65-77.

183. Gao, D., et al., *Evaluating Antibody Monomer Separation from Associated Aggregates Using Mixed-Mode Chromatography.* Journal of Chromatography A, 2013. **1294**: p. 70-75.

184. Bischoff, R. and L.W. McLaughlin, *Nucleic Acid Resolution by Mixed-Mode Chromatography.* Journal of Chromatography A, 1984. **296**: p. 329-337.

185. Arakawa, T., et al., *Capto Mmc Mixed-Mode Chromatography of Murine and Rabbit Antibodies.* Protein Expression and Purification, 2016. **127**: p. 105-110.

186. White, C.W., *Product and Process for Liquefaction of Mucus or Sputum*. 2007, Google Patents.

187. Johansson, B.-L., et al., *Chemical Characterisation of Different Separation Media Based on Agarose by Static Time-of-Flight Secondary Ion Mass Spectrometry.* Journal of Chromatography A, 2004. **1023**(1): p. 49-56.

188. Arnér, E.S.J. and A. Holmgren, *Measurement of Thioredoxin and Thioredoxin Reductase.* Current Protocols in Toxicology, 2005. **24**(1): p. 7.4.1-7.4.14.

189. Jorgensen, W.L., et al., *Comparison of Simple Potential Functions for Simulating Liquid Water.* The Journal of Chemical Physics, 1983. **79**(2): p. 926-935.

190. Spyrou, G., et al., *Cloning and Expression of a Novel Mammalian Thioredoxin.* Journal of Biological Chemistry, 1997. **272**(5): p. 2936-2941.

191. Guo, S., et al., *Exploring the Separation Power of Mixed-Modal Resins for Purification of Recombinant Osteopontin from Clarified Escherichia coli Lysates.* Biotechnology Progress, 2018.

192. Parimal, S., S. Garde, and S.M. Cramer, *Effect of Guanidine and Arginine on Protein–Ligand Interactions in Multimodal Cation-Exchange Chromatography.* Biotechnology Progress, 2017. **33**(2): p. 435-447.

APPENDIX A

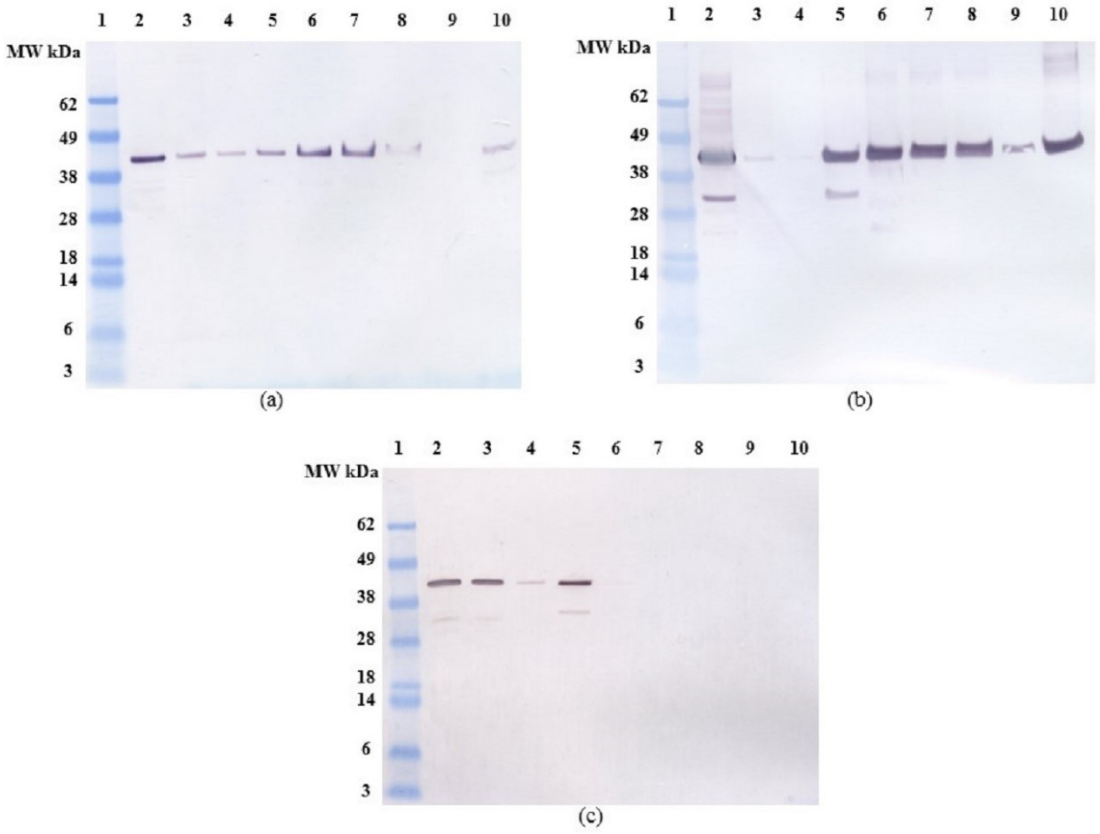

Figure A1 Anti-FLAG western blot of (a) *E. coli* OPN binding and elution profile without 250 mM NaCl (b) *C. reinhardtii* OPN binding and elution profile with 250 mM NaCl (c) *E. coli* OPN binding and elution profile with 250 mM NaCl from ceramic hydroxyapatite (CHT) resin. All samples diluted to <1 mg/mL total soluble protein (TSP). Lane 1. Molecular weight (MW) marker, lane 2. Clarified lysate, lane 3. Supernatant, lane 4. Washes 3 column volumes (CV), lane 5. Elution with 100 mM NaP, lane 6. Elution with 250 mM NaP, lane 7. Elution with 500 mM NaP, lane 8. Elution with 1000 mM NaP, lane 9. Elution with 1500 mM NaP, lane 10. Elution with 100 mM NaOH. All elutions were performed with 5 CV of the respective buffer

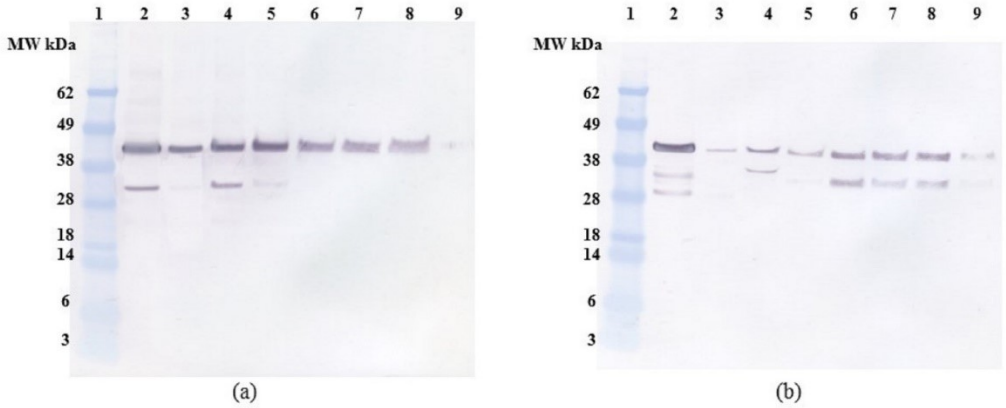

Figure A2 Anti-FLAG western blot of (a) *C. reinhardtii* OPN (b) *E. coli* OPN binding and elution profile from Ga-IMAC resin. All samples diluted to <1 mg/mL TSP. Lane 1. MW marker, lane 2. Clarified lysate, lane 3. Supernatant, lane 4. Washes (3 CV), lane 5. Elution with 100 mM NaP, lane 6. Elution with 250 mM NaP, lane 7. Elution with 500 mM NaP, lane 8. Elution with 1000 mM NaP, lane 9. Elution with 1500 mM NaP. All elutions were performed with 5 CV of the respective buffer

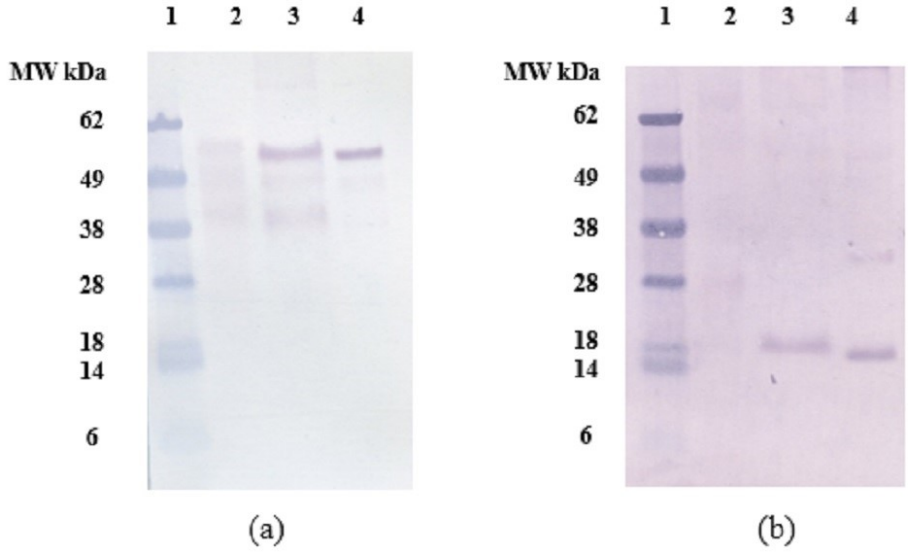

Figure A3 (a) Anti-Rubisco large subunit (b) Anti-Rubisco small subunit western blots of *C. reinhardtii* OPN samples. All samples diluted to <1 mg/mL TSP. Lane 1. MW marker, lane 2. *C. reinhardtii* clarified lysate, lane 3. Elution with 100 mM NaOH from ceramic hydroxyapatite (CHT) resin, lane 4. Elution with 200 mM NaCl from Capto Q resin. All elutions were performed with 5 CV of the respective buffer

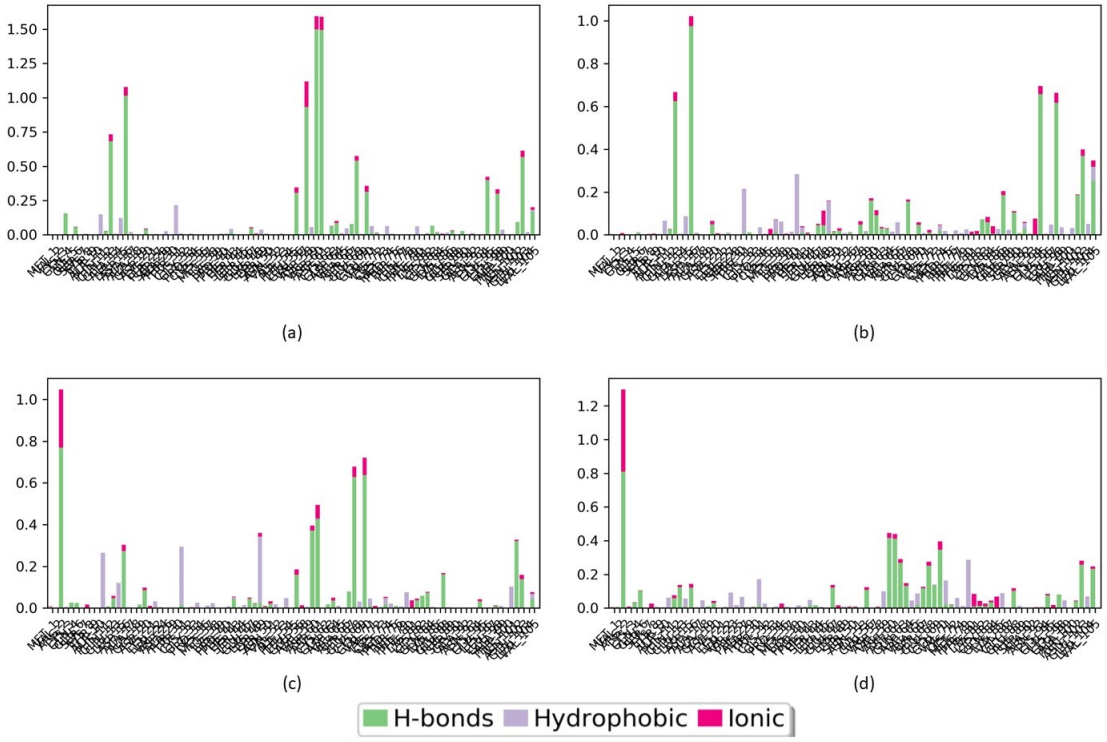

Figure A4 Interaction fraction (or contact period) over the course of the trajectory (240ns) for hTrx amino acids with HEA ligand are shown in bar chart under the following simulation conditions (a) 0.05 M NaCl, (b) 1 M NaCl, (c) 0.2 M arginine and (d) 1 M NaCl + 0.2 M arginine. The values over one are possible as some protein residue may make multiple contacts of same subtype with the ligand.